



UNIVERSITAT DE
BARCELONA

Plasma membrane mechanosensing upon stretch-induced topography remodelling

Xarxa Quiroga Alvarez



Aquesta tesi doctoral està subjecta a la llicència *Reconeixement- SenseObraDerivada 4.0.
Espanya de Creative Commons.*

Esta tesis doctoral está sujeta a la licencia *Reconocimiento - SinObraDerivada 4.0.
España de Creative Commons.*

This doctoral thesis is licensed under the *Creative Commons Attribution-NoDerivatives 4.0.
Spain License.*



UNIVERSITAT DE
BARCELONA

Tesi Doctoral

Plasma membrane mechanosensing upon stretch-induced topography remodelling

Memòria per optar al grau de Doctor en el Programa de Doctorat en
Biomedicina

Barcelona, Universitat de Barcelona, Maig 2021.

Presentada per Xarxa Quiroga Álvarez

Dirigida pel Dr. Pere Roca-Cusachs Soulere

Codirigida per la Dr. Anabel-Lise Le Roux

“Intelligence is what you use when you don't
know what to do: when neither innateness
nor learning has prepared you for the particular
situation.”

Jean Piaget

AGRADECEMENTOS

Inda me acorda cando estaba facendo o mestrado de xenética e xenómica do desenvolvemento, estudando como emerxen os patróns corporais e como as células indiferenciadas migran e se colocan para dar lugar a estruturas en 3D. Eran cuestións que me fascinaban. Eu quería entender a regulación bioquímica de todo aquilo. Obviamente, naquel momento non tiña nin idea do que era a mecanobioloxía nin de que moitas das respostas que eu buscaba se agochaban nesta disciplina. A casualidade quixo que o coordinador do mestrado organizase as aulas coma unha serie de palestras con poñentes invitados. Entón sucedeu: Xavi veu e explicounos o traballo de Anna sobre como os CAFs facían dragging das células tumorais axudándoas a escapar do agregado no que se atopaban. Iso era! Eu tiña que traballar aí. Así que ao rematar a charla, Macià e máis eu fomos inquirir a ver se había oco para dous estudantes de mestrado highly-motivated. Naquel momento eu era inocente a toda a física que se agochaba detrás daquel proxecto (e todos os proxectos do laboratorio de Xavi). Afortunadamente, el si o soubo ver e presentoume a Pere. “Tengo un compañero que hace cosas mucho más moleculares que yo y que está buscando estudiantes”. Así que, contraintuitivamente a como comezan os agradecementos da maioría das teses, merci Xavi, per presentar-me a en Pere, si no fossi per això no estaria on estic avui. Quina sort que vaig tenir aquell dia! Pere, quan em vaig plantar al teu despatx i em vas acollir sense importar el meu expedient o si tenia una beca, només tenint en compte la meva il·lusió i el meu interès per la recerca, vas ser molt generós. I t’ho agrairé sempre. Em vas donar la oportunitat amb la que vaig passar anys somniant i em sento en deute amb tu per això. Tambièn tengo que agradecerle a Anita haberme acogido en el lab, no solo como su estudiante, sino tambièn como a una amiga. Anabel-Lise, tu vas arriver après. Mais heureusement

que tu vas y arriver! Merci de tout mon cœur pour m'avoir guidé en tout moment et pour être devenue ma maman de la science. Tu sais que, justement comme avec une mère, je me suis fâchée avec toi et je t'ai aimé avec toutes mes forces. Mais tu sais que c'est justement parce que tu avais raison, et on déteste qu'ils nous dissent ce qu'on sait déjà mais qu'on ne veut pas voir. Merci encore pour avoir eu toute la patience du monde avec moi. Je ne vais jamais l'oublier. A continuación, tengo que agradecerles a todas mis compañeras de laboratorio que me han acompañado durante este largo, LARGO, camino. Nucleoporinos, gràcies per existir a la pecera, perquè m'ho he passat tan, tan be amb vosaltres aquets anys que us trobaré massa a faltar. I gràcies també perquè es per vosaltres que avui parlo català (tot i que sigui una mica xungo...). Ion, eskerrik asko por hacerme las comidas más ricas de mi vida y, sobre todo, ¡por enseñarme a hacerlas! Compartir piso contigo fue genial, tu calma es un ejemplo para mí. Leonucio, grazie per non farmi sentire mai scomoda chiedendoti cose scientifiche. Mi sento fiera di sapere che ho amici tan intelligenti come te e che in più amano mangiare della orella e ballare nel Avante. Juanfra, ir contigo a Baeza fue uno de los mejores momentos de toda la tesis. No voy a seguir en ciencia, pero si lo hiciese me gustaría ser como tú. Eres un ejemplo de integridad, inteligencia y bondad y estas son palabras muy grandes para unos agradecimientos, así que mejor evoco la imagen del Juanfra bailongo a la que también quiero parecerme. Annie, merci pour me montrer comment faire des western blots, même si ça fut à prix de détruire les échantillons de quelqu'un. Je grade toujours dans mon cœur tous nos moments rentrant chez nous après le bootchamp. Jennyko, ευχαριστώ for being always so sweet to me and preparing the best trip to Greece ever imagined. I just want to finish this thesis and do a girl's night with lots of κλασί. Amy, thank you for being our source of gossips, I just hope that you will equally be a source of dessert recipes soon. Laura, merci pour me faire souvenir que mon français c'était merde et que je devais toujours pratiquer et apprendre ces petits proverbes que tu connais. Sefo, Giulia, Davia, grazie per lasciarmi essere italiana con voi. Le nostre cene mi fanno sempre sentire a casa mia in paese e questo vale oro in una città come Barcelona. Carlos, nadie grita más que tú en la pecera, pero nadie tiene el corazón más grande. Te echo mucho de menos y ojalá seguirmos viendo para echar unas birras de vez en cuando (espero que en Galicia pronto). Flor, gracias por toda la ayuda que me diste y por esos consultorios psicológicos que nos montamos en la sala de virus. Gerardinho da Sousa, estoy muy feliz de que hayas vuelto a ser tú después de la publicación del paper. Pronto más y mejor en el parc de la Espanya Industrial.

Nimesh, my friend, thanks for all the things about communism I have learnt with you (and some science too), but specially for establishing the habit of going at parc industrial for beers every Friday. That is the best contribution that you have made to this lab. Sri, you are very likely the person that I know that reads the most. Looking forward to share all of that knowledge in front of a beer at parc industrial. Oriol, merci per ser el tècnic de laboratori més riquiño que mai hem tingut, i ara ja gairebé PhD student! Miguel, é unha mágoa que non coincidísemos máis tempo, tería sido xenial facer a tese cun medio irmão. Macià, ets el baríton mes impressionant que mai ha vist el lab. I gràcies també per parlar-me en català quan encara estàvem al màster, si ho parlo avui també es gràcies a tu. I a la Ari! Que a més de ensenyar-me la llengua em vas ensenyar com ser assertiva i no rallar-me per dir les coses que penso. Ja saps que t'admiro molt per això. Susana, Jari, gracias por ser las más mejores en técnicos del mundo. Y además dos amores de persona. ¡Ojalá poder trabajar siempre con gente como vosotras! Ali, thanks for all the efforts you made to help with the project. If we can publish an article it is also thanks to you. Y gracias a todo el resto de compañeras del laboratorio (las que están y las que ya se fueron): Alberto, Roger, Marina, Pilar, Manu, Ernest, Raimon, Dobryna, Sabrina, Marilena, Tom, Marina PD, Marija, Ona, Natxo, Aina, Mar, Aurora, Alice, Miquel, Isabela, Marc T... Gracias, gracias, gracias por todo lo que aprendo de vosotras cada día. Me lo he pasado genial en estos años y creo que eso es lo más importante de esta experiencia.

Víctor, ya lo sabes, pero gracias por estar a mi lado cada día durante casi toda la tesis, literalmente, y toda la tesis sin ser literal. Aunque te haya odiado más que a nadie por haberme creado un trauma con los stainings sabes que también te quiero por todo lo demás. ¡Pronto lo celebraremos en Plataforma, no lo dudes!

Thank you also to the PhD Committee fellows: those retreats will remain for ever recorded on my mind!

E xa para concluír, grazas aos Canecos por recibirme cada vez que volvía a Lugo coma se non pasase o tempo, e a ti especialmente, Pérez, por ser o mellor amigo que unha pode desexar e cubrirme de mimos e ánimos cada vez que o necesitei. Primas, el veranito en Ghalisia estanos agardando e xa non me dá chegado a hora de estar con vós e recuperar todo o tempo perdido. Mamá e papá, por ter tido conta de min cada vez que andei langrada e por terme animado sempre a dar un paso máis, a seguir adiante, inda que iso fose a calquera custo para vós. Sei que sodes o meu apoio e que estades aí para min sempre, sempre. Bebé, grazas por acocharte comigo na cama e compartir as nosas cousas, ver vídeos de make up e

xogar ao pokemon. Tamén polos vraos na Veiguiña escoitando paxaros e bañándonos na chapacuña. Estar contigo éme sempre a maior das sanacións. Pablo, pecho contigo. Esta tese nunca tería chegado ao seu termo se non fose por ti, sábelo, ou? Con toda a paciencia do mundo recolliches cada cachiño de min cada vez que chegaba esgazada a casa, respectaches os meus tempos e coidaches de min inda cando ti andabas tan eslabazado ou máis cá min. Pasar esta experiencia xuntos úneme a ti. Grazas meu amor, aquí estou, “heguei”!

CONTENTS

PREFACE	12
CHAPTER 1 - INTRODUCTION	15
1.1. THE PLASMA MEMBRANE - A GENERAL VIEW.....	15
1.1.1. Physicochemical properties of PM.....	18
1.1.2. PM topography.....	21
1.1.3. PM reservoir	25
1.1. ACTIN-THE SUPPORTIVE SCAFFOLD UNDER THE PM	26
1.1.1. Cortical actin.....	29
1.1.2. PM regulation of actin polymerization events	31
1.2. MECHANOSENSING AND SIGNAL INTEGRATION AT THE PM.....	33
1.2.1. What is mechanosensing?.....	33
1.2.2. The PM as a mechanosensitive structure.....	34
1.2.3. Physical stimuli altering PM state in physiological conditions	35
1.2.4. Tools to study PM mechanosensing and molecular responses associated to them	36
1.3. MECHANOSENSING EVENTS TRIGGERED AT THE PM.....	40
1.3.1. Protein conformational changes	40
1.3.2. Protein relocation	41
1.3.3. Curvature sensing proteins.....	42
CHAPTER 2 - AIMS OF THE THESIS.....	45
2.1. GENERAL AIM	45
2.2. SPECIFIC AIMS	45
CHAPTER 3 - METHODS	46
3.1. CELL CULTURE AND EXPRESSION VECTORS.....	46
3.2. CELL TRANSFECTION	47
3.3. STABLE CELL LINE PRODUCTION.....	47
3.4. DRUG TREATMENTS.....	48
3.5. PDMS MEMBRANE FABRICATION.....	48
3.6. STRETCH EXPERIMENTS.....	49
3.7. OSMOLARITY EXPERIMENTS.....	50
3.8. SCANNING ELECTRON MICROSCOPY EXPERIMENTS	50
3.9. TRANSMISSION ELECTRON MICROSCOPY EXPERIMENTS	51
3.10. APEX LABELLING FOR TEM IMAGING	51
3.11. IMAGE ACQUISITION	52
3.12. FLUORESCENCE ANALYSIS	52
3.13. AREA ANALYSIS.....	53
3.14. QUANTIFICATION OF NUMBER AND PM AREA % STORED BY EVAGINATIONS ..	53
3.15. FLUORESCENCE AND SEM CORRELATION	54
3.16. STATISTICAL ANALYSIS	54
3.17. TEORETHICAL MODEL.....	54
CHAPTER 4 - RESULTS.....	59
4.1. COMPRESSION GENERATES DYNAMIC PM EVAGINATIONS IN THE SCALE OF 100NM WIDTH.....	60

4.2.	THE INVOLVEMENT OF ACTIN IN EVAGINATION RESORPTION AFTER STRETCH	64
4.3.	WHICH IS THE MOLECULAR LINK BETWEEN PM AND ACTIN REMODELLING?	65
4.4.	THE PM REMODELLING EVENT TRIGGERED BY STRETCH-RELEASE IS LOCAL	69
4.5.	HOMEOSTASIS RECOVERY AFTER STRETCH REQUIRES INTEGRITY OF SH3 AND IBAR IRSP53 DOMAINS	71
4.6.	IRSP53 ACTS AS A MECHANOSENSOR OF PM CURVATURE	73
4.7.	ACTIN POLYMERIZATION IS DRIVEN BY RAC1 AND ARP2/3 ACTIVATION.....	79
4.8.	A MECHANICAL MECHANISM FOR ACTIN-MEDIATED EVAGINATION FLATTENING.....	84
CHAPTER 5 -	DISCUSSION	87
CHAPTER 6 -	CONCLUSIONS.....	93
APPENDIX A – IMMUNOSTAINING PROTOCOL FOR PM BOUND PROTEINS.....		95
PROTOCOL: IF FOR PM ASSOCIATED PROTEINS.....		99
<i>List of materials</i>		99
<i>Steps</i>		100
APPENDIX B – BAR PROTEINS KNOCK-DOWN GENERATION.....		102
APPENDIX C – MECHANICAL EFFECTS ON AMPHYPHISIN TUBULATION IN CELLS		105
APPENDIX D – SEM IMAGES OF COMPRESSION-GENERATED EVAGINATIONS IN IRSP53^{-/-} AND IRSP53^{-/-R} MEF		107
APPENDIX E – IRSP53 PLASMIDS SEQUENCING.....		109
APPENDIX F – ANALYSIS CODE FOR MEMBRANE EVAGINATIONS DYNAMICS		112
APPENDIX G – PUBLICATIONS AND CONFERENCES		116
LIST OF ABREBIATIONS.....		118
REFERENCES.....		122

PREFACE

Five years ago, I started walking this path that now seems like an entire life. Although everyone around tried to explain how this would feel, none of their explanations could have match what it has been in the end. And this is exactly how living systems are, at all levels. The harder the scientists try to feed our curiosity taking closer looks to them, inspecting the question from a different angle, and despite all the previous knowledge that we could gather; the more they surprise us and reveal new ways of sensing, reacting and adapting to the environment. And I think this is exactly what drove me here. I wanted to understand how this is done. I wanted to “see” it. How is it possible that a cell “understands” what is going on around? Which are the parameters that they sense? Biochemistry alone does not answer the question.

In a crowded environment, such as it is our body, cells are exposed to thousands of mechanical stimuli too. And those can be also harnessed and transformed into chemical responses as a way of signalling. While the classical biochemical inputs have long been studied, loads of questions remain open about how cells interpret those physical stimuli around them, and microscopy comes as a powerful technique to try to answer these queries.

In that sense, this thesis represents a small approach in trying to unravel how the plasma membrane, the first boundary between the cell and the extracellular media, can receive mechanical stimuli and convert them into biochemical signals amenable for the cell. To try to answer this question, this work starts with an introduction to the structure and physicochemical characteristics of the plasma membrane. An overview of the cortical component of the cytoskeleton, intrinsically interconnected to this structure, is also provided. Next, a summary of the literature available on how the plasma membrane can perceive mechanical

stimuli and which are the associated biochemical responses triggered by them is included as well. This part is based on a review article published by my colleague and co-supervisor Dr. Le Roux and myself at *Philosophical Transactions B* as part of the 2019 issue "Forces in cancer" [1].

After the introduction, chapter 2 describes the objectives of this study, which can be summarised as trying to unravel the way in which cells couple mechanical signals at their plasma membrane to biochemical cascades that mediate a response to those. Following, chapters 3 and 4 compose the main body of this thesis, including the methods and the experimental results coming from this research work. Both sections constitute a scientific article that has been recently submitted for publication. In chapter 3 the simplified model chosen to study the question of how cells sense and integrate mechanical stimuli at their plasma membrane is described. This consisted in submitting fibroblast to a controlled stretch-release cycle, forcing them to quickly adapt their shape, mimicking a highly-relevant scenario in physiology. Chapter 4 recapitulates the way in which plasma membrane reacted to this mechanical perturbation. In the first place, the structure reacted by passively forming evaginations on the nanometric scale of homogeneous size and shape. These evaginations are next recognised by the I-BAR protein IRSp53, which subsequently organizes a node of actin polymerisation dependent on Rac1 and Arp2/3 that mediates the flattening of the structures. Absence of IRSp53 results, thus, in an impaired recovery of homeostasis after stretch. To reinforce the obtained experimental results, theoretical framework to model the mechanics of the system was generated in collaboration with the group of Dr. Arroyo at the Centre Internacional de Mètodes Numèrics en Enginyeria (CIMNE). The aim of this model was to describe how a network generated by the Arp2/3 complex, until now described to push, is able to generate in-plane forces that mediate the ironing of the evagination. Chapter 5 includes a discussion about the limitations of the technique, the novelty of the presented findings, the possible physiological scenarios where the described mechanochemical pathway can be of relevance and, finally, some exciting and unexplored questions that remained open after this work.

Additionally, other scientific production obtained during this thesis consisting in unexplored results or work belonging to other publications, has been added at the end of this manuscript in four appendixes. On the first one, I describe all the efforts made during the first 1 year and a half of the PhD to improve immunostaining technique for plasma membrane bound proteins in order to try

to stain endogenous BAR proteins. The second appendix gathers the findings obtained from the silencing assay of BAR candidates likely to recognise the curved shape of the stretch-release generated evaginations. The third appendix contains experimental results part of a different publication from Le Roux et al. now under review in Nature Communications [2]. Here, I studied the response of the N-BAR protein Amphiphysin after mechanical stimulation in cells. A fourth appendix including scanning electron microscopy representative images of stretch-release generated evaginations in other cell lines is also added. Finally, I included two more appendix containing the sequencing of all the IRSp53 plasmids used for the body of the work of this thesis and the MATLAB code used for analysis of evaginations flattening dynamics after stretch.

Chaper 1 -INTRODUCTION

1.1.THE PLASMA MEMBRANE - A GENERAL VIEW

For the development of life, the formation of a physical boundary that compartmentalized nucleic acids and proteins from the extracellular milieu, was a fundamental fact. This boundary, known as the plasma membrane (PM), is in its majority formed by lipids together with a variable fraction of proteins.

Three groups of lipids constitute the PM, phospholipids, sphingolipids and sterols [3].

Phospholipids are amphipathic molecules composed by a polar head, containing a phosphate group, and two hydrophobic tails that tend to arrange facing to the tails of the other phospholipids in order to stay away from water molecules. This arrangement imposes a bilayer type of structure, which is the most energetically favourable configuration for this type of molecules when they are surrounded by water [4].

Phospholipids are differentiated between them depending on their polar heads and on the type of hydrophobic tails bound to it. The most abundant type of phospholipids in membranes are glycerophospholipids, which have diacylglycerol as a backbone for the addition of two hydrophobic carbon tails, and a phosphate as a linker for the head group. Lipids within this group can be classified in function of the chemical group esterified to the phosphate head. Choline gives rise to Phosphatidylcholine (PC), the most abundant of glycerophospholipids. Serine results in Phosphatidylserine (PS). From Ethanolamine, Phosphatidylethanoamine (PE) is obtained. Inositol results in Phosphatidilinositol (PI), which can be modified by phosphorylation giving rise to the family phosphoinositides (PIPs). Finally, when no group is linked to the

Chapter 1 – INTRODUCTION

phosphate head, Phosphatidic Acid (PA) is obtained [5]. From this set of lipids, only PS, PI and PA carry a negative charge at physiological pH [4], which is of great importance for protein binding (discussed in the next section). The size of the head of these lipids confers them different geometrical structure, which has an impact in the bilayer's shape. For example, PC and PS have a cylindrical shape which makes them self-organize in flat bilayers. On the other hand, PA and PE display conic shape which imposes positive curvature¹ to the flat bilayer, and, opposite, PI and PIPs display an inverted conical shape conferring negative curvature to membranes [6,7].

In addition to glycerophospholipids, membranes are also composed by sphingolipids, which have ceramides as backbones and can be modified by the addition of sugars in their polar heads by a glycosidic bond, forming glycosphingolipids. Sphingomyelin is the most important representant of this family, as it is the most enriched in PM [8]. These glycolipids contribute to the glycocalyx, an outer structure surrounding cell membrane composed by sugar chains which function is to contribute to cell shape, adhesion and intercellular recognition [4,9].

The last lipidic component of PM are sterols. In animal membranes, the most abundant one is cholesterol, which is non-polar, in contrast with the rest of lipids described [5].

These different types of lipid species distribute differently within the two leaflets of the PM, giving rise to asymmetry [10]. Not the same types of lipids distribute equally across each one of the sides of the bilayer, and the components of one side may influence what is found on the other. For instance, PS and PE are mostly present at the cytosolic side of the membrane, whereas PC and Sphingomyelin are by majority located facing the extracellular media [11]

But lipids are not the only type of molecule forming the PM, proteins are also a big part of it. In animal cells, they constitute around the 50% of the total mass (although this amount can vary in other types of membranes within the cell) [4]. These proteins can be enclosed in the bilayer, in which case they are referred to as integral proteins, or adjacent to it, in which case they are named peripheral proteins. Integral proteins usually possess big hydrophobic regions which allow for insertion into the bilayer. Opposite, peripheral proteins interact with the

¹ By convention, the sign of PM curvature is positive when the center of the curvature is in the side of the membrane opposite to extracellular medium. This gives rise to invaginations. Oppositely, when the center of curvature is in the same side of the extracellular medium it is considered negative, which depicts the shape of evaginations.

components of the bilayer through weak electrostatic or hydrophobic interactions as well as non-covalent bonds [4,12]. Membrane proteins can vary on their functions and features. First, they can present glycosidic modifications contributing to the glycocalyx. Second, they can act as channels or transporters allowing the passage of water molecules and ions. They can also act as surface receptors, being involved in external signal reception and transduction to the inner of the cell. Some of them perform as anchors, maintaining the architecture of the PM on top of the cytoskeleton and other present enzymatic activity [4]. However, this thesis will only address more in detail the roles of anchoring and signalling transduction proteins, which are the ones of interest for the study here presented.

The interactions between proteins and lipids within the bilayer give rise to its 2D conformation. During the last 50 years different models to explain PM structure have been proposed. Since the beginning of the 70's the PM has been described following the model of the fluid mosaic. In this model, the PM is understood as a heterogeneous fluid interface of around 7-10 Å thick in which lipids form a matrix where proteins are embedded [13]. However, this model was over simplistic considering simple Brownian movement of proteins embedded in the lipid fluid, which was not observed under experimental conditions. Since that, other models have appeared, each one trying to explain determinate features of the PM. Currently, the working paradigm is the “fence-and-pickets” model (Fig. 1), in which the influence of the cytoskeleton over the PM is accounted. In this model, some integral proteins (pickets) would be bound to the underlying cortex which would create a sort of fence limiting the diffusion of non-anchored integral proteins [14–17].

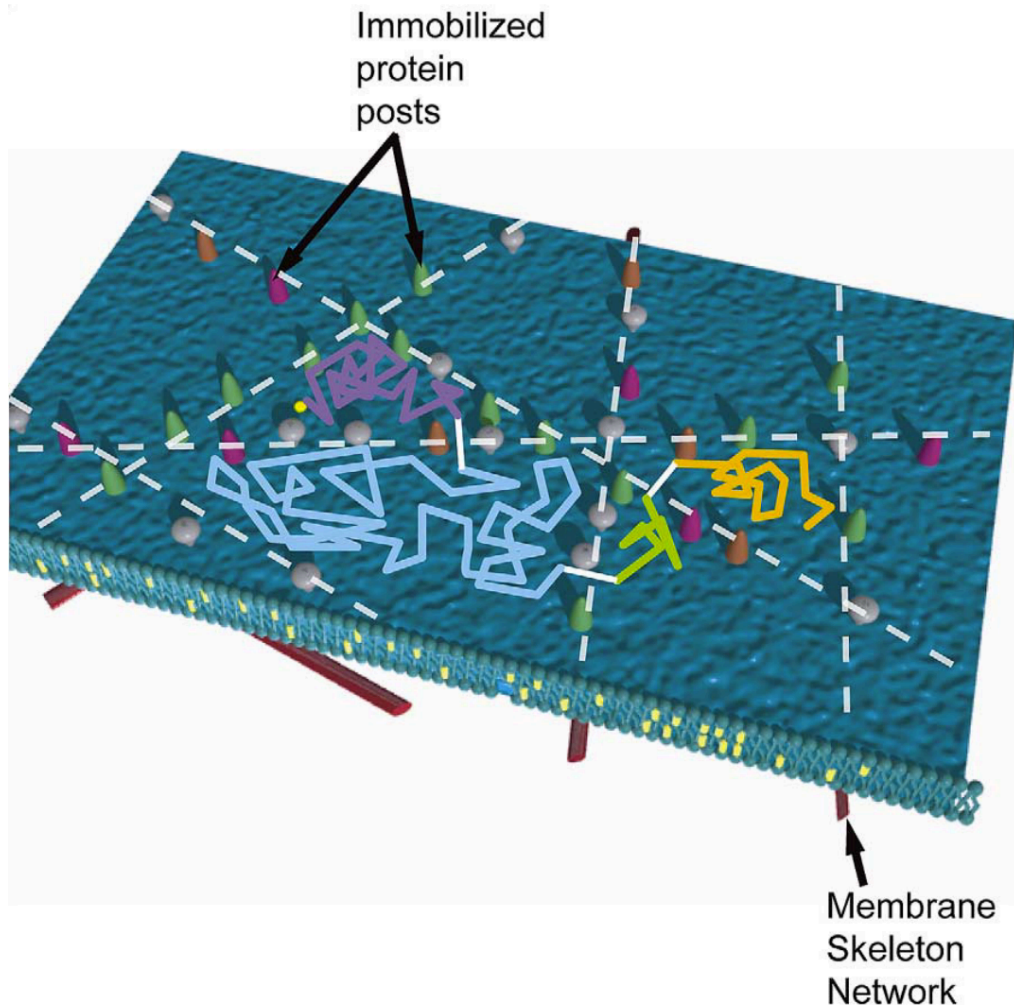


Figure 1: The fence-and-pickets model (extracted from [14]). The actin cytoskeleton interacts with the PM anchoring the integral proteins on it. This connections act as a fence with pickets limiting protein and lipid mobility within discrete domains. One protein trajectory within a certain domain followed by hopping into another one is designed as lines in blue, green, yellow and purple.

Nevertheless, the complexity of this organelle is great, and a simple model cannot recapitulate all of its features. In the next chapters, some of its characteristics will be analysed in more detail to elaborate a clearer picture on this tangled structure.

1.1.1. Physicochemical properties of PM

As explained in the previous section, the plasma membrane is composed by different types of phospholipids and the differences arising from their structures plus the plethora of chemical variations that they can present both on their polar heads or in the carbon chains, confer different properties to each one of the leaflets of the PM.

The carbon chains in both glycerophospholipids and sphingolipids can proceed from different types of fatty acids. Those can be saturated if all the carbons composing the chain are saturated with hydrogen atoms; or unsaturated, when some of the carbons are covalently bound to its neighbour by a double bond [6]. Glycerophospholipids usually carry one monounsaturated or saturated chain and a polyunsaturated one, whereas sphingolipids are usually saturated. This translates in the type of arrangement that they adopt in the bilayer. The unsaturated carbon tails, usually present in glycerophospholipids, have kinks that make them occupy a wider space, making the membrane less packed. On the contrary, sphingolipids carry saturated acyl chain, which makes them to arrange in a more packed way [5]. This behaviour induces an asymmetrical distribution of lipid species, which, *in vitro*, results in the formation of membrane phases with different degrees of order. The liquid disordered phase (L_d), involves a fluid state and it arises from the gathering of lipids carrying unsaturations on their chains. Opposite to this, the enrichment on sphingolipids with their saturated chains results in the formation of packed and low mobile fraction defined as solid-like phase (S_o) [5]. Cholesterol, being non-polar, needs to be shielded by the polar heads of phospholipids in order stay away from the aqueous media [18]. This results in a distribution where the long, saturated carbon chains of sphingolipids and certain phospholipids arrange together with cholesterol forming highly ordered phases that retain high lateral mobility known as liquid ordered phases (L_o) [5,11,19].

Although well characterized, this type of arrangement is still a matter of debate in physiological systems [11]. In cells, the existence of L_o domains, known as lipid rafts, that serve as platforms for spatial segregation of proteins with signalling function has long been debated [19]. The existence of rafts could not be proven *in vivo*, which has led to hypothesize that, if existing, these domains are 10-200nm in size (which makes them hard to image) and their dynamics are very fast [11,19–21]

Altogether, this behaviour defines the packing of a membrane and its viscosity. For the PM, the order is usually high, defined by notorious amounts of saturated phospholipids and cholesterol [22] and with variable viscosities depending on the changes in lipid composition of the different domains [16,23].

The distribution of different types of phospholipids within the two leaflets of the PM, known as asymmetry, results in a differential in charges between both sides. As mentioned before, the inner leaflet is usually enriched negatively charged phospholipids, specially PS and PIPs. This distribution results in the creation of

Chapter 1 – INTRODUCTION

a binding surface for positively charged proteins (discussed in the next section) and cations [24]. On their side, changes in the amount of negative charges on PIPs through phosphorylation and dephosphorylation modulates the interaction of these lipids with different types of proteins [22,25]. This is the case of phosphatidylinositol-3,4,5-triphosphate (PIP3), which has been described to tag Rac1 to determinate areas of the PM [26]; or phosphatidylinositol-4,5-biphosphate (PIP2), involved in sequestering TORC2 in yeast to PM folds where it remains inactive [27].

Other than electrical properties, the PM is also defined by its mechanical properties. As any solid material, the PM presents an energy cost to be deformed. This is known as the bending stiffness and it is defined by the Young's modulus. This energy depends on the type of lipids that compose the PM. Notably, bigger amounts of cholesterol and saturated lipids increase the bending stiffness, while the presence of lipids with unsaturations decreases it. In terms of elasticity (how stiff is the PM under tension), this structure is considered highly inextensible, which is characterised by a small stretch modulus [23,28]. This has an important impact on cell function, because it means that an important reservoir of membrane has to be provided in order to perform processes such as migration, division or phagocytosis. The nature of this membrane stock will be discussed more in detail in the next section, but it is important to highlight that it comes from PM folds of different sizes together with endomembrane reserves provided by other organelles.

The last mechanical characteristic is PM tension. This is defined by the energetic cost of stretching PM surface and it arises from the tight lipid packaging in order to avoid contact with the aqueous media. Although in synthetic lipid bilayers tension can be measured by simply pulling a tube from a vesicle and then measuring the in-plane tension of the bilayer, in the PM this simplification cannot be done. In the cell, PM tension is considered the measurement of the bilayer tension itself plus the influence of the underlying cortex and the molecules crosslinking these two structures [23,29]. In the last years, PM tension has risen a lot of interest due to its influence in controlling important cellular processes, such as endo and exocytosis, migration and cell shape. However, it is still not clear how PM tension propagates within the ensemble of the PM envelope [30,31]. Although the traditional view stated that tension propagated fast across PM in order to modulate cell response, a recent study by Shi et al. [32] has challenged this hypothesis. In their work, Shi and colleagues observed that tension propagated quickly when they were pulling two tethers separated 5-15 μ m away inside a bleb,

however, when those tethers were pulled on PM attached to the cortex, tension decayed fast and could not propagate further than 5 μ m.

Integration of this two opposite points of view arises from the fact that components interacting with the bilayer introduce obstacles in tension propagation. On one hand, the cytoskeleton acts as a network withstanding and dispersing tension modifications. However, the presence of transmembrane proteins and the presence of PM-cortex linkers hinders this propagation. Moreover, the curvature arising from protein insertion in the bilayer can recruit curvature-sensing proteins which will further impact the propagation (see section 1.4. Mechanotransduction events triggered at the PM) [30].

1.1.2. PM topography

Lipid composition can not only produce chemically differentiated domains, but also structurally different ones. As mentioned before, the different phospholipids in membranes have different shapes, which confers different sign of curvature to the PM [6,22]. The nanotopography generated by these changes in composition becomes of high importance when we talk about protein recruitment, as a lot of proteins are able to sense a number of bilayer shape deformations. Among these proteins, probably, the best known are the BAR superfamily of proteins, which possess a positively charged banana-shaped BAR domain that is able to sense the curved bilayer and shape it by scaffolding or aggregation [33].

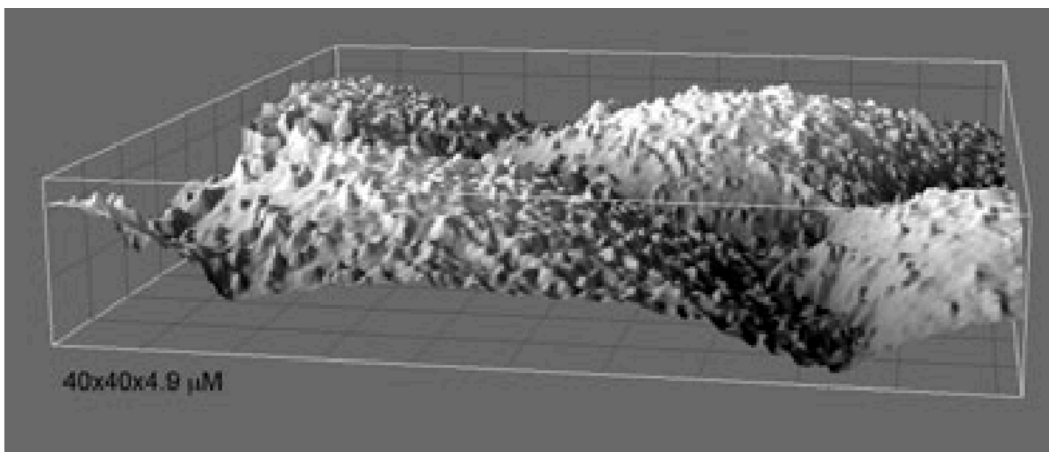


Figure 2: Scanning-ion conductance microscopy image of cell surface (extracted from [34]). Although in fluorescence microscopy cell surface appears to be flat, higher resolution techniques reveal the abundance of topography.

Chapter 1 – INTRODUCTION

A second type of change in PM topography is a lipid packing defect. This type of arrangement emerges when lipids with small head sizes and tails with different properties (length and level of saturation) induce bending of the membrane. This is the case of PE or PA, that introduce positive PM bending, while, as mentioned before, the presence of PI generates the opposite type of curvature [6]. The presence of these lipid species increases the degree in which PM hydrophobic side is exposed to water, causing an imperfection in the bilayer surface that can be sensed by proteins containing certain types of motifs. The best known example of this mechanisms is represented by proteins containing an amphipathic lipid-packing sensor motif (ALPS), which can even show specificity for certain types of lipids forming the defect [6,22,35]. Other examples include simply the presence of amphipathic α -helices that can be inserted in deformations created in the bilayer by those defects. For instance, this is the case of CCT α , one of the enzymes in charge of synthesising PC. This protein has been shown to display sensitivity to the lack of PC in membranes by using its amphipathic helix to scan for lipid packing defects appearing when this lipid is absent [36]. CCT α becomes active when bound to the membrane, so, although this mechanism has only been proven *in vitro*, it could represent a way of regulating lipid synthesis in function of PM topographical properties.

It is also possible that the gathering of transmembrane proteins with a conical shape results in membrane bending, which has been proposed to be acting as a sorting process to support endocytosis [37].

Protein crowding can also result in bending membranes. A high coverage of the membrane by proteins, especially those containing long intrinsically disordered regions, would exert a pressure that would eventually provoke the bending of its surface [38]. Although this process does not involve solely the PM, it is equally important to mention. In a physiological system, such it is the cell, the PM cannot be conceived by exclusively the lipids and proteins contained within the two leaflets that compose it. Peripheral proteins, which constantly interact with the cytosolic face of the membrane, also need to be taken into account. An example of this mechanism is also represented by BAR proteins, that, when oligomerising on a membrane template, impose their preferred curvature [2].

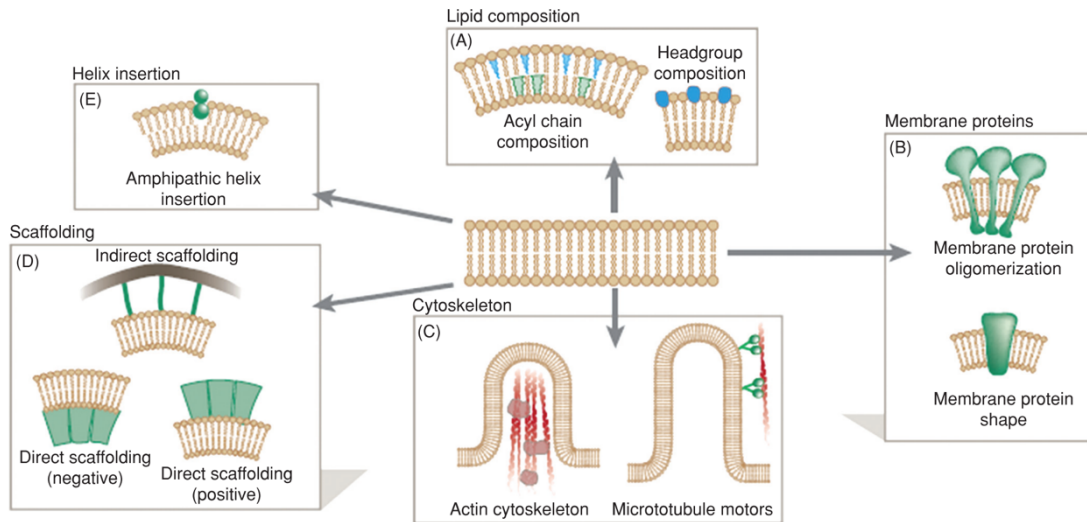


Figure 3: Mechanisms of topography generation at the PM (extracted from [39]). Topography can emerge by (A) changes in lipid composition; (B) insertion of transmembrane proteins or clustering of those; (C) evaginating or invaginating the PM by the pulling or pushing forces generated by the cytoskeleton; (D) protein crowding and scaffolding effects, and (E) amphipathic helix insertion.

Micron-sized architecture also exist at the PM. Nevertheless, given the inextensibility of this structure and the fact that it is under hydrostatic pressure exerted by the cytosol, imposes the need for a machinery to overcome this force and maintain this microtopography [31,34]. In this context, the tension needed for this structures to be maintained comes from actin and myosin together applying forces to the PM, which results in both keeping the fold's structure and prompting their fast rearrangement when required [40,41].

Additionally, other modulators can assist in overcoming this tension. For example, curvature-sensing BAR proteins can act as scaffolds lowering the tension and maintaining the curvature [38]. Further, it has been recently shown that also the glycocalyx plays a role in maintaining PM microtopography, as demonstrated in this study, where, by changing the amount of molecules present in the glycocalyx, authors could influence different shapes of PM folds and protrusions [9].

The shape and architecture of the cytoskeleton that lies underneath these structures allows for categorization of their different natures. According to this, we can separate them into structures filled with bundled actin filaments, structures enriched in branched actin and, finally, those that lack it.

Within the first category, we have filopodia, thin long protrusions filled with parallel bundles of actin filaments. Filopodia perform a variety of roles, being the most prominent among them migration, but also adhesion between cells or

Chapter 1 – INTRODUCTION

aiding phagocytic cup formation in macrophages. The formation of these structures has not been totally elucidated yet; however, a model mechanism would comprise the pushing force produced by Formins nucleation of actin filaments together with BAR proteins that would help in the outward bending of the PM [42,43]. Microspikes also belong to this group of micron-scaled PM structures. They could be described as a type of filopodia, as these are also thin tubular structures that protrude outside the PM. The difference is found in the fact that those never reach further than the cell perimeter, by opposition to filopodia, which are often used to “explore” and probe the substrate for migration, outside the leading edge of the cell.

Both structures originate in lamellipodia. Lamellipodia are thin and flat motile protrusions that originate at the leading edge of a cell and that are parallel to the substrate. Within the ~1-5 μ m width of cytoplasm that they contain, a lot of actin branches, polymerized by the actin-related protein-2/3 (ARP2/3) complex, are constantly formed, pushing the front of the cell, and making the membrane to protrude. Their main role is to establish adhesions to make migration possible, but they can also bend upwards, forming ruffles, which are rich in branched actin and are involved in phagocytosis [44]. Additionally, there is also the existence of smaller folds called wrinkles, which depend on an actin scaffold and which function is to buffer small changes in membrane tension [45].

In the category of membrane structures that are not supported by an actin scaffold, we find Blebs. They form when the PM detaches from the underlying actin cortex which keeps it under tension, and can freely bend outwards into a balloon as a result of the hydrostatic pressure exerted by the cytoplasm. At this moment, they still keep a thin layer of actin of 10-20nm, which does not provide support to the structure and that will thicken later, during the retraction phase [46,47]. Traditionally, blebs have been associated with dying cells, but it is now known that they actually fulfil very important roles as regulating cell membrane and cortical tensions [48], drive ameboid migration [49,50] or even participate in the process of lumen formation in capillaries [51].

Vacuole-like Dilations (VLDs) share with blebs that they are also depleted from actin. However, VLDs form on the interface between the PM and the substrate and they are the result of the confinement of water expelled from cells against a non-porous substrate as a result of an osmotic shock. Yet, and more related to physiological scenarios, VLDs can also form due to water flows emerging from compression of poroelastic substrates in which cells are laying, as demonstrated in [52]. Independently of the mechanism that lead to their formation, they tend

to form in areas where the actin meshwork is weaker between adhesion sites within the cell [53].

Other topography arising from the PM include different types of endocytic pits, which shape can be maintained or not due to actin, exocytic buds and caveolae, flask-shaped invaginations formed by assembly of caveolins in cholesterol rich domains [54,55].

1.1.3. PM reservoir

It is important to highlight the role of some of these folds as reservoirs to provide extra membrane when the cell needs to adapt its shape, move or divide. As mentioned before, the PM is poorly inextensible, reaching only a 3-5% extension before breakage [56]. This creates the need for a buffer to unfold and prevent PM rupture under increases in tension.

The actin machinery supporting large folds, such as ruffles, wrinkles or filopodia, can flatten those structures upon requirement [52,53].

Additionally to those, the PM reservoir contained in endomembranes represents another source to respond to increasing or decreasing demand in cell area. Under tension increases, exocytosis is activated thereby supplying extra lipids to the membrane [55,57,58]. Oppositely, when there is a drop of tension, endocytosis gets activated, primarily through the clathrin-independent carries and GPI-anchored proteins enriched early endosomal compartments (CLIC-GEEC) pathway, which has been recently proven to show very specific regulation upon PM tension changes [59,60].

Nonetheless, folds devoid of actin also constitute an important and fast mechanism to protect the cell when it is exposed to stretch. This is the case of caveolae, which have been long studied for their mechanoprotective effects upon sudden increases in membrane tension [61–63]. However, the quantity of buffer that they can provide is small in comparison to that furnished by bigger membrane folds, although this amount can vary in function of the cell type [1,53]. Overall, this stock of membrane depends on the actin cytoskeleton to be rearranged in response to changes in PM tension and topography. During the next chapter, the function and structure of the actin supportive scaffold will be addressed more in detail to try to understand how PM and cytoskeleton are interconnected and communicate to each other, allowing for cell adaptation to the changing environment.

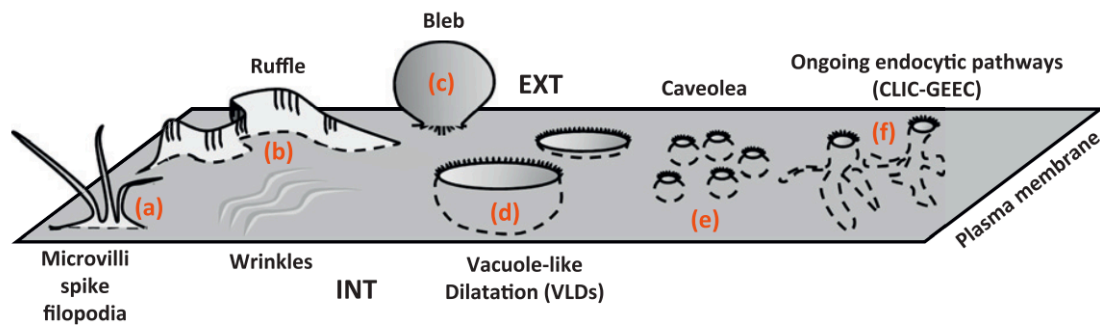


Figure 4: Types of PM topography (extracted from [53]). The cartoon describes the different architectures providing membrane reservoir to regulate PM surface and tension.

1.1. ACTIN-THE SUPPORTIVE SCAFFOLD UNDER THE PM

In order to maintain their shape, divide, move and mechanically interact with their environment and neighbours, cells need a scaffold that can support their volume. This structure is the cytoskeleton, a supportive assemblage composed by filaments that are dynamically rearranged in response to cell needs. The cytoskeleton is composed by intermediate filaments, microtubules, and actin filaments. During this introduction, the focus will be set in the last group, the actin filaments. They are the main component of the meshwork that stands below the PM., providing the support and the force to remodel this structure. Other than actin, the cortex is also rich in anchor proteins, such as spectrin and septins, that bridge the PM and the actin polymers together [64,65].

The actin cytoskeleton minimal unit are actin monomers (G-actin), globular polypeptides containing a pocket for ATP binding that form long flexible filaments (F-actin). The assembly of these filaments is polar, which means that the monomers always dispose in the same direction, head-to-tail, producing a plus or barbed end and a minus or pointed end. Although G-actin is bound to either ATP or ADP, ATP hydrolysis is not needed for filament elongation. However, ATP-bound actin is more readily to polymerize. When these monomers bind together, ATP gets hydrolysed and ADP-actin becomes more easily detached from the filament that the one in association with ATP. Because of this fact, the plus end of the filament, where ATP-actin monomers are being constantly added grows faster; whereas the minus end, where the monomers are bound to ADP elongates slower. This type of behaviour, representing the way in which actin filaments are formed, can only be observed *in vitro*, and it has the name of treadmilling [4,66]. It is also important to note that, as a consequence of

the way in which elongation is done, pushing forces of actin filaments are always exerted in the direction of the plus side [67].

Nevertheless, polymerization in living systems is tightly directed by regulatory molecules that control nucleation, elongation, and disassembly of filaments. In a cell, free actin monomers are bound to thymosin, an actin sequestering protein which role is to prevent polymerization. To achieve it, monomers have to be released from thymosin by profilin, a protein that competes for their binding and promotes addition to a filament but impairs their self-association. This last function of profilin may seem contradictory, but in fact, it is of high relevance in order to avoid unregulated spontaneous actin polymerization within the cell. Indeed, the activity of profilin is carefully regulated by phosphorylation and binding to phosphoinositides, which targets actin polymerization to the inner side of the PM [4].

In order to start a new filament, actin monomers have to associate in a trimeric complex. This process is called nucleation of a new filament and it is energetically very unfavourable. This means that the initiation of polymerization has to be achieved by other means, which involves a subset of proteins that precisely coordinate the process: formins, ARP2/3 complex and the tandem-monomer-binding (TMB) nucleators [68].

Formins polymerize long filaments that arrange in parallel arrays with the help of bundling proteins. They can nucleate the filament, but the way in which this is done is still unknown, although it has been shown that it involves actin monomer binding by their formin homology 2 (FH2) domain [66]. The details of the way in which they perform elongation are also currently under debate, but the broad description of the process involves binding of the FH2 domain to the plus end of a filament, where it fosters actin assembly. The supply of actin monomers for this process involves the formin homology 1 (FH1) domain, which binds several profilin-bound actin monomers and keeps them in close proximity of the FH2 domain [69]. The fact that the FH2 domain is associated with the barbed end avoids the attachment of capping proteins, which would stop elongation.

Crystallographic studies show that formins are auto-inhibited in their resting state, revealing that FH1 domain interacts with the FH2 impairing its activity. To release this blocking, FH1 domain has to interact with Rho GTPases. This interaction also influences the protein location within the cell, although some formins already contain lipid modifications that directly tether them to the PM [70].

Chapter 1 – INTRODUCTION

Elongation by formins needs the support of bundling proteins that proportion stability to filaments. Provided that when those exceed 700 nm length they tend to collapse due to the force generated in the elongation process, association with bundling proteins creating fibres makes them able to stand a bigger load [67].

The ARP2/3 complex represents the other side of actin polymerization. It is composed by 7 subunits, two of them sharing similarities with actin monomers, ARP2 and ARP3. Its function is that of establishing an actin meshwork by synthesizing new actin filaments from pre-existing ones. The new-born filaments grow with an angle of $\sim 70^\circ$ while the ARP2/3 stays bound to the mother filament making a link between both and forming a web [69,71]. It has not been elucidated yet how the event of nucleation is achieved, but the current view supports the idea that ARP2 and ARP3 act together with one actin monomer to establish the trimeric complex needed to trigger the formation of a filament. However, in the crystallographic structure of the complex, these two proteins are located distanced from each other, which suggest that the complex has to undergo a conformational change in order to get active.

But in order to overcome this separation and achieve nucleation, ARP2/3 cannot act alone. ATP hydrolysis and association to nucleating promoting factors (NPFs) are necessary. NPFs are a group of molecules that are able to recruit the actin monomers that will form the template for nucleation together with the ARP2 and ARP3 subunits. There are two main groups of NPFs: type I and type II. Type I NPFs are characterised for the possession of a verprolin homology (also called WH2 for WASP homology), connecting region and acidic (VCA) domain that has the ability to bind actin moieties throughout the VC motif and to interact with the ARP2/3 complex by the CA motifs. This conformation makes possible the formation of the nucleation complex [69,72]. In mammals, this group is composed by the WASP and WAVE family of proteins (discussed more extensively in the 1.1.2 section: PM regulation of actin polymerization events). Type II NPFs include cortactin in mammals, which does not contain a verprolin homology domain, but instead a central tandem repeat that allows binding to F-actin. This interaction, although sufficient to activate the ARP2/3 complex is far less effective in vitro than that of NPFs type I [72].

TBM nucleators constitute a series of different proteins that contain WH2 domains in a variable number. These domains, as previously mentioned, are able to bind actin monomers and to form a complex that allows the nucleation of a filament. All TMBs can exclusively polymerize filamentous actin, except the junction-mediating regulatory (JMY) protein, which possess both filament

and branched actin polymerization activity. Although the last one is mediated in partnership with the ARP2/3 complex, by binding to it through its CA motif, and therefore making JMY to function as an NPF [68].

1.1.1. Cortical actin

Underlying the PM stands a hundred nanometre sheet of actin arranged as a meshwork known as the cell cortex. Its main functions are to provide support, stiffness, and movement to the bilayer and, overall, governing full cell shape. The cortex is not uniform, neither in composition, nor in the distribution of its components. Actin is the main molecule found at the cortex, but a lot of actin binding proteins can be found together with it. And, importantly, a good amount of non-muscle myosin II, which accomplishes the task of generating forces over the actin filaments providing contractility to the mesh [73].

Studies using high resolution imaging techniques have shown that the cortex does not have the same type of network arrangement in all cell types and structures [74,75]. Typically, round cells display an isotropic cortex, characterized by a loosen actin meshwork with scarce anchorage points. In contrast, the cortex of spread cells is characterized by an anisotropic alignment of the actin bundles. This is due to the bigger number in anchorage points, which allows myosin II to exert bigger forces and therefore impose the alignment [73,76].

The composition of the cortex includes the main molecules in charge of actin polymerization, ARP2/3 and formins [77], which have a different impact in polymerization rate depending on the cell type. But other types of proteins involved in regulating actin polymerization are present too, such as capping proteins, sequestering proteins and different crosslinking proteins. Myosin motors are available too, as previously mentioned. In general, myosin II isoforms are predominant, but other types as, for instance, myosin I have also been found colocalizing there.

The ezrin, radixin and moesin (ERM) family of proteins are in charge of anchoring the cortex to the PM. They do so through their actin binding domain and their Four-point-one ERM (FERM) domain, which is able to interact with PIP2 in the PM and with some transmembrane proteins. Due to this linker function, they have a crucial role in regulating cortex mechanical properties [78,79], as shown in this study where moesin was demonstrated to play a crucial

Chapter 1 – INTRODUCTION

role in regulating cortex stiffening to correctly perform mitosis in S2 *D. melanogaster* cells [80].

Overall, this array of proteins constitutes a layer of less than 200 nm thickness, with a pore size of 50-200 nm (depending on whether we look at it from the PM side or the cytoplasmic side) with a given set of mechanical properties. Myosin II motors apply forces that generate what is known as cortical tension or contractility, a parameter that is understood as the force per unit length exerted in a given area of the cortex. This parameter is intrinsically linked to PM tension, as the forces generated by those motors influence the tensional state of the lipid bilayer in an interplay that governs cell shape [31].

On top of myosin forces other components, such as the degree of crosslinking and rate of actin turnover, influence cortical tension. Regarding crosslinking, the number of attachment points influences the propagation of stresses generated by myosins: the more anchors, the more rigid the network will be, and therefore, less propagation. On the other hand, a fewer number of connections will prevent transmission of forces, limiting the tension on the cortex. Actin filaments turnover might have an impact too, as for tension to be kept, the edges of the filament where myosins are bound have to remain polymerized although the rest of the filament can suffer remodelling. The thickness of the cortex has been recently shown to regulate cortical tension too, as demonstrated in this study where knocking-down of several capping proteins and the formin DIAPH1 resulted in either an increase or a decrease in width of the cortex and a subsequent decrease in cortical tension, even though myosin II remained untouched [76].

The cortex is considered a viscoelastic material, which means that it behaves as an elastic solid at short time scales and like a viscous liquid at longer times. The flow of this viscous liquid within the cell generates friction against the components of the PM, the cytosol and the adhesion proteins that mediate interaction with other cells and the extracellular media (ECM), which in turn influences the contractility of this structure [73,81].

All these properties make the cortex a highly polymorphic structure involved in governing the main morphological arrangements in cells, but to fully understand the physiological consequences of the remodelling done by this structure it is indispensable to look at its direct crosstalk with the PM.

1.1.2. PM regulation of actin polymerization events

The cell cortex is in close relationship with the PM. Changes in lipid composition can orchestrate actin polymerization events and transmembrane proteins can modify the location of the anchor points where actin filaments are attached. But this interaction is bidirectional, and the cortex can modulate and compartmentalize the components of the PM in a feedback loop between both structures.

The main actors in directing the crosstalk between the PM and the cytoskeleton are PIPs. All of them come from the modification of PI by different kinases which create seven unique derivatives through phosphorylating the hydroxyl groups of the inositol head in the positions -3,-4 and -5 [82]. Among these family of PIPs, the most abundant is PIP₂, composing roughly 1% of the total lipids in the PM. Consequently, it has been targeted as the main lipid organizing polymerization events.

The high density of negative charges in these molecules can topographically orchestrate the recruitment of proteins, which are, often, the ones starting the process of actin nucleation. These proteins possess an assortment of lipid-interacting domains (PH, PX, FERM, FYVE and others) that allow the interplay between them and the different PIPs, notably, those that are phosphorylated in the -3 position. Some of them have preferential binding for PIP₂, as it is the case of the PH domain of the Phospholipase-C δ , but this does not happen for all PH domain-containing proteins. The specificity on PIPs binding does not depend strictly on a concrete domain, but rather on a combination of it together with electrostatic interactions between other domains of the protein and the PM [83]. Within the collection of players that interact with PIPs we find the Wiskott-Aldrich Syndrome protein (WASP) and WASP-family verprolin-homologous protein (WAVE) family of proteins. These two are NPFs that share very common architectures. Both have a VCA domain that allows for the trigger of filament nucleation through ARP2/3 binding, and both share a polybasic region that interacts with PIP₂, in the case of WASP, and PIP₃, in the case of WAVE. The binding to this PIPs mediates the location of the protein to the places where polymerization is needed. WASP was the first protein of this group in being identified, however, it is not widely expressed in animal tissues and it is restricted to hematopoietic cells. Another member of this group is the Neural-WASP (N-WASP), and although it was called like that because it is over-expressed in brain tissue, this protein is widely present in all cell types. In the

Chapter 1 – INTRODUCTION

case of N-WASP, upon contact of its polybasic region with PIP₂, a conformational change releases the interaction between this motif and the VCA region, allowing for the interaction with ARP2/3. Regarding WAVE, three homologs exist, WAVE1, WAVE2 and WAVE3. They are differentially expressed across tissues, being WAVE2 the most ubiquitous. WAVE proteins cannot act alone, they do it with other partners forming an heteropentameric complex known as the WAVE regulatory complex (WRC) that directly triggers ARP2/3-dependent actin polymerization [84,85].

As well as WASP and WAVE proteins, the mouse formins mDia1 and mDia2 have been shown to be dependent on PIP₂ clustering to mediate tethering to the PM, where they nucleate actin filaments [86,87]. Also, the ERM family of proteins modulates the attachment of the PM and the cortex through the interaction of their FERM domain with PIP₂, which, in turn, influences the mechanical properties these two structures [88].

There are also proteins that can interact with the whole molecule of PIP₂ (head and tails), as for instance, profilin or the severing proteins cofilin and gelsolin [89,90]. Indeed, all the spectrum of actin-binding proteins influencing polymerization and depolymerization can interact and are regulated by PIP₂, which confers this lipid opposite effects to influence this pathway. Interestingly, there is a correlation between the levels of PIP₂ in the cell and the amount of actin polymerized. In general, high levels of PIP₂ in the PM correlate with an increase in F-actin formation, whereas low levels of PIP₂ in the PM have been related to a decrease in the polymerization activity and a loosen attachment of the cortex to the PM [41,91]

On top of regulating PM recruitment of NPFs, capping, and severing, PIPs also influence the distribution of small GTPases and their GEFs and GAPs in this structure. Within this group, the Rho family of small GTPases, which regulate cytoskeletal dynamics, influence motility, and have a key role in maintaining cell shape; are known to relocate across cell membranes in a way highly influenced by PIP clustering. Rac1 is known to group in PM nanodomains where PIP₃ is enriched, associating to them through its polybasic C-terminal domain [92]. This areas with an increased amount of PIP₃ do not only recruit Rac1, but also WAVE2, which gets stimulated by the synergistic action of Rac1 and the BAR protein IRSp53, to start the nucleation of actin filaments together with ARP2/3 [26,84,93]. Another example is represented in the BAR-domain protein GRAF1. This protein is a GAP of the small G proteins Cdc42 and RhoA and it has also been shown to bind PIP₂ enriched domains where it acts modulating the activity

of this two GTPases [82,94]. Indeed, the influence of PIPs over GAPs is not only limited to its topographical distribution, but it can also be extended to the modification of the preferential binding of these molecules for their different substrates [95].

Also, the turnover of different PIP species at the PM allows a precise temporal and topographical distribution of the polymerization process. This turnover is catalysed by PIP kinases and phosphatases. For instance, PIP5K phosphorylates Phosphatidyl-inositol-4-phosphate at position -5 to produce phosphatidyl-inositol-4,5-biphosphate (PIP2) [83]. The location of this kinase is in turn influenced by Rac1 [96], which can also activate PLC, a phosphatase mediating PIP2 degradation [97]. This generates a dynamical interplay between the generation and degradation of PIP2 that ensures that only at a given spot within the PM actin polymerization would be achieved.

Transmembrane proteins location can also modulate actin underneath. Some of these proteins can directly bind actin, as it is the case of the EGF receptor. Whereas in other cases this link is indirect, through adaptor proteins, such as integrins [41].

Actin turnover can be induced by extracellular signals, generating a cascade that eventually remodels both the cortex and the PM. At this point, the need for coordination and signal processing at the PM-cytoskeleton interface emerges clearly. In order to properly transduce the inputs coming from the extracellular environment, a fine regulation involving the integration of PM composition and cytosolic molecular players that will lead to actin nucleation has to be executed.

1.2. MECHANOSENSING AND SIGNAL INTEGRATION AT THE PM

1.2.1. What is mechanosensing?

Not only chemical changes can induce signalling cascades. Mechanical inputs can too. It has long been shown that upon mechanical stimulation, signalling pathways can get activated with the subsequent reaction of the cell to the sensed stimulus. This process is what we know as mechanosensing and it is often accompanied by mechanotransduction, which would involve the further transmission of the signal to trigger cell response. To make both possible it becomes patent that the different structures within the cell need to be mechanically connected so the transmission of forces can be done. The scaffold making this connection is, of course, the cytoskeleton and it is through the

Chapter 1 – INTRODUCTION

different types of filaments that compose it that the mechanical inputs can travel. These stimuli can come from the external media, being this the ECM and/or the neighbouring cells; but they can also be generated by the contraction of the aforementioned myosin II motors pulling on actin filaments [98].

Classically, the best studied mechanosensing structures have been cell adhesion points. Starting with focal adhesions, these points represent the locations where integrins mediate the binding between the ECM and the actin cytoskeleton. But further that that, focal adhesions are composed by a broad spectrum of proteins, which include protein kinases and actin binding proteins, some of them mechanically sensitive to pulling forces, as it is the case of talin [99,100]. This makes the structure sensitive to forces, either coming from the ECM to the cytoskeleton, or the other way around, which has an impact on their growth and maturation (substitution of some protein components by others). Altogether, focal adhesions constitute an integrative platform that can be used by the cell to probe the environment and sense its mechanical properties.

But not only focal adhesions sense the physical inputs from the environment. In recent year, the role of the PM as a mechanosensitive structure has gained more attention. The way in which this structure can integrate mechanical stimuli and transform them into biochemical signalling will be the focus of the next section.

1.2.2. The PM as a mechanosensitive structure

As discussed in the first chapter, the PM constitutes the physical boundary than insulates the intracellular media from the exterior and, as so, its function is also to receive and integrate all the stimuli coming from the outside and transmit them intracellularly, where those inputs will turn into changes in cell behaviour. Given the huge extension that the PM represents with respect to other structures in the cell, it must be considered as highly relevant in transmitting all these signals.

In the next sections, the type of stimuli that alter PM state (tensional and or topographical) and the tools that can be used in the lab to reproduce them will be addressed. Further, the knowledge existing around molecular sensors recognising those changes in PM state and the mechanotransduction cascades associated to them will also be subject of this introduction in the last section.

1.2.3. Physical stimuli altering PM state in physiological conditions

The traditional biological view has always focused on the biochemical signalling perspective. This englobes mechanisms such as a ligand binding to its receptor or a lipidic messengers, soluble across the PM barrier, diffusing and binding to transcription factors in the nucleus. However, physical stimuli can trigger the same type of response too. And throughout topographical rearrangements of the PM, changes in protein structure, phase separation of lipid types or the recruitment of molecular players; end up triggering changes in the behavioural profile of a cell [101].

In this line, in the background of a physiological context, the PM can be exposed to several different types of physical stimuli depending on the external mechanical force received [1]:

i. Tensile Stresses

This category englobes stimuli exerting pulling forces on the membrane, which might be also associated with an increase in PM tension if the force applied is great enough [102]. Numerous cell types in our body constantly experience such input: muscle cells [103], all type of epithelia [101,104] and even fibroblasts embedded in connective tissue [105] are submitted to stretches, either cyclically or with no periodicity. On the other hand, circulating cells are exposed to changes in osmolarity that can trigger swelling [106]. Tensile stresses can also be applied locally, in the form of a receptor bound to its ligand, as it is the case of f T-cell receptor activation, which has been shown to activate upon binding and force pulling on it [107].

ii. Compressive Stresses

In tissues, cells are confined between the ECM and the neighbouring cells. If tissue homeostasis is broken and proliferation gets out of control, as it is the case of a tumorigenic environment, cells might experience compression [108]. Another example comes for hypertonicity of the media, which turns active a set of mechanisms like changes in the expression profile of different ion channels to adapt to the new environment [109]. Also, the release of a tensile stimulus, such as it is the case of cyclic stretches experienced by beating cells, represents another type of compression.

iii. Shear flows

For endothelial and circulating cells, this is probably the most important type of physical stimulus that they can experience. Shear flow is caused by the movement of a fluid through a vessel, which applies a stress over the PM of cells composing such structure and the ones navigating through it [110]. Changes in this force can be sensed by cells, although it is still not clear how this is achieved [111]. However, we know some examples as, for instance, the primary cilia of endothelial cells in zebrafish, which have been shown to move accordingly to the strength of the vascular flow and transmitting this physical information into a cascade involved in angiogenesis in the embryo [112]; or the determination of the arterial versus de venous tree in the yolk sac in chicken embryos depending on blood flow rate [113].

iv. Topography

In their normal milieu, cells are constrained by the ECM and other cells around them. Altogether, this creates a landscape full of irregularities, integrated by fibres disposed aligned or misaligned, where the spatial distribution of ligands and its abundance can greatly vary from different tissues inducing different types of signalling [114]. Also, cells have to deform to adapt to this environment, which entails PM remodelling and dynamic accommodation to the new shapes [115].

1.2.4. Tools to study PM mechanosensing and molecular responses associated to them

Given the high complexity of all these phenomena, researchers have aimed at simplifying the way in which those can be study in the laboratory by engineering different types of systems and experimental set-ups that allow for the manipulation of one or several of these parameters in a controlled way.

Tensile stresses can be emulated by stretching cells, both by seeding them on top of flexible membranes and by exposing them to a medium where the salts concentration has been lowered down (hypo-osmotic) in comparison with physiological (iso-osmotic) medium. In the case of the osmotic shock, the extension in PM has been shown to be small [52], whereas by the use of stretchable membranes the extension can be biaxially or uniaxially and managed to be finely tuned and adapted to mimic both physiological conditions and pathological ones [104].

In both cases the PM responds in the first place by unfolding different types of structures acting as membrane supply, among them, caveolae, which deserve to be highlighted due to their protective role in preventing membrane breakage [62,63]. When these folds have extended, if the stimulus continues, other mechanisms are triggered to supply extra lipids in order to prevent rupture. One of them is exocytosis, which activation has been related to an increase in PM tension [55]. Lipid biosynthesis has also been shown to switch on upon stretch exposure, which would represent an ultimate source of material for the PM [116].

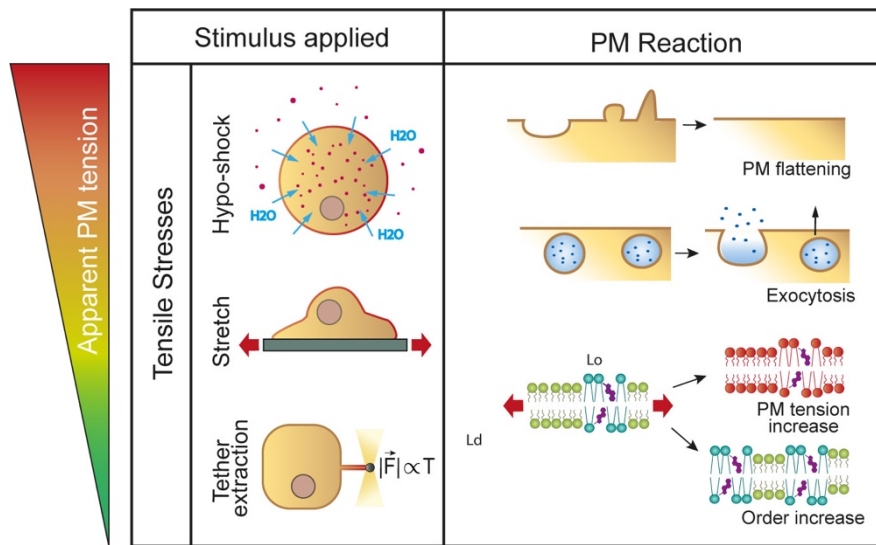


Figure 5: Tensile stresses applied to PM and its triggered response (adapted from [1]). Experimentally, tensile stresses can be applied by hypotonic shocks, cell stretching and tether pulling. As a response, PM folds flatten and exocytosis increases. Once the reservoir has been depleted, PM tension and order increase.

Last, when the cell has unfolded all of its membrane reservoirs, PM tension increases [1]. However, the resting tension of different cell types can vary a lot, which influences the magnitude of stretch or osmotic force that has to be applied in order to observe a raise in tension. Nonetheless, when this happens, the PM experiences changes at the molecular level too. It has been previously reported that increases in membrane tension in synthetic systems can lead to a dynamical binding of ALPS-containing proteins due to the appearance of lipid packing defects in the bilayer [117]. In living systems, endothelial cells submitted to stretch displayed an increase in order and a decrease in fluidity on their PMs [1]. Tensile stresses can be applied too by pulling tethers through atomic force microscopy (AFM) or magnetic or optical tweezers [31,118]. However, the increase in tension applied by tether pulling has been recently shown to be local and to not propagate across the PM due to cytoskeleton effects [32]. AFM, on its

Chapter 1 – INTRODUCTION

side, can also be used to apply an increase in tension by indentation, locally pressing a cell [119].

Compression can be accomplished by the release of stretch (which will be referred as stretch-release stimulus in the results section) or by the exposure to a hyper-osmotic medium. In both cases the PM folds and generates highly curved structures at the micron and submicron scales such as caveolae [61], nanometric tubes, or buds [52]. These last two have also been shown to appear in synthetic lipid bilayers under the same type of compressive stimulus [120]. Under hyper-osmotic treatment of cells seeded on non-permeable substrates or compression of cells on a porous matrix, VLDs form [52]. Last, endocytosis also becomes active under compression, leading to material removal from the PM to recover its resting tension [56,59,121]. The decrease in tension, if achieved, can activate other type of responses such as the recruitment of determinate proteins [122]. At the molecular level, PM compression have broad effects too. For instance, the formation of lipid packing defects in curved folds upon application of compression was shown in giant unilamellar vesicles (GUVs), which could in turn facilitate the insertion of proteins containing ALPS motifs [123]. Most of these studies have been performed in synthetic systems, so it is still not clear how this can relate to living systems. However, major advances in the field are being done, such as this recent work in which Colom et al. synthesised a probe able to sense PM tension, and therefore the level of lipid packing, through the changing in emission lifetime [124]. Indeed, by using this tool it was shown that a decrease in PM drove PIP2 clustering in small curved domains where TORC2 was sequestered and inactivated in yeast [27].

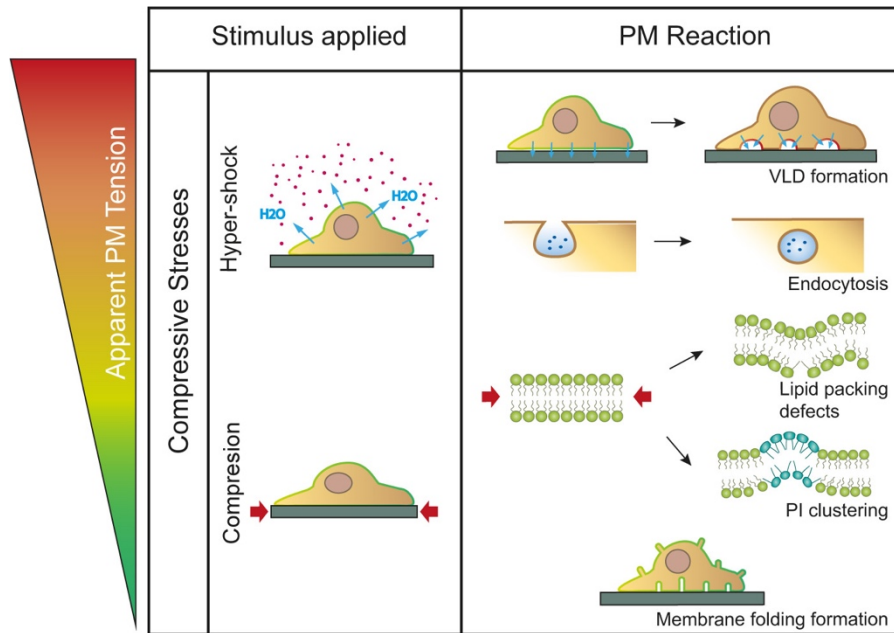


Figure 6: Compressive stresses applied to the PM and their associated responses (adapted from [1]). Compression can be achieved through hyper-osmotic shocks and stretch-release stimulus. Their associated PM responses englobe different type of fold formation (VLDs, tubes, buds), endocytosis increase, emergence of lipid packing defects associated to highly curved areas and PI clustering.

Shear flow is usually applied through microfluidic systems, where cells are cultured in chambers by which a fluid is constantly circulating in a given direction [125,126]. Effects of this kind of stimulus are difficult to dissect, because shear flows exert both hydrostatic pressure and a tensile stress over the PM. Nonetheless, decreases in membrane ordered domains have been consistently identified [1].

The shape of the substrate that is contact with the PM can also be tuned to achieve different effects on it. For instance, seeding cells on top of nanocones or nanoneedles to force them to adapt to this topography [1]. This type of procedures would involve a temporary increase in PM tension at the areas in contact with the structures, which can unleash a variety of responses. One is the triggering of endocytosis in the highly curved areas where membrane has bent to adapt to the pillar [127]. Other works have identified BAR proteins and actin recruitment to this highly curved areas [115].

Other types of topography tuning include protein patterns that determine the shape and size of the areas to which cells can attach [128]. The use of those has led to striking results, such as determining mesenchymal stem cells fate through membrane reorganization and signalling depending on pattern shape [129].

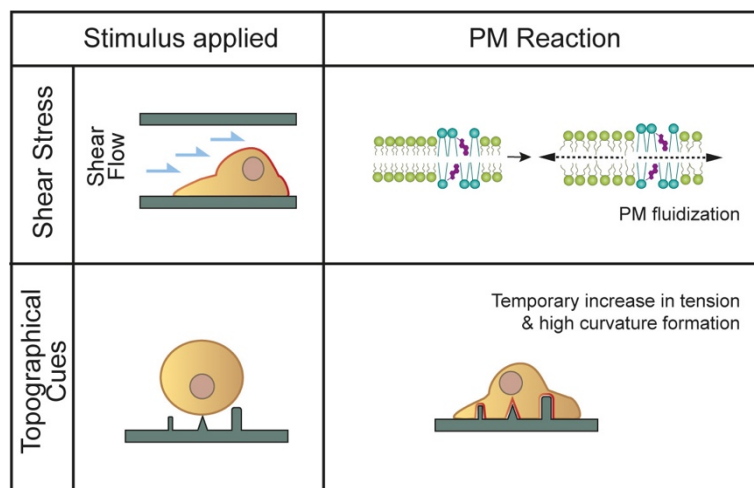


Figure 7: Shear stress and topographical cues applied to the PM and their associated responses (adapted from [1]). Shear stress application results in increased PM fluidity. The interaction with topographical cues involves PM adaptation to substrate architecture, likely triggering a temporary increase in PM tension which can lead to other responses, like endocytosis.

Altogether, these methods share one important characteristic: allowing PM controlled remodelling to be able to study molecular responses to the applied physical stimulus in a simplified way. However, the nature of the signalling cascades triggered and the mechanosensing mechanism underlying their activation can vary a lot from one situation to another.

1.3. MECHANOSENSING EVENTS TRIGGERED AT THE PM

1.3.1. Protein conformational changes

Within this category, the best-known example is the family of mechanically gated channels (MGCs). These are integral proteins embedded in the PM which respond to raises in tension involving PM expansion by opening and allowing the pass of ions. Eukaryotic channels include Transient Receptor Potential (TRP) channels, Piezo channels and Potassium channels. TRP channels are non-selective cation channels and they can be activated by different types of physical stimuli, such as temperature and voltage. Potassium channels allow the pass of K^+ ions lowering the PM potential and thus, helping in balancing the effects produced by other types of MGCs. Finally, Piezo channels are cationic channels involved in a variety of responses from sensing the rigidity of the environment to touch [130,131].

GPCRs also undergo conformational changes when exposed to physical stimuli. In this case, shear flow, which has been related to induce fluidization of the PM,

appear to have an effect in these transmembrane receptors, increasing the mobility of their subunits and facilitating the exchange of GDP by GTP [1]. An example of this is the recent work developed by Xu et al. in which they show the activation of GPR8 (a type o GPCR) when cells are submitted to flows parallel to their surface [132].

1.3.2. Protein relocation

Increases in PM tension lead to unfolding of membrane reservoirs. Among them, caveolae are one of the best studied. Flattening of caveolae has a direct mechanoprotective role, as it avoids sudden increases in tension which could cause PM rupture [62,63], but also an indirect role, as buffering PM tension increase could prevent the activation of MGC [133]. The disassemble of caveolae components occurs in a passive way, depending only in physical forces applied to the structure. This involves the release of Caveolins and Cavins (their main protein components) into the cytoplasm, which leads to the activation of biochemical cascades [61,134]. A beautiful example of this mechanism is this recent study by Torrino et al. where they observe the translocation of the EHD2 ATPase from caveolae to the nucleus upon mechanical stress [135].

Additionally to caveolae, other types of membrane folds can flatten upon tensile stress application. For instance, in yeast, unfolding of invaginations called eisosomes led to the relocation of Slm1/2 proteins, which subsequently bind to TORC2, mediating its activation. TORC2, in turn, modulates sphingolipids synthesis, providing a mechanosensory pathway where PM stresses transduce into lipid synthesis [136]. A similar mechanism was also shown in mammalian cells, where increases in PM tension induced release of PLD2 from the membrane. This impacted the activity of mTORC2, which resulted in a decrease in actin polymerisation in an attempt to buffer the raise in tension [122].

BAR proteins can also unbind from membrane folds upon PM flattening and, if accompanied by an increase in PM tension, theoretical modelling predicts that oligomerisation of this proteins becomes unfavourable [137]. However, as BAR proteins possess curvature-sensing domains, the mechanosensing events triggered by their binding and unbinding from curved membranes will be addressed more thoroughly on the next point.

Chapter 1 – INTRODUCTION

1.3.3. Curvature sensing proteins

The formation of curved PM structures through mechanical stimulation involves the recognition of these templates by curvature sensitive proteins. The best known are BAR proteins, a superfamily of proteins characteristic for possessing a positively charged banana-shaped BAR domain which is able to bind to curved regions of the PM. This domain is enriched in positively charged amino acids that allow for electrostatic interactions with the negatively charged phospholipids of the membrane.

There are different types of BAR proteins depending on the topography of the BAR domain. Canonical BAR and N-BAR display domains that bind positively curved membranes. N-BARs usually possess additionally amphipathic helices in their N-terminal side which can help in the sensing. F-BARs also bind to positively curved membranes. However, the curvature displayed by their BAR domains is shallower than that of N-BARs and BARs. This makes them induce tubules with diameters between 60 and 100 nm, contrary to the 20-60 nm tubes created by N-BARs and classical BARs. F-BARs do not possess amphipathic helices, but they can display short loops that can be inserted in the PM like a wedge. Opposite to these groups, there is the category of I-BAR domain containing proteins, which characterises for binding to negatively curved membranes [138]. Some members of the I-BAR family do contain amphipathic helices that, as in the case of N-BARs, can help on the sensing.

At the molecular level, there are several mechanisms that contribute to the curvature sensing ability of these proteins. First, the presence of the curved BAR domain has been shown to have affinity for curved membranes, enriching the most when the curvature of the template matches the intrinsic curvature of the protein [139]. Second, the presence of negative charges in the PM can contribute both due to electrostatic interactions and because of curvature generation due to crowding of those lipid species. An example of this type of mechanism are PIPs, which carry a lot of negative charges, a fact that could lead to more intense electrostatic interactions between these lipids and the BAR domains [93]. Also, BARs that possess amphipathic motifs could scan the PM looking for lipid packing defects where to get inserted. The curved areas of the PM are often more prone to have this type of defects, which would confer them the curvature-sensing ability [35].

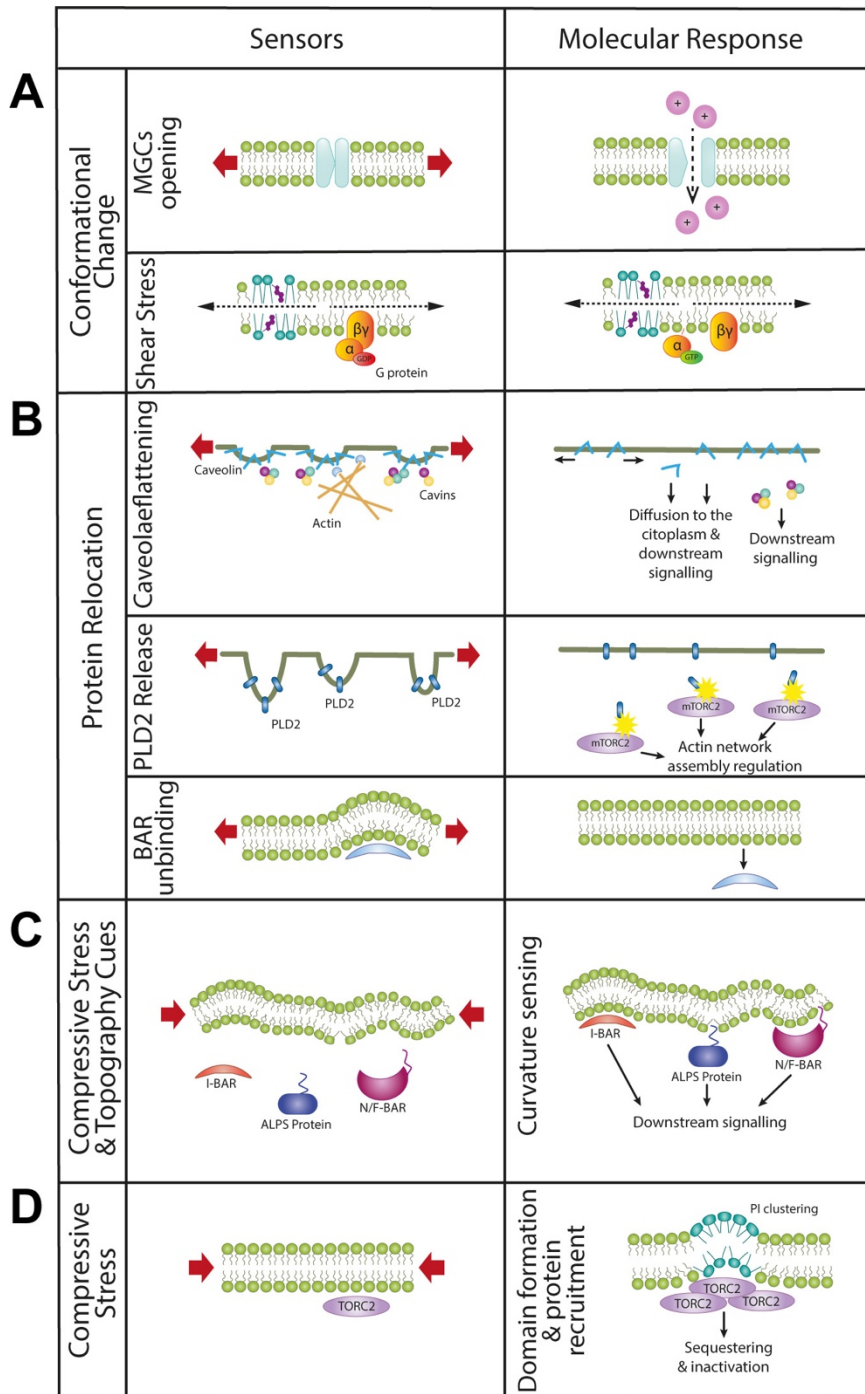


Figure 8: Mechanochemical events triggered at the PM. (A) MGC opening upon stretch. (B) Mechanically induced protein relocation events. (top) With increased PM tension, caveolae flatten and its protein components relocate, subsequently activating signalling pathways. (middle) Unfold of PM invaginations where PLD2 is sequestered provoke its released and activation of its partner mTORC2. (bottom) BAR proteins respond to fold flattening by unbinding from the PM and diffusing into the cytoplasm. (C) Compressive stresses and topographical cues result in the formation of different types of PM curvature that can be recognized by BAR proteins through their positively charged BAR domain. Proteins containing ALPS motifs can also sense curvature by inserting their amphipathic helix in curved PM areas, where lipid packing defects are more abundant. (D) Clustering of PIs due to compressive stresses leads to TORC2 sequestering and inhibition of its activity

Chapter 1 – INTRODUCTION

Whatever the nature of the sensing, to uncouple this mechanism from the ability of these proteins to generate curvature (scaffolding of membrane tubes) *in vivo* is still a pending issue on the field. Studies performed *in vitro* have shown that, when contained at low density in the bulk, BAR proteins are able to sense curvature. However, at higher concentrations, the activity of these proteins switches into scaffolding and they nucleate around the curved structure imposing their preferred curvature [2,140]

In cells, BAR domain containing proteins are found in membrane spots displaying curvature [33,141]. However, this does not necessarily involve sensing. An attempt to unveil the sensing mechanism in cells has been done by Zhao and colleagues [142] by seeding cells on top of nanocones of different diameters, which resulted in the recruitment of BAR proteins depending on the curvature of the topographically induced PM templates. An exciting possibility derived from this work would involve the response to PM topography alteration through curvature-sensing proteins. Recent studies have already addressed this question, as the one by Echarri et al. [143], in which they observed cells submitted to osmotic shocks react by phosphorylating the curvature-sensing F-BAR protein FBP17, which in turn acts on formin mDia1 to regulate actin dynamics.

In this line, previous work done in our lab has identified passive membrane deformations generated by stretch-release stimulation that depend on actin and ATP to be resorbed by the cell [52]. Such curved folds represent a putative target for curvature-sensing molecules to mediate the matching between the mechanically induced curvature and the subsequent active biochemical process that leads to cell recovery after the stimulus is ceased.

Chaper 2 - AIMS OF THE THESIS

2.1. GENERAL AIM

The aim of this project is to unveil the molecular mechanisms by which cells detect and respond to mechanically induced deformations in their PM upon the application of stretch-release stimulus.

2.2. SPECIFIC AIMS

This general aim will be divided into following specific objectives:

1. To analyse the ultrastructure of the PM folds generated when cells are submitted to stretch-release stimulation:
 - a. To unveil the sign of the curvature of such structures.
 - b. To analyse the size and shape of such structures.
2. To investigate the molecular mechanism driving PM homeostasis recovery after stretch:
 - a. To understand the role of actin in the process of stretch-induced membrane remodelling.
 - b. To test for possible molecular candidates mediating the mechanosensing mechanism matching the PM structures described in point 1 to a molecular cascade leading to recovery of the original topography.
 - c. To unveil all the steps involved in the aforementioned molecular cascade.

Chaper 3 - METHODS

3.1. CELL CULTURE AND EXPRESSION VECTORS

NHDF were purchased from Lonza (CC-2511) and cultured in DMEM without pyruvate (ThermoFisher 41965-039) supplemented with 10% FBS (v/v), 1% penicillin-streptomycin (v/v) and 1% Insulin-Transferrin-Selenium (v/v) (ThermoFisher 41400045). IRSp53^{-/-} MEF infected with an empty pBABE or a pBABE-IRSp53-WT retroviral vector were generated by G. Scita (IFOM, Milan) as previously described [144–146]. The culture was maintained in DMEM supplemented with 1 % penicillin-streptomycin (v/v) and 1 μ /mL puromycin to selectively maintain cells expressing the selection vector. CO₂ independent media (ThermoFisher 18045088) was used for microscopy imaging and was supplemented with 10 μ g/mL of rutin (Sigma R5143) to prevent photobleaching [147]. HEK293T were cultured in DMEM (ThermoFisher 41965-039) supplemented with 10% FBS (v/v) and 1% penicillin-streptomycin (v/v). mCherry, EGFP and EYFP membrane markers contained a fusion protein consisting in one of the three fluorophores coupled to the 20 last amino acids of Neuromodulin which is post-translationally palmitoylated and targets the fluorophore to PM [52]. IRSp53 60950 shRNA and control Non-Targeting shRNA were purchased from Sigma Mission for viral transfection and stable cell line creation. To produce the lentiviral particles, the pHDM-HgpM2 plasmid, encoding the Gag and Pol genes was used together with the pRC-CMV-Reb-1b, the pHDM-Tat1b and the pHDM-G, encoding the VSV-G envelope protein, all of them kindly provided by Johan de Rooij (UMC-Utrecht). mEmerald-Ezrin was from Addgene (#54090). IRSp53 WT [148], 4KE-IBAR, I268N-CRIB [149] and I403P-SH3 [144] contained isoform 2 of the murine protein

either wild type or carrying the mentioned mutations in the pC1-EGFP backbone. IRSp53 W413G-SH3, Δ IBAR and IBAR-domain alone [144] were created based on the sequence of isoform 4 of the human protein inserted in the pC1-EGFP backbone. A point mutation was included in the SH3, the first 312 amino acids were removed in the case of the Δ IBAR and the first 250 amino acids were expressed to obtain the IBAR-domain. The dominant constitutively active Rac1-G12V and the dominant negative Rac1-T17N were described previously [150]. Actin was marked using the mammalian expression vector encoding the cytoskeleton marker Actin-V_HH fused to either or RFP or GFP2 and commercially sold as Actin-Chromobody® (Chromotek).

3.2. CELL TRANSFECTION

48h prior to the experiments, cells were trypsinised and split to reach the desired confluency of 75% flask coverage most suitable for transfection. On the day prior to the experiment, cells were electroporated with the selected plasmids using the Neon™ Transfection System (Invitrogene) by exposing the cells to a 1350V pulse for 30ms, according to instructions provided by the company. Plasmid concentration was always kept between 1 and 2.4 $\mu\text{g}/\mu\text{L}$ and amount used for transfection ranged from 3 to 6 μg for 10^6 cells.

3.3. STABLE CELL LINE PRODUCTION

To produce cell lines stably expressing the shRNAs for BAR protein silencing, lentiviral particles were created from HEK293T cells transfected with Lipofectamine® 3000 (Invitrogene™) and the 4 plasmids encoding the Rev, Tat and Pol genes needed for viral particles production together with the plasmid encoding the viral envelope protein and the plasmid to be inserted in the genome. On the next day, medium was replaced, and cells were let to produce virus for 24 more hours. After this time, medium was collected and filtered through a 0.45 μm filter. New medium was added, and the process was repeated 24 h later. The virus containing medium was kept at -80°C for further use. To transduce the cells, NHDF were seeded of 6 well plates 24 h prior to viral transduction in order to reach a 75% confluency on the day of exposure. On that day, cells were treated with 8 $\mu\text{g}/\text{mL}$ of Polybrene (107689 Sigma) and 1 mL of viral filtrate. The culture was incubated for overnight at 37°C and on the next morning, efficiency was checked by using an optical microscope. Viral filtrate was aspirated and replaced

Chapter 3 – METHODS

by new media. At this stage, cells were left to recover until the next day and then successfully transduced cells were selected by keeping the culture in fresh medium supplemented with 3 µg/mL of puromycin (A1113803 Invitrogene) for at least 72 h. An untransfected well was always left as a control and death of all cells was checked to verify antibiotic selectivity.

After puromycin selection, cells were expanded, frozen and kept in culture with 1 µg/mL of puromycin supplementation to ensure vector expression.

3.4. DRUG TREATMENTS

CK-666 was purchased from Merck (Ref 182515), SMIFH2 was from Abcam (ab218296), Wiskostatin was bought from Sigma (W2270) and Para-Nitro-Blebbistatin was from Optopharma (DR-N-111). All compounds were diluted in DMSO and conserved according to manufacturer's instructions. On the day of the experiment, drugs were diluted in culture media, filtered through a 0.22 µm filter and warmed up to 37°C prior to addition to the culture. Cells were treated with 25 µM of CK-666 for 30 min, 10 µM of PNB for 30-40 min and 10 µM Wiskostatin or 15 µM SMIFH for 1 h prior to the experiment. Corresponding controls were done by diluting DMSO to the same amount as drugs in culture media, filtered through a 0.22 µm filter, warmed up to 37°C and incubated with the culture for the same amount of time than their corresponding treatment.

3.5. PDMS MEMBRANE FABRICATION

The stretchable PDMS membranes were prepared by mixing the polymeric base 10:1 with the curing agent (SYLGARD-184 silicone elastomer kit - Dow) for 5 min and then the mixture was let to degas for 1 h. Membranes were spun on top of PMMA dishes according to the following settings:

- 5 seconds at 500 rpm and acceleration = 0.02 m·s⁻¹
- 1 minute at 500 rpm and acceleration = 300 m·s⁻¹

After spinning, membranes were cured in the oven at 65°C for 18-24 h.

To produce a patterned support to further obtain patterned-PDMS membranes PMMA dishes were plasma cleaned for 20 min and warmed up to 95°C for 5 min. After cooling down using a nitrogen gun, SU 2010 resin was spun on top of the dish to create a 10 µm layer and prebaked 2,5 min at 95°C. Dishes were then placed on a mask aligner and exposed for 7,5 s in presence of the designed acetate mask. After post-baking for 3,5 min at 95°C, the pattern was revealed for 1 min

and subsequently extensively washed with isopropanol and verified under the microscope. Finally, PMMA dishes were silanised by 30 s plasma cleaning activation followed by 1 h silane treatment under vacuum. Patterns were designed as a grid with letters and numbers to allow for correct orientation.

3.6. STRETCH EXPERIMENTS

Standard or patterned PDMS membranes were carefully cut from PMMA dishes and transferred to PMMA rings using some 96% ethanol to ease the task. After ethanol dried, another PMMA ring was used to sandwich the membrane. The lower part of the metal rings used to stretch the cells was then placed on top a custom-made 3D printed support and the PMMA-PDMS sandwich was placed on top and carefully pushed until reaching the mounting surface to introduce some tension in the membrane. While holding the membrane with a weigh, the upper part of the metal ring was placed on top and both metal parts were screwed together. Finally, remaining PDMS was cut to release the metal ring with the stretchable membrane from the PMMA ring holder.

To proceed for experiments, the rings were coated with 10 $\mu\text{g}/\text{mL}$ fibronectin (Sigma) overnight at 4°C PDMS membranes were then quickly washed, and 3000 cells were seeded on top and allowed to spread for 45 min to 1 h in the incubator. Then, rings were mounted on a loading post coupled to the microscope stage and vacuum was applied for 3 min to stretch the membrane. After this time, vacuum was released to come back to the initial shape as described in [52]. Calibration of the system was done by measuring the displacement of fluorescent beads attached to the top of the membranes to adjust the vacuum applied to obtain 7% stretch of the PDMS surface in the case of NHDF and 5% for MEF cells. These two magnitudes of PDMS nominal stretch were used to obtain ~5% cell stretch.

Chapter 3 – METHODS

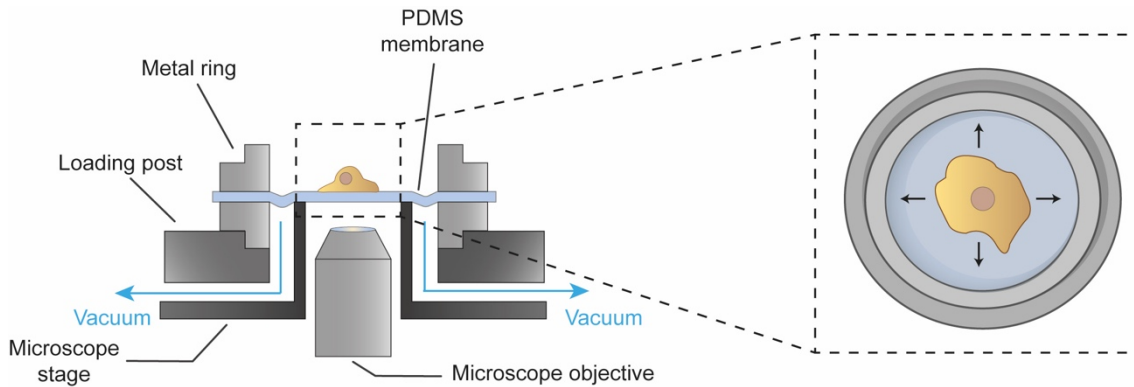


Figure 9: Stretch system components. The two metal rings clamp a PDMS stretchable membrane on top of which cells are seeded. Once mounted, the ring with the cells is placed on a loading post coupled to the microscope to perform imaging. The loading post is connected to a controlled vacuum source that allows for sucking and therefore stretching the PDMS membrane.

3.7. OSMOLARITY EXPERIMENTS

6 well glass-bottom dishes No. 0 (MatTek) Hypo-osmotic shocks were performed by exposing cells during 3 min to CO_2 independent medium mixed at 50% with de-ionized water in which the concentrations of Ca^{+2} and Mg^{+2} had been corrected. Iso-osmotic medium was added after the 3 min incubation period and cell recovery was imaged by using an inverted fluorescence microscope.

3.8. SCANNING ELECTRON MICROSCOPY EXPERIMENTS

Cells were prepared as explained in the previous section. Right after stretch release, the sample was fixed in 2.5% glutaraldehyde EM grade (Electron Microscopy Sciences 16220) plus 2% PFA (Electron Microscopy Sciences 15710-S) diluted in 0.1 M PB buffer at 37°C for 1 h. Samples were then washed 4 x for 10 min in 0.1 M Phosphate Buffer (PB) and imaged with epifluorescence microscopy as described below to acquire fluorescence images of the cell PM. PDMS membranes were then cut into 1 x 0.5 cm rectangles in which the pattern was centred and placed on top of 12 mm coverslips for further processing. Dehydration was carried out by soaking samples in increasing ethanol concentrations (50, 70, 90, 96 and 100 %). After this, samples were critical point dried and covered with a thin layer of gold to be imaged.

3.9. TRANSMISSION ELECTRON MICROSCOPY EXPERIMENTS

Cells were fixed, washed and PDMS membranes were cut and mounted as for SEM imaging. After this, samples were postfixed with 1% OsO₄ and 0.8% K₃Fe(CN)₆ for 1 h at 4°C in the dark. Next, dehydration in increasing ethanol concentrations (50, 70, 90, 96 and 100%) was done. Samples were then embedded in increasing concentrations of Pelco® EPONATE 12™ resin (Pelco 18010) mixed with acetone. 1:3 infiltration was done for 1 h then 2:2 for 1 h and finally 3:1 overnight. On the next day, embedding was continued with EPON12 without catalyser for 3x2 h washes and then overnight. Last, samples were embedded in EPON12 plus catalyser DMP-30 (Pelco 18010) for 2x3 h. To finish, blocks were mounted and polymerized for 48 h at 60°C. PDMS membrane was next peeled off and ultrathin sections were cut and mounted on grids for imaging.

3.10. APEX LABELLING FOR TEM IMAGING

Two days prior to the experiment, cells were co-transfected by electroporation with mKate2-P2A-APEX2-csGBP (Addgene #108875) and EGFP-IRSp53-WT in a 3:1 ratio, using the Neon™ Transfection System (Invitrogene) following the protocol provided by the company. Before seeding, cells were sorted for double positive mKate and GFP fluorescence, excluding very high and very low transfection levels. Cells were subsequently seeded and stretched in the same conditions as explained in the stretch experiments section. Right after stretch release, the sample was fixed in 2.5% glutaraldehyde EM grade (Electron Microscopy Sciences 16220) diluted in 0.1 M Cacodylate buffer at 37°C for 10 min, followed by incubation on ice for 50 min in presence of the fixative. All subsequent steps were performed on ice. The sample was washed 3 times with cold 0.1 M Cacodylate buffer, and next cut into 1 x 0.5 cm rectangles containing the fixed cells. Cells were washed for 2 min with a fresh cold 1 mg/mL 3,3'-diaminobenzidine (DAB) (tablets, Sigmafast, D4293) solution in 0.1 M Cacodylate buffer. Cells were immediately incubated with a fresh cold 1 mg/mL DAB solution in cold 0.1 M Cacodylate buffer supplemented with 5,88 mM hydrogen peroxidase (PERDROGEN™ 30% H₂O₂, 31642, Sigma). The samples were washed 3 times with cold 0.1 M Cacodylate buffer, and subsequently incubated for 30 minutes with cold 1% OsO₄. Dehydration, resin embedding, and block mounting was done as described in the TEM experiments section.

Chapter 3 – METHODS

3.11. IMAGE ACQUISITION

Fluorescence images were acquired with Metamorph software using an upright microscope (Nikon eclipse Ni-U) for the stretch experiments, and an inverted microscope (Nikon eclipse Ti-E) for the osmolarity set up, both equipped with an Orca Flash 4.0 camera (Hamamatsu). Images were always acquired with a 60x water dipping objective (NIR Apo 60X/WD 2.8, Nikon). Fluorophore emission was collected every 3 s. Cells were imaged in a relaxed state and then for 3 min at 5% stretch, and for 3 min during the release of stretch. SEM images were taken using the xTm Microscope Control software in a NOVA NanoSEM 230 microscope (FEI Company) under the high vacuum mode using ET and TL detectors to acquire high and ultra-high resolution images of the cell surface. TEM Samples were observed in a Jeol 1010 microscope (Gatan, Japan) equipped with a tungsten cathode in the CCI/TUB EM and Cryomicroscopy Units. Images were acquired at 80 kv with a CCD Megaview 1kx1k.

3.12. FLUORESCENCE ANALYSIS

All images used for time course analysis were aligned using the Template Matching plugin from Fiji to correct the drift. To assess the evolution of PM evaginations, VLDs or the different marked proteins, their fluorescence was quantified. To ensure that we only considered the fluorescence of structures induced by stretch or osmotic shocks, the analysis was carried out in regions devoid of visible endomembrane structures before the application of stretch or osmotic shocks. For each evagination, we calculated the integrated fluorescence signal of a small region of interest containing the evagination (I_{evag}), the integrated fluorescence signal of a neighbouring region of interest of the same size and devoid of any structures (I_{PM}), the integrated fluorescence signal of the entire cell (I_{cell}) and the integrated fluorescence signal of a background region of the same size as the cell (I_{BG}). Then, the final evagination signal I_{final} was computed as:

$$I_{final} = \frac{(I_{evag} - I_{PM})}{(I_{cell} - I_{BG})}$$

The numerator of this expression corrects evagination fluorescence so that only the signal coming from the evagination itself and not neighbouring PM is quantified. The denominator normalizes by total cell fluorescence, and also

accounts for progressive photobleaching. All control curves were normalized to 1 (maximal fluorescence after stretch release) and the rest of the data represented in the same graph were normalized to the control. Exceptionally, actin and ezrin curves were normalized to 0.5 (maximal fluorescence after the release of stretch) for visualization purposes. To quantify the degree of resorption of the evaginations, as the experimental data could not always be fitted with single exponential decay curve, we adopted the strategy of comparing the residual fluorescence intensity of the PM marker at the last timepoint of acquisition (t_{180s}), on which statistical analysis can be performed. Full reabsorption of evaginations leads to a complete return to fluorescent baseline (≈ 0), while presence of a residual fluorescence indicates non-reabsorbed evaginations. Lag time was calculated by identifying the maximum intensity timepoints in the protein and PM channels, and subtracting them to obtain the time between the two events.

3.13. AREA ANALYSIS

To compute the changes in cell area with time after stretch, automated area analysis for each timepoint was done using CellProfiler [151] (<https://cellprofiler.org/>). To calculate the time constant (k) of each experimental curve, data was fitted to a one-phase decay (for time course dynamics of PM evaginations, VLDs and protein markers) or one-phase association equation (area analysis after stretch) using GraphPad and k was extracted from the fittings to be further compared by statistical analysis.

3.14. QUANTIFICATION OF NUMBER AND PM AREA % STORED BY EVAGINATIONS

3 regions of different parts of the cell were randomly chosen from every cell at the timepoint t_0s (right after the release of stretch) and the number of evaginations was manually counted by comparing the analysed images with the images of the cell during stretch, to discard PM structures not formed by stretch-release. For stored area calculation, the membrane area fraction mf contained in evaginations was estimated as:

$$mf = \frac{i_{ze} - i_{zf}}{i_{zf} - bg}$$

Chapter 3 – METHODS

Where i_{ze} is the average fluorescence intensity of a cell zone (containing evaginations), i_{zf} is the average fluorescence intensity of a neighbouring flat patch of membrane (small enough so that it does not contain any evaginations), and bg is the average intensity of background. For each cell, this was done for 3 random regions containing evaginations.

3.15. FLUORESCENCE AND SEM CORRELATION

Images of the fixed sample were acquired in fluorescence and brightfield and positions of the imaged cells in the pattern were noted down. Sample was then processed for SEM imaging and the same cells were found by manually following their location on the pattern and visual verification was done to check for correct matching. Fluorescent and SEM images were then aligned by using the BigWrap plugin on Fiji.

3.16. STATISTICAL ANALYSIS

In the case of data following a normal distribution, T-test or ANOVA was done depending on whether there were 2 or more datasets to compare. For data not following normal distributions, Mann-Whitney or Kruskal-Wallis test were applied depending on whether there were 2 or more datasets to test. When measurements were paired and data not normal, the Wilcoxon matched-pairs test was used.

All data are shown as mean \pm SEM. Specific P and N values can be found in each one of the graphs shown in the figures or in their respective legends.

3.17. TEORETHICAL MODEL

To understand the physical mechanism leading to the active flattening of membrane evaginations caused by compression of the PM, we focused on a single evagination and described it mathematically under the assumption of axisymmetry. We modelled the membrane as locally inextensible thin sheet with bending rigidity $\kappa = 20 k_B T$ using the Helfrich model and accounted for the viscous stresses due to membrane shearing with membrane 2D viscosity $\eta_m = 3 \cdot 10^{-3} \text{ pN s}/\mu\text{m}$ [32,120,152]. We modelled the cortex as a 2D planar active gel adjacent to the membrane. We thus ignored the out-of-plane protrusive forces caused by localized actin polymerization at evaginations enriched in IRSp53,

which in a classical view can lead to further protrusion rather than flattening [153]. Instead, we focused on the in-plane effect of localized actin polymerization to explain active flattening. In the actual system, we expect both effects to compete.

To model the interaction between the membrane and the cortex, we considered an adhesion potential depending on the distance between the membrane and the cortex enabling decohesion with an adhesion tension of $\gamma = 1.5 \cdot 10^{-5}$ N/m [120], (Fig. XX). We also considered in-plane frictional tractions between the membrane and the cortex proportional to their relative velocity, $\tau = \mu(v_m - v_c)$ where v_m is the membrane velocity, v_c is the cortex velocity, and μ is a friction coefficient, which we took as $\mu = 20$ nN s/mm³ [32].

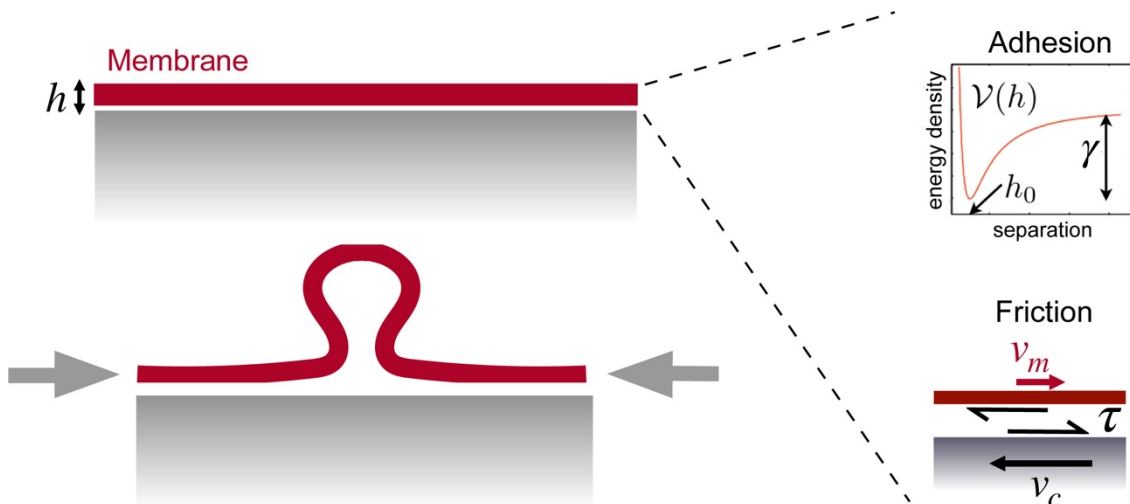


Figure 10: Considerations for the model. Schematic of the interaction between the membrane and the 2D underlying cortex, separated by a distance h before evaginations form. The interaction is modelled through an adhesion potential $v(h)$ with a minimum at separation h_0 , with adhesion tension γ and a tangential fictional traction τ in the adhered part of the membrane proportional to the slippage velocity $v_m - v_c$.

We generated evaginations with dimensions comparable to those obtained by experimental procedures (Fig. 12) by laterally compressing an adhered membrane patch of radius R_0 as discussed in [120]. We considered $R_0 = 150$ nm, consistent with the typical separation between evaginations (Fig. 12 A). After formation of the evagination, we applied at the boundary of our computational domain the surface tension required to stabilize the evagination, consistent with the long-time stability of such compression-generated evaginations of the PM when cellular activity is abrogated [52].

We then considered the model in [154] to capture the interaction between an ensemble of curved proteins (IRSp53) and a membrane. In this model, proteins

are described by their area fraction ϕ . We fixed the chemical potential of such proteins at the boundary of our computational domain, corresponding to a relatively low area fraction of proteins, $\bar{\phi} = 0.05$. We set the saturation coverage to $\phi^{\max} = 0.35$ due to crowding by other species but in our calculations, coverage did not come close to this limit. We considered an effective surface area per dimer of 300 nm². In this model, the curvature energy density of the membrane-protein system is given by $\frac{\kappa}{2}(H - C_0\phi)$ where H is the mean curvature and C_0 is a parameter combining the intrinsic curvature of proteins and their stiffness [154]. We took $C_0 = 3 \cdot 10^{-3}$ nm⁻¹, which lead to curvature sensing but no significant protein-induced membrane reshaping. With a protein diffusivity of 0.1 mm²/s, we obtained protein enrichments on the evagination of about 3-fold within 0.5 s.

To model in a coarse grained manner the signalling pathway triggered by IRSp53 localization and leading to actin polymerization, we considered a regulator species given by a normalized surface density ψ , which was produced with a rate depending on IRSp53 enrichment and given by $r\left(\frac{\phi}{\bar{\phi}}\right) = k_1 \min\left\{\left\langle\frac{\phi}{\bar{\phi}} - e_t\right\rangle; e_s - e_t\right\}$, where e_t is a threshold IRSp53 enrichment for signaling, e_s is an enrichment saturation threshold beyond which the production of ψ saturates, and $\langle a \rangle$ is 0 if $a < 0$ and a otherwise. We considered $e_t = 2$, $e_s = 3$ and $k_1 = 1$ s⁻¹. This regulator was degraded with rate $k_2\psi$, with $k_2 = 1$ s⁻¹ and diffused with an effective diffusivity of $D = 0.1 \cdot 10^{-3}$ mm²/s, much smaller than that of membrane proteins since the regulator is viewed as an actin-binding species. In polar coordinates, the governing equation for the transport of this regulator is thus:

$$\frac{\partial\psi}{\partial t} = \frac{1}{r} \frac{\partial}{\partial r} \left(rD \frac{\partial\psi}{\partial r} \right) + r(\phi/\bar{\phi}) - k_2\psi$$

This equation results in a region enriched with ψ , co-localizing with the evagination, and reaching a maximum value of about 1 within about 10 s, comparable to the typical times of actin dynamics. Not being a detailed description of a specific network, the details of this model for ψ are not essential. The key points are that the production of ψ is triggered by IRSp53 enrichment, and that k_1 , k_2 and D are such that over the time-scales of actin dynamics (significantly slower than those of IRSp53 enrichment) a region of high ψ develops close to the evagination.

The effect of this regulator is to locally favour actin polymerization by the Arp2/3 complex. The cortex can be viewed as a composite system of interpenetrating

actin networks, one polymerized by formins leading to linear filaments and producing contractile forces through the action of myosins and other crosslinkers, and one polymerized by the Arp2/3 complex, with a branched architecture and producing extensile forces by polymerization [73]. Combining these two effects, the net active force generation in the actin cortex is contractile. These two networks compete for actin monomers [155], and hence a local enrichment in the regulator leading to enhanced polymerization of the branched network should bias this competition and locally lower contractility in the vicinity of the evagination. In turn, the resulting contractility gradient should generate an in-plane centrifugal cortical flow, which if large enough, might drag the membrane outwards due to frictional forces and actively flatten the evagination.

To model such actin flow, we considered simple active gel model where the cortical velocity v_c is obtained by force balance between viscous and active forces in the cortex, and given by the following equation:

$$0 = 2\eta_c \left[-\frac{1}{r} \frac{\partial}{\partial r} \left(r \frac{\partial v_c}{\partial r} \right) \right] + \frac{\partial \sigma^a}{\partial r}$$

Where η_c is the viscosity of the cortex and $\sigma^a(\psi)$ is the active tension, which we assume to be a function of the regulator ψ . We note that we neglect in the equation above the force caused by friction between the membrane and the cortex as they slip past each other. This is justified because the hydrodynamic length for the cortex is in the order of microns and above, and hence in the smaller length-scales considered here viscosity dominates over friction. In our calculations, we took $\sigma^a(\psi) = \sigma^0 \left(1 - \frac{\psi}{2} \right)$, so that active tension is approximately halved near the evagination when the normalized regulator density ψ reaches about 1 and is equal to σ^0 far away from it. As boundary conditions, we considered $v_c(0) = 0$ consistent with polar symmetry and $\partial \frac{v_c}{\partial r}(R) = 0$, so that at $r = R$ the stress at the gel is σ^0 . We chose σ^0/η_c so that the resulting cortical velocities due to gradients in active tension gradients were of about 0.1 mm/s, comparable to the typical actin velocities due to polymerization in the lamellipodium [156].

The formation of the evagination triggered in this model a sequence of chemo-mechanical signalling event restoring autonomously homeostasis of membrane shape and of all the signalling network. Indeed, within a few seconds, IRSp53 became enriched in the evagination by curvature sensing. Then, over a about 10 seconds, the actin regulator ψ progressively built up in the vicinity of the

Chapter 3 – METHODS

evagination, creating a gradient in active tension σ , which in turn created a centrifugal cortical flow. This flow frictionally dragged the membrane outward ironing out the evagination. In the absence of curvature, the IRSp53 domain rapidly dissolved and according to Eq. (1) ψ dropped to zero everywhere, eventually stopping the cortical flow and thus recovering a homeostatic state with a planar membrane and a quiescent cortex.

We note that our model is consistent with the fact that myosin inhibition does not affect the resorption process. Indeed, myosin inhibition should lower the baseline active tension, σ_0 , but should not change the fact that localized polymerization would locally induce an extensile stress, and hence establish a tension gradient and an actin flow.

One important difference between our model and the experiments is that, in our calculations, the evaginations rapidly flattened once the contact angle of the evagination became smaller than 90 degrees, whereas in the experiments, the decay of membrane fluorescence was more gradual over a timescale of 3 minutes. We hypothesize that this may be due to the fact that localized actin polymerization may fill the evagination with a branched actin network, which should apply an out-of-plane force competing with the flattening force causing the centrifugal flow and whose material needs to be cleared out even when localized polymerization has stopped. Both of these effects should slow down the resorption process.

Chaper 4 - RESULTS

As mentioned before, the objective of this study was to discover how cells can detect the mechanically induced changes in their PM and harness those to interact with their environment. Here, the chosen method to apply mechanical deformations to the PM was stretch. As a result, the remodelling generated came in the form of PM folds, membrane accumulations with a given topography smaller than $1\ \mu\text{m}$ that were quickly flattened through an active cell response [52]. Given the small size of those folds, image accessibility, especially in the Z plane, was a challenge. Also, they were structures without marker, which complicated even more the task of recognising them through other techniques. This is why in the beginning of the study, we decided to address the problem through different points of view, including staining of curvature-sensing proteins related to membrane remodelling processes (which we suspected could be involved in the observed cell response), silencing assays of those proteins and electron microscopy techniques to gain a better understanding on the shape and curvature of the generated folds.

Although only some of these approaches yielded significant results for the work here presented, the rest of negative results and unexplored paths have been gathered in appendixes A, B, C and D at the end of this thesis. Therefore, the work presented in the results section corresponds exclusively to the story resulting from all the meaningful results obtained and its deeper analysis and comprehension, which fructified in a publication which is currently under submission on a high impact journal.

Chapter 4 – RESULTS

4.1. COMPRESSION GENERATES DYNAMIC PM EVAGINATIONS IN THE SCALE OF 100NM WIDTH

To study how PM topography is regulated, we submitted normal human dermal fibroblasts (NHDF) transfected with an EGFP-membrane marker to a physiologically relevant 5-6% equibiaxial stretch (Fig. 11 A) by using a custom-made stretch system composed by a PDMS stretchable membrane clamped between two metal rings, as previously described in [157] (see methods). After an arbitrary time of 3min to allow for equilibration, stretch was released. Cell response during and after stretch (stretch-release cycle) was monitored by live fluorescence imaging. As previously described, when tensile stress was applied cells increased their area by depleting PM reservoirs such as ruffles and caveolae [52,53]. After 3 minutes, stretch was released, resulting in a compression stimulus. At this point, excess membrane was stored again in folds, visualized as bright fluorescent spots of ≈ 500 nm (Fig. 11 D). These spots incorporate approximately 1.5% of PM area (Fig. 11 B), and thus store an important fraction of the area modified by cell stretch. Previous work done in the lab [52] showed that these spots are formed passively by the PM to accommodate the extra-material added during the stretch phase by fusion of membrane reserves. In this way, extra PM area gets stored in numerous structures each of them containing a small volume as a result of the compression generated when the stretch is released. This same behaviour was previously described when compressing synthetic lipid bilayers [120]. In cells however, passive fold formation is followed by active resorption involving actin cytoskeleton rearrangements. To monitor this process, changes in fluorescence intensity in the area where these structures were formed were tracked throughout a lapse of 180s and images were taken every 3s (see methods). Coinciding with which was previously published [52], compression-generated PM folds disappeared within 120s (Fig. 11 C and D) describing a decreasing exponential and reaching values close to 0 (baseline fluorescence, meaning flat PM) after this time.

The mechanism described allows for equilibration of PM topography and tension after perturbation in short timescales. However, the molecular mechanism underlying the process was poorly described and a lot of questions remained open. In previous lab work it was shown that when inhibiting actin polymerisation either by treating the cells with Cytochalasin D or with Latrunculin A, the PM remodelling following passive fold formation was blocked [52]. Further, ATP depletion led to the same result, confirming fold

resorption after stretch release is an active process relying on the need of remodel actin cytoskeleton.

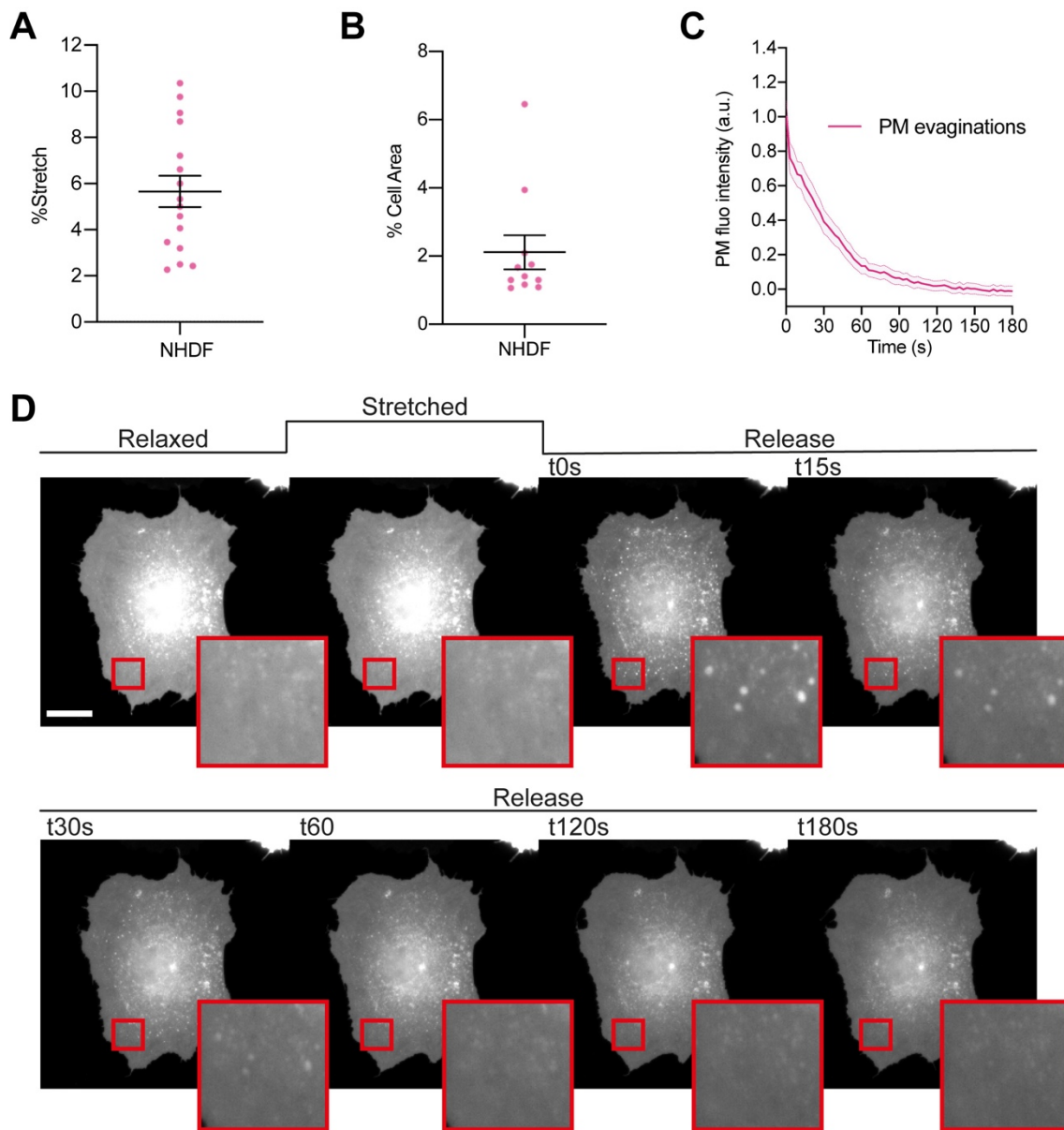


Figure 11: Effects of stretch-compression cycle in fibroblasts. (A) Average areal stretch experienced by NHDF. N=18 cells from 3 independent experiments. (B) % of cell area stored in evaginations upon stretch-release. N= 11 cells from 3 independent experiments. (C) Dynamics of PM evaginations after stretch release quantified as the change in fluorescence of the structure with time. N=12 cells from 3 independent experiments. (D) Time course images of a NHDF transfected with EGFP-membrane marker before, during and after stretch application. PM evaginations are seen as bright fluorescent spots after the release of the stretch due to compression of the PM. Lower images show a magnification of the areas marked in red un upper images. Scale bar is 20 μ m. Data show mean \pm s.e.m.

Although having identified the basic molecular mechanism of this process, its fine description requires characterisation of the topography generated by stretch-

Chapter 4 – RESULTS

release. As the diffraction limit of a standard fluorescence microscope lays in the range of 500 nm, characterisation of the compression-generated folds' structure in more detail was done through electron microscopy.

Cells transfected with a PM marker were seeded in a 3D patterned PDMS membrane, stretched for 3min and immediately fixed after the release of the stimulus. Next, brightfield and fluorescent images of the 3D pattern and the cells on it were acquired and samples were further processed for scanning electron microscopy (SEM) imaging. Computational alignment tools allowed for correlation between brightfield, fluorescence and SEM images. Observation of stretched and released cells under the SEM revealed numerous bud-shaped evaginations at their apical PM side that correlated with the bright spots seen by fluorescence (Figs. 12 A and B), showing that the PM bends outwards in a way that friction with the underlying cortex is minimised.

Because SEM samples are covered with a thin layer of gold, some bias can arise when structures are measured with this technique. To avoid this problem, transmission electron microscopy (TEM) was used to take measurements of the compression-generated evaginations and further characterise its shape. By comparing non stretched to stretched-released cells, we observed that the first displayed a homogeneously flat PM, while the second group displayed bud-shaped evaginations on the apical side (Fig. 12 C). The procedure used to create TEM samples involves peeling off the PDMS membrane in which the cells are seeded, which results in partial loss of the basal PM. Given this situation, analysis of the type of structures that may be created at the basal side of the cell remains unknown.

Analysis of the shape profile of compression-induced apical evaginations yielded an average diameter in the neck (cylindrical shape) of 83nm and of 115nm in the head (spherical shape), and average curvatures of 0.03 and 0.02 nm⁻¹ respectively (Figs. 12 D, E and F). These data indicate that PM compression led primarily to the formation of evaginations of regular size and shape at the apical side, which are immediately resorbed by the cell in an active process to re-equilibrate PM topography and tension.

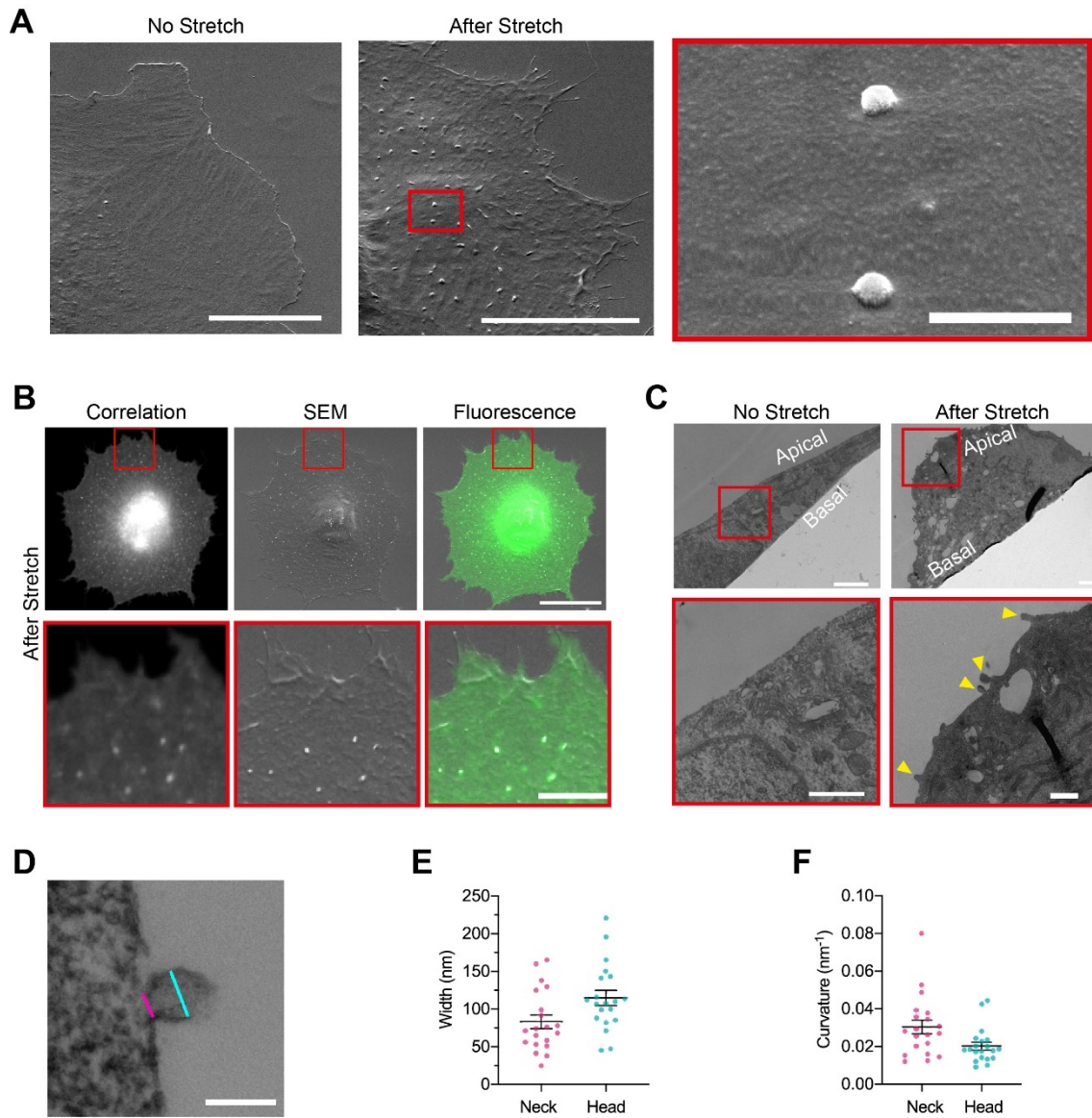


Figure 12: Cellular stretch generates PM evaginations with a defined curvature. (A) NHDF imaged through SEM. A non-stretched cell (left), and a cell just after stretch release (middle) are shown. Scale bars are 10 μm . Image on the right show a magnification of the area marked in red. Scale bar is 500 nm. (B) Correlation between fluorescence and SEM images of a non-stretched and stretched-released NHDF. Matching was achieved by using a patterned substrate together with computational tools for alignment. Scale bar is 20 μm for the main images and 2 μm for the insets. (C) TEM images of a non-stretched and a stretched-released NHDF. Yellow arrows in zoomed image point at PM evaginations formed at the apical side of the cell. Scale bars are 1 μm for the main images and 500 nm for the insets. (D) Detail of an evagination, cyan and magenta lines show evagination's head and neck diameters, respectively. Scale bar is 100nm. (E, F) Corresponding evagination neck and head diameters (E) and curvatures (F). N=22 evaginations from 3 independent experiments. Data show mean \pm s.e.m. In B and C lower images show a magnification of the areas marked in red un upper images.

4.2. THE INVOLVEMENT OF ACTIN IN EVAGINATION RESORPTION AFTER STRETCH

The clear pattern observed after the study of the shape of compression-generated PM evaginations reinforced the idea that the homogeneity of the population of structures made them good templates to be detected by the cell, triggering a unique mechanism to recover PM shape.

Further, after having observed that either depolymerization or stabilisation of the actin cytoskeleton led to the blocking of PM remodelling after stretch, prompted the idea that reattachment between the PM and the underlying actin cortex could be the first step mediating the reshaping process. To assess the role of actin in this mechanism, NHDFs co-transfected with a PM marker together with a plasmid expressing an actin nanobody bound to a GFP fluorophore (ACG) were submitted to a cycle of stretch-release stimulation and dynamics of both markers were recorded under the microscope. As hypothesised, while evaginations were being resorbed, actin was recruited to the same spot (Fig. 13 A). Quantification of fluorescence intensity of PM and ACG markers showed an increase in actin fluorescence during the first 9 s of resorption, followed by a decrease in the intensity of both markers that concluded when evaginations were resorbed (Fig. 13 B). These data suggest that PM quickly reattaches to the underlying cortex, which then mediates remodelling of the structure. Calculation of the average timepoint at which maximal actin fluorescence was achieved yielded an average of 14.70 ± 2.70 s after the release of stretch. However, maximal PM fluorescence was reached at an average timepoint of 6.30 ± 1.61 s after the release of stretch, which did not match the previous control (only membrane marker transfected cells) data, where maximal PM intensity was achieved at 0.70 ± 0.55 s after the release of stretch. This suggested that actin manipulation could be affecting PM dynamics, as already demonstrated in other studies [158]. Therefore, to further confirm the hypothesis of PM reattachment to the cortex and to prevent any mechanical interference caused by actin manipulation, the same experiment was repeated over-expressing the PM-cortex linker ezrin [78,159]. mEmerald-Ezrin also co-localized with evaginations during their resorption (Fig. 13 D) and fluorescence analysis of PM and ezrin markers revealed a recruitment of the protein that mimicked, with a delay of 10s the one seen with actin (Fig. 13 C, E and F). In this case, the average time of mEm-Ezrin maximal fluorescence was 24.64 ± 3.97 s and PM displayed values concordant with the ones observed in controls (average time of maximal PM fluorescence was 0.64 ± 0.34 s).

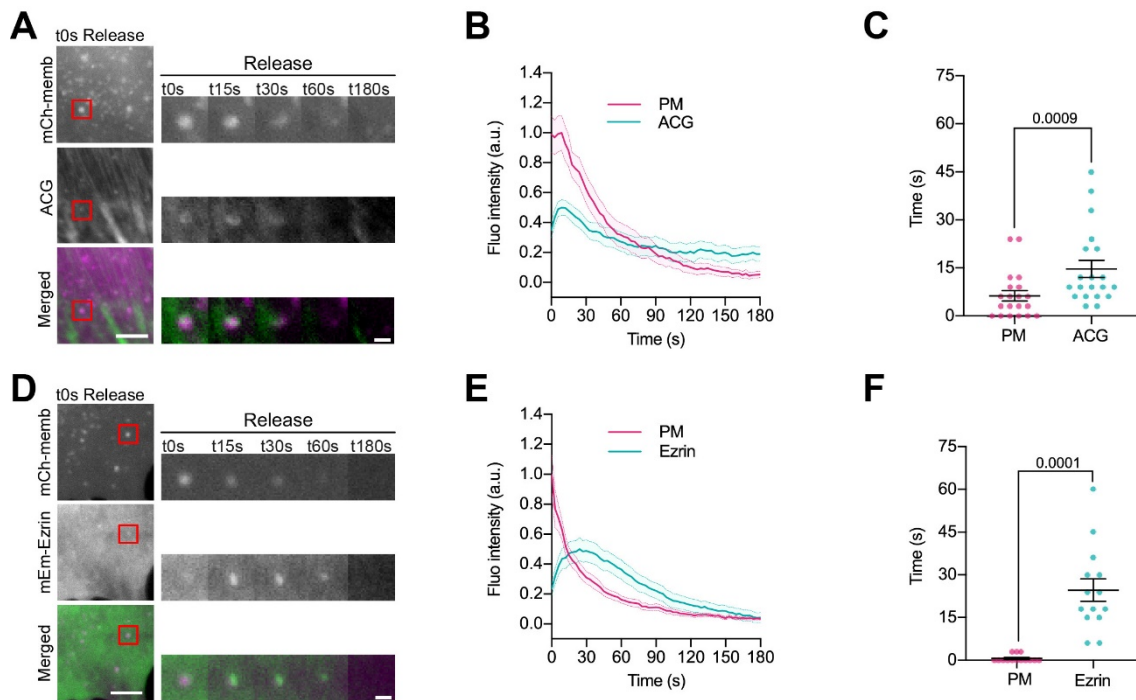


Figure 13: PM evaginations trigger local actin recruitment. (A) Time course images of mCherry-membrane and Actin Chromobody-GFP (ACG) marking PM evaginations in NHDF after stretch release. (B) Dynamics of PM evaginations quantified through mCh-membrane or ACG fluorescence markers during stretch release in NHDF. N= 20 cells from 3 independent experiments. (C) Timepoint of maximal fluorescence intensity of PM and ACG. Statistical significance was assessed through Wilcoxon test. N= 20 cells from 3 independent experiments. (D) Time course images of mCherry-membrane and mEmerald-Ezrin marking PM evaginations in NHDF after the release of the stretch. (E) Dynamics of PM evaginations quantified through mCh-membrane and mEmerald-Ezrin fluorescence markers after stretch release in NHDF. N= 14 cells from 2 independent experiments. (F) Timepoint of maximal fluorescence intensity of PM and ezrin markers. Statistical significance was assessed through Wilcoxon test. N= 14 cells from 2 independent experiments. For panels A, B, and C, scale bars are 5 μ m and 1 μ m for insets. Data show mean \pm s.e.m.

4.3. WHICH IS THE MOLECULAR LINK BETWEEN PM AND ACTIN REMODELLING?

The burst in actin polymerization at the evaginated PM and the simultaneous reattachment to the cortex suggest that the local topography generated by compression may act as the mechanical input triggering the subsequent polymerization event. Indeed, membrane curvature can recruit different signalling molecules [27,31,38,143,160]. And, among them, as already reviewed in the introduction, the superfamily of curvature-sensing BAR proteins [94,161–163]. This group of proteins accounts for molecules containing different curvature sensing and generating BAR domains: The N-BAR and F-BAR domains, which interact with positively curved membranes (invaginations), and

Chapter 4 – RESULTS

the I-BAR domain for the opposite type of curvature (negatively curved membranes or evaginations). In addition, these proteins also contain other domains, many of them reported to recruit actin nucleation promoting factors (NPFs) or even directly binding actin monomers [138].

Interestingly, a recent work described how ezrin needs to act in partnership with the I-BAR protein IRSp53 to enrich in negatively curved membranes [164]. Previous work done on IRSp53 has related this protein to PM ruffling [165,166], filopodia formation [167–170] and endocytosis [149], but, so far, no mechanosensing mechanism relying on its capacity to bind negatively-curved membranes has been described. Moreover, recent studies *in vitro* and *in cell* have pointed out that the IBAR domain of IRSp53 displays a peak of sorting at evaginations with curvatures of 0.05nm^{-1} , and that lower curvature values comparable to the ones obtained by TEM imaging of stretch-release induced evaginations also led to a two-fold enrichment of this domain with respect to a control membrane marker [168,171]. Prompted by this idea, we tested if IRSp53 could be the molecular linker between PM shape and actin dynamics in our system. To do so, stable cell lines expressing IRSp53 shRNA and control Non-Targeting shRNA (NT-shRNA) were generated and resorption dynamics of compression-generated evaginations were studied by plotting the decrease of their fluorescence with time (Fig. 14 A and B). Although the proper way of comparing both curves would involve fitting of the experimental data with an exponential equation, this could not be achieved in every case. Therefore, comparisons were done by contrasting the residual PM fluorescence at the places of evaginations 180s after the release of stretch. This parameter can now be used to perform statistical analysis and provides a meaning on the degree of resorption of evaginations, being full reabsorption of evaginations a complete return to fluorescent baseline, whereas non-reabsorbed evaginations imply presence of residual fluorescence.

Concordant with our hypothesis, IRSp53-depleted NHDFs did not complete bud resorption after 180s (Fig. 14 C), even though they stretched by the same amount as non-depleted cells (Fig. 14 D).

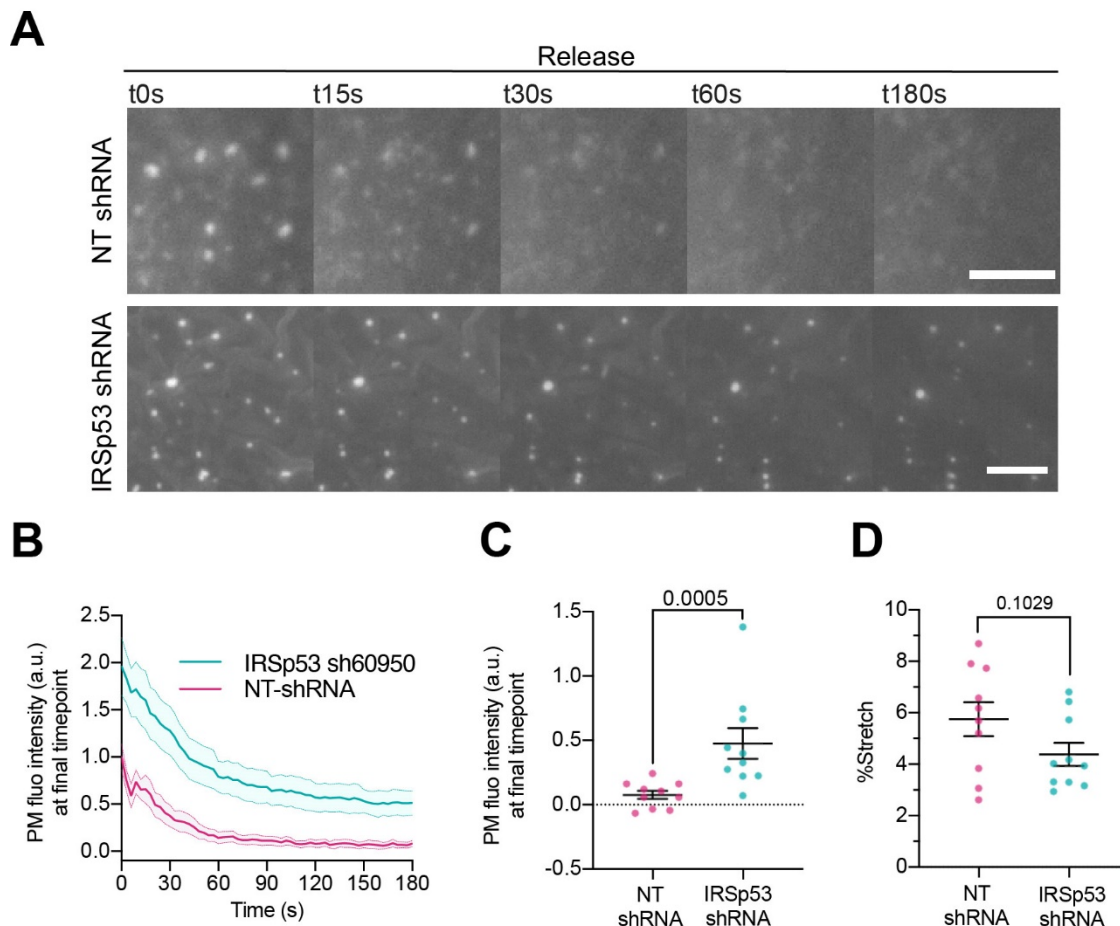


Figure 14: IRSp53 silencing impairs compression-generated PM evagination resorption in NHDF. (A) Time course images after stretch release of stable NHDF cell lines expressing either a non-targeting (NT) shRNA or an shRNA specifically targeting IRSp53. PM is marked with EGFP-membrane. Scale bars are 5 μ m. (B) Quantification dynamics of EGFP-membrane tagged PM evaginations after stretch release in NT-shRNA and IRSp53 shRNA expressing cells. (C) Differences in EGFP-membrane fluorescence intensity at the final timepoint of acquisition after stretch in the conditions mentioned above. Significance was calculated through Mann-Whitney test. (D) Areal stretch experienced by NT-shRNA and IRSp53 shRNA expressing cells under exposure to 7% PDMS membrane nominal stretch. Statistical differences were tested through unpaired T-test. N=8 and 10 cells from 2 independent experiments.

As the use of shRNAs implies only a partial removal of the protein, two different cell lines, one lacking IRSp53 and the other one expressing it, were used to validate the result. The cells used were previously described in [144–146], and they were generated using isogenic mouse embryonic fibroblasts (MEFs) derived from IRSp53 null mice that were stably infected either with a control (IRSp53^{-/-}) or an IRSp53-retroviral vector (IRSp53^{-/-}R) to restore expression levels of IRSp53 similar to wild type fibroblasts.

IRSp53^{-/-} cells stretched by the same amount as IRSp53^{-/-}R cells (Fig. 15 A) and did not display a significant change in the number of evaginations generated after

Chapter 4 – RESULTS

compression (Fig. 15 B) or in the area stored by those (Fig. 15 C), However, and reinforcing the previous result, they showed a severe impairment in the resorption of the evaginations even 180s after stretch release in comparison to their IRSp53^{-R} controls. In agreement with this result, transient expression of wild type (WT) IRSp53-GFP, fully recovered PM topography by resorbing the compression-generated evaginations in a lapse of 90s (Fig.8 D-F).

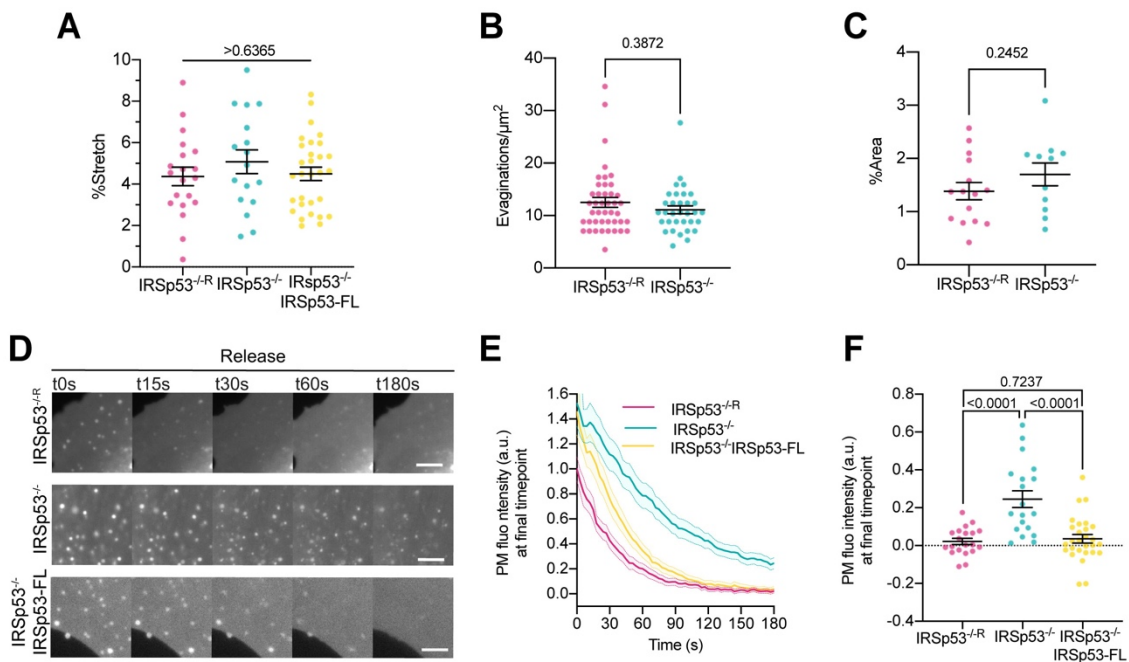


Figure 15: IRSp53 removal from MEF impairs compression-generated evaginations resorption after stretch. (A) Areal stretch experienced by IRSp53^{-R}, IRSp53^{-/-} and IRSp53^{-/-}EGFP-IRSp53-FL under exposure to 5% PDMS membrane nominal stretch. (B) Number of PM evaginations per μm^2 formed after stretch in IRSp53^{-R} and IRSp53^{-/-} MEF. N= 43 and 33 regions from 15 and 11 cells from 3 independent experiments. Differences were tested through Mann-Whitney test. (C) % of cell area stored in PM evaginations after stretch in IRSp53^{-R} and IRSp53^{-/-} MEF. N = 15 and 11 cells from 3 independent experiments. Differences were teste through unpaired T-test. (D) Time course images of PM evaginations tagged by mCherry-membrane in IRSp53^{-R}, IRSp53^{-/-} and IRSp53^{-/-} EGFP-FL-IRSp53 cells after the release of stretch. (E) Dynamics of PM evaginations (mCh-membrane marker) after stretch in IRSp53^{-R}, IRSp53^{-/-} and IRSp53^{-/-} EGFP-FL-IRSp53. (F) Differences in PM fluorescence intensity at the final timepoint of acquisition (180s after the release of the stretch). For panels A, E and F, N= 20, 19 and 28 cells from 3, 3 and 5 independent experiments. Statistical differences were tested through Mann-Whitney test. For all graphs data show mean \pm s.e.m.

Knowing that IRSp53 is a protein involved in scaffolding numerous NPFs [153] and can even itself directly nucleate actin monomers [167,172,173], it seemed logical to check for a direct effect of the lack of this protein on the recruitment of actin to compression-generated evaginations. To do so, IRSp53^{-/-} and its controls were transiently transfected with ACG-GFP together with mCh-membrane, and

dynamics of PM and this protein were monitored as described previously. Indeed, IRSp53^{-/-} cells exhibited a recruitment of actin to PM evaginations that was weakened with respect to IRSp53^{-/-R} cells (Fig. 16 A-D), illustrating that actin assembly at the PM evaginations is dependent on the presence of the I-BAR protein.

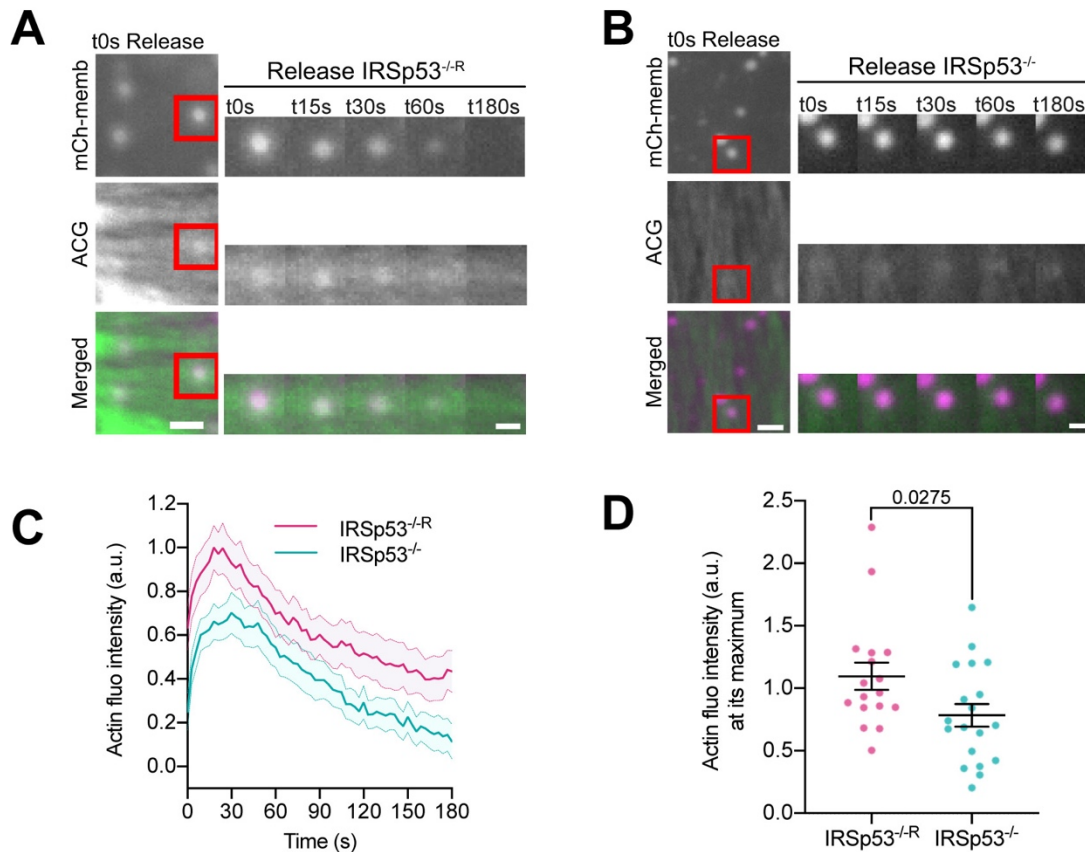


Figure 16: Actin is differently recruited to evaginations depending on the presence of IRSp53. (A, B) Time course images of mCherry-membrane and ACG marking the evolution of both PM evaginations and actin after the release of the stretch in IRSp53^{-/-R} MEF cells (A) and IRSp53^{-/-} MEF (B). Scale bars are 2 μm and 1 μm for insets. (C) ACG dynamics at PM evaginations after stretch in both IRSp53^{-/-R} and IRSp53^{-/-} MEF. (D) Maximal fluorescence intensity of ACG during the resorption process for IRSp53^{-/-R} and IRSp53^{-/-} cells. N= 17 and 19 cells from 4 independent experiments. Statistical significance was assessed through Man-Whitney test.

4.4. THE PM REMODELLING EVENT TRIGGERED BY STRETCH-RELEASE IS LOCAL

The next point to address was to check whether the effect of IRSp53 in actin remodelling was local at evaginations or, instead, it was rather a general non-specific cell-level effect due to the ability of IRSp53 to organize different NPFs [84,153]. To solve this question, PM folds of very different nature and curvature

Chapter 4 – RESULTS

were generated, and their dynamics were studied under IRSp53^{-/-} and IRSp53^{-/-R} conditions. The first strategy to achieve a different type of PM remodelling was to submit cells a hypo-osmotic shock. IRSp53^{-/-} and IRSp53^{-/-R} were transiently exposed to hypo-osmotic medium, leading to cell swelling. As previously described [52], re-exposure to iso-osmotic medium generates a water outflow from cells. When those are attached to a non-porous substrate such as PDMS, expelled water becomes trapped between the cell and the substrate, forming the dome-shaped invaginations known as vesicle-like dilations (VLDs) [174,175]. VLDs are much larger than compression-generated bud-shaped evaginations (several μm in size), with much lower curvature, and resorb in the order of minutes [52]. Confirming the local, evagination-specific effect of IRSp53, VLD resorption was equivalent in IRSp53^{-/-} and IRSp53^{-/-R} cells (Fig. 17 A-C).

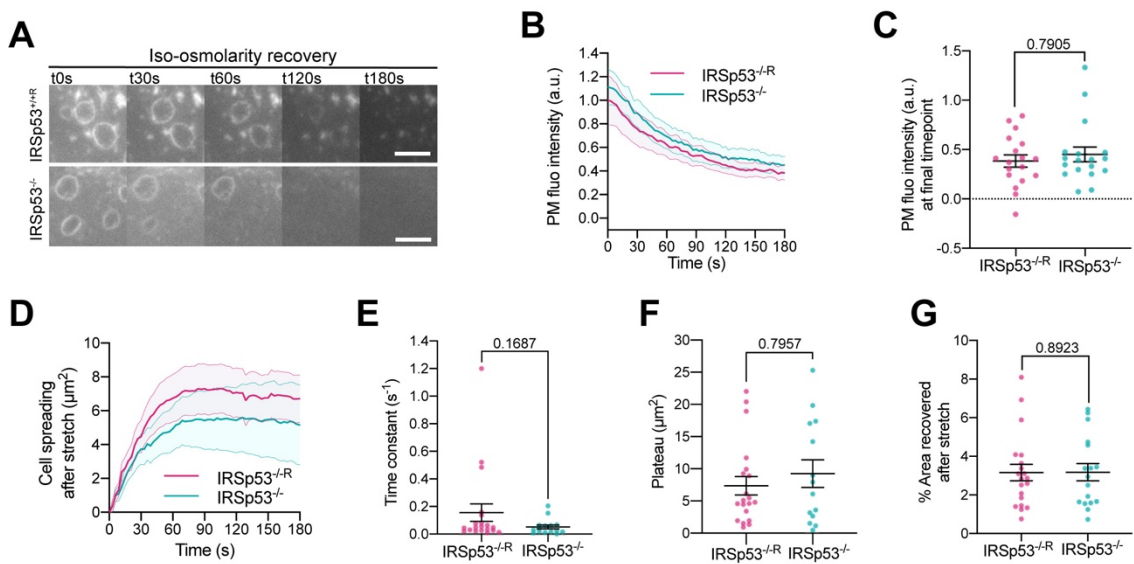


Figure 17: The role of IRSp53 is local and specific to PM evaginations. (A) Time course images of VLDs (observed with a pYFP-membrane fluorescent marker transfection) formed by exposing cells to iso-osmolar medium after a transient exposure to a 50% hypo-osmotic medium. Results for IRSp53^{-/-R} and IRSp53^{-/-} cells are shown. Scale bars are 5 μm . (B) VLDs fluorescence quantification as a function of time. (C) Comparison of PM fluorescence intensity of VLDs at the last frame of acquisition (180s after the iso-osmotic medium recovery). Significance was assessed through Mann-Whitney test. N=18 cells from 3 independent experiments. (D) Cell spreading during PM recovery phase. 0 = cell area after the release of stretch. (E) Comparison of time constants resulting from the exponential fitting of the curves obtained from cell spreading during the recovery phase after stretch. (F) Comparison of plateau values resulting from the same exponential fitting. (G) Quantification of % of area recovered after stretch. N=20 and 17 cells from 4 independent experiments. Statistical significance was assessed through Mann-Whitney test. Data show mean \pm s.e.m.

IRSp53 has also been related to actin polymerization in lamellipodia [165,176]. To discard that flattening of the evaginations was due to potential lamellipodial extension (cell spreading) after compression, we analysed cell spreading dynamics. After a stretch-release cycle, cells did extend lamellipodia and spread during approximately 1 minute (Fig. 17 D). However, the time constant of spreading (obtained by fitting an exponential curve to the experimental curve) and the amount of area recovered were not altered by IRSp53 (Fig. 17 E-G), discarding an effect of this factor.

4.5. HOMEOSTASIS RECOVERY AFTER STRETCH REQUIRES INTEGRITY OF SH3 AND IBAR IRSP53 DOMAINS

So far, it was shown that PM remodelling of compression-generated evaginations is a local event, which depends on IRSp53 to organize a burst of actin polymerization that flattens the PM. The next objective was to investigate if this could be part of a mechanosensing mechanism and to gain deeper knowledge in the molecular organisation of the cascade mediating PM flattening. Indeed, the I-BAR domain of IRSp53 may recognize the curvature generated at the evaginations and further recruit NPFs to coordinate the polymerization event through any of the other domains (Fig. 18 A). First, the I-BAR domain of IRSp53 can interact with charged curved membranes, but it further contains a sequence known as Rac Binding domain (RCB) which enables binding to active Rac1. Additionally, this domain has been described to have the ability to bundle actin [172]. IRSp53 also contains an atypical CRIB domain that binds to activated Cdc42, but not Rac1 [177] and, further, an SH3 domain that recruits different NPFs, such as WAVE2, Eps8 or N-WASP [153].

The mutants used to elucidate the interactions of IRSp53 during this process are described in Fig. 18 B. They comprise modifications targeting all of the domains described before, thus, impeding each one a specific interaction.

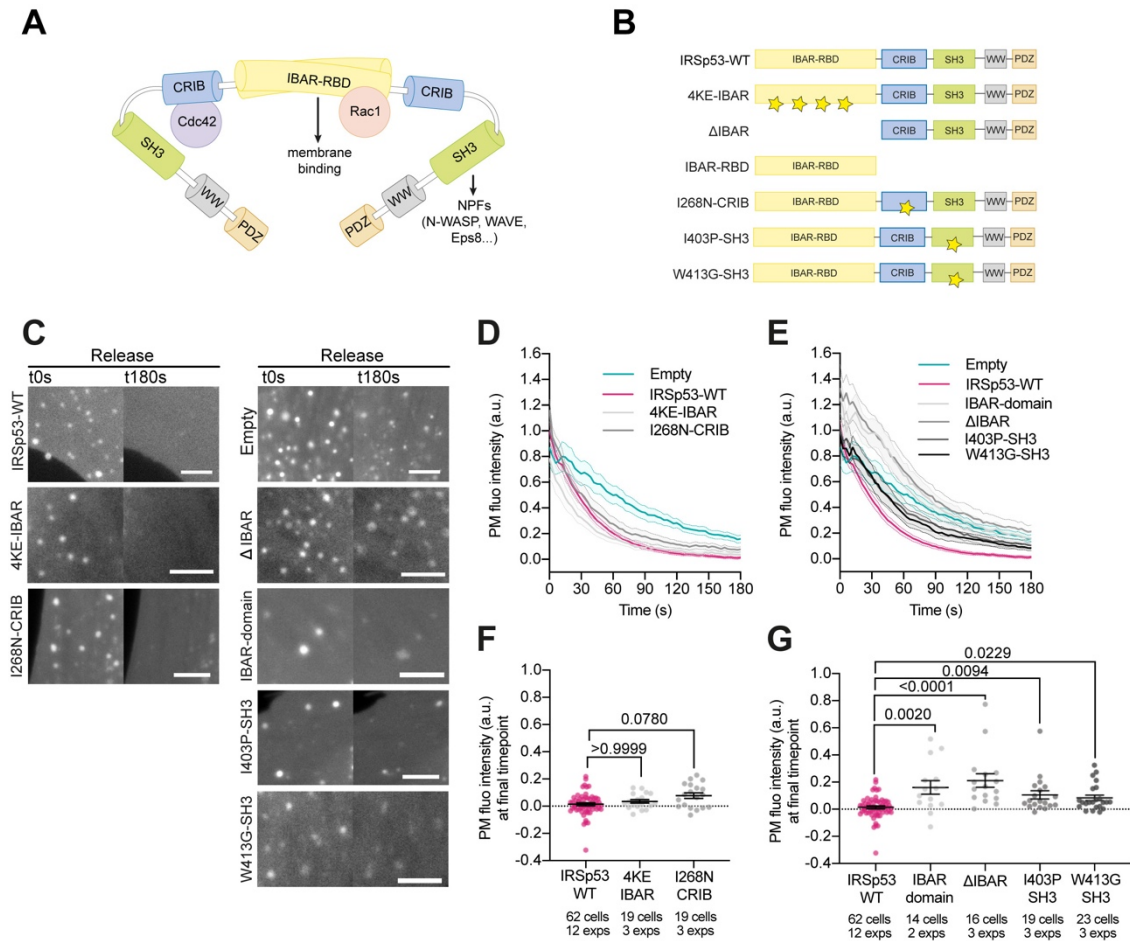


Figure 18: IBAR and SH3 domains of IRSp53 regulate the resorption of PM evaginations. (A) Schematics representing the IBAR protein IRSp53 and the different molecules interacting with its different domains. **(B)** Schematics of the IRSp53 mutants used in this study. Stars denote the location of mutations impairing the function of the different domains. **(C)** Images of PM evaginations of mCh-membrane transfected IRSp53^{-/-} cells (empty) or reconstituted with the different wild type (WT) or mutant forms of EGFP-IRSp53 at the first (t0 s) and last (t180 s) timepoint of acquisition after stretch. Scale bars are 5 μm. **(D-E)** Time course dynamics of PM evaginations of mCh-membrane transfected IRSp53^{-/-} cells either empty or reconstituted with the different WT or mutant forms of IRSp53. (D) shows IRSp53 mutants that rescue PM recovery after stretch, (E) shows IRSp53 mutants that do not rescue PM recovery after stretch. **(F-G)** Corresponding fluorescence intensity of PM evaginations at the last timepoint of acquisition (t180 s) after the release of stretch. Statistical significance was assessed through Kruskal-Wallis test. Data show mean ± s.e.m.

GFP-labelled mutants were expressed in the background of IRSp53^{-/-} cells, and PM remodelling after stretch was observed through fluorescence decay analysis with time. Whereas a set of mutants was able to rescue the wild type phenotype (Fig. 18 C, D and F), another group was not (Fig. 18 C, E and G). The I-BAR mutant 4KE (IRSp53^{-/-}-EGFP-IRSp53-4KE), in which Lysines 142, 143, 145 and 147 were replaced by Glutamic Acid rescued the phenotype when over-expressed in IRSp53^{-/-} cells. These amino acids belong to a basic patch which function involves

PM and actin monomers binding. The substitution of the positive charges coming from Lysines by the negative charges provided by Glutamic Acids was expected to mildly affect this interaction [172,178], although here no effect was observed. The same outcome was observed with the I268N-CRIB mutant (IRSp53^{-/-}-EGFP-IRSp53-I268N), which impairs the interaction with Cdc42. However, the full deletion of the I-BAR domain (IRSp53^{-/-}-EGFP-IRSp53-DIBAR) or point mutations I403P and W413G in the SH3 domain (IRSp53^{-/-}-EGFP-IRSp53-I403P and IRSp53^{-/-}-EGFP-IRSp53-W413G), that impair the association of IRSp53 with all its SH3 interactors, including WAVE2 [179], VASP and Eps8 [144,148], did not rescue homeostasis recovery after stretch release. Moreover, the over-expression of the I-BAR domain alone (IRSp53^{-/-}-EGFP-IBAR) also failed to rescue the phenotype, suggesting that the interaction with the PM and active Rac1 is not sufficient to drive PM flattening in response to stretch. This ensemble of results points at a mechanism where the I-BAR domain of IRSp53 would interact with the curved membrane of evaginations, leading to actin polymerization via active Rac1 and activation of NPFs through its SH3 domain.

4.6. IRSP53 ACTS AS A MECHANOSENSOR OF PM CURVATURE

To evaluate whether IRSp53 itself was directly recruited to evaginations, images of the dynamics of EGFP-labelled WT or mutant IRSp53 constructs, expressed in IRSp53^{-/-} cells, were taken. Co-localisation of the fluorescently labelled protein, either WT or mutated, and the PM marker was found in all cases (Fig. 19 A-G), indicating that the presence of IRSp53 in the PM is not mediated exclusively by the I-BAR domain and rather occurs as an interplay of all different domains, as already suggested in previous studies [180,181]. The dynamics of EGFP-IRSp53-WT at the resorbing evaginations were next analysed. Because IRSp53 is already bound to the PM, co-localisation of the protein with the evaginations was observed from the first timepoint after stretch release. However, the decay in fluorescence of the IRSp53 coupled fluorophore was significantly slower than that of the PM marker (Fig. 19 H and I), indicating that there is a progressive enrichment of IRSp53 to the evaginations while those are disappearing.

Chapter 4 – RESULTS

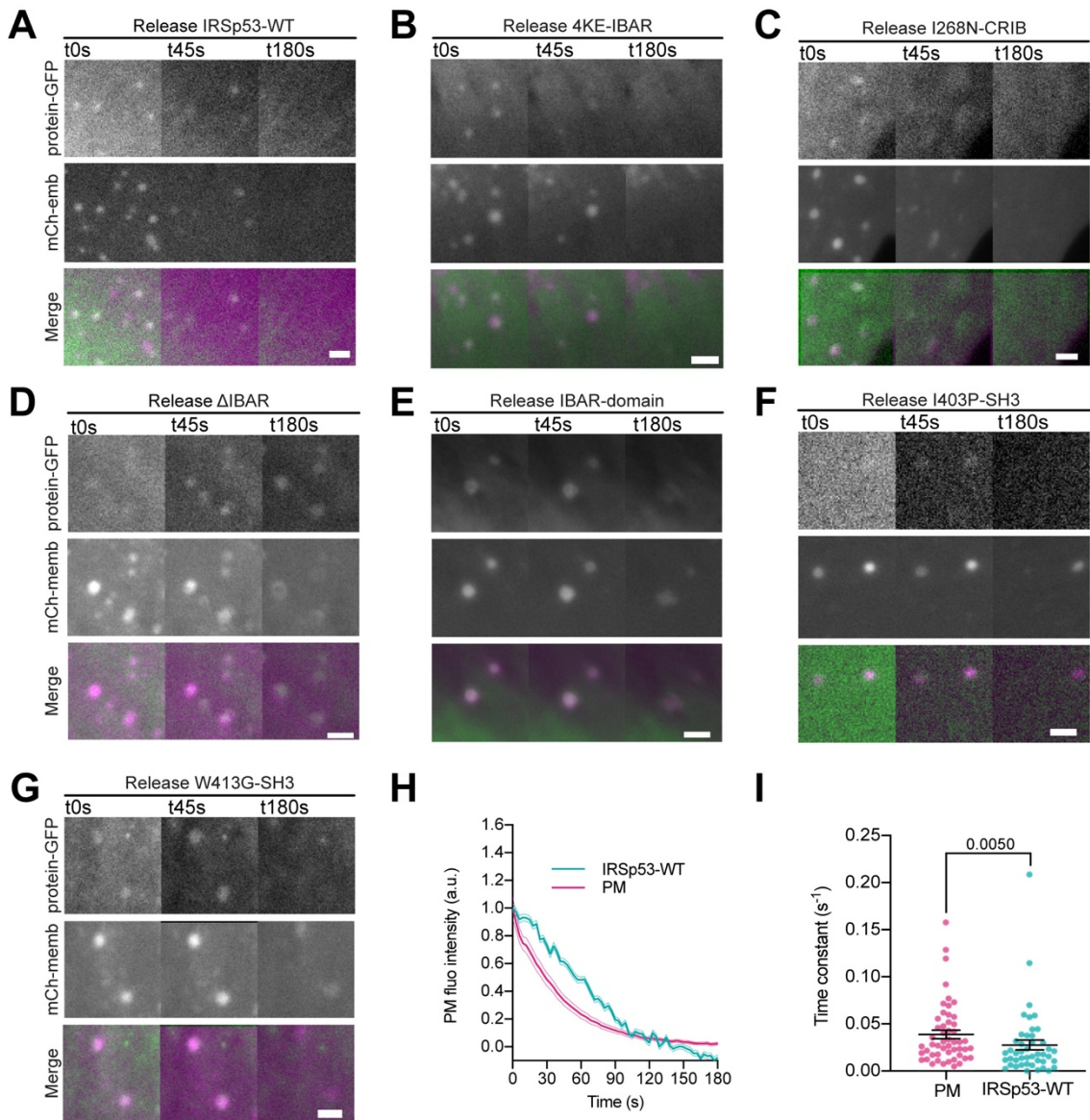


Figure 19: IRSp53 mutants' behaviour during homeostasis recovery after stretch. (A-G) Images of IRSp53^{-/-} cells after stretch release transfected with mCh-membrane and either the FL form of IRSp53 or different mutant forms of the protein coupled to EGFP. Scale bars are 2 μ m. (H) Corresponding dynamics of PM evaginations upon stretch release quantified through mCh-membrane or GFP coupled to EGFP-IRSp53-WT. (I) Time constants obtained by exponential fitting of the evagination resorption curves in the PM and EGFP-IRSp53-WT channels. Statistical significance was assessed through Mann-Whitney test. N=53 cells from 12 independent experiments. Data show mean \pm s.e.m

To confirm this recruitment, APEX (enhanced ascorbate peroxidase) staining for TEM samples was used. APEX is a monomeric heme enzyme that turns diaminobenzidine (DAB) and H₂O₂ into an insoluble polymer that becomes an electrodense product visible by TEM after OsO₄ staining. This polymer cannot diffuse, which confers a high spatial resolution to the technique [182,183], allowing to verify if IRSp53 was indeed specifically enriched at PM evaginations.

To perform these experiments, APEX2, an improved form of APEX which performs a better incorporation of heme group and provides a more intense staining, was used in preference to standard APEX [182].

IRSp53^{-/-} cells were co-transfected with csAPEX2-GBP, a conditionally stable APEX2 marker bound to a nanobody specifically recognizing GFP (also called GFP-binding protein, GBP), together with EGFP-IRSp53-WT or a GFP-bound mitochondrial marker (Mito-GFP). Evaginations were generated by a stretch-release cycle and samples were treated with DAB and H₂O₂ after fixation to visualize the APEX staining. As expected, a strong APEX signal (observed as electrodense areas in the TEM images) was observed around the mitochondrial membrane in the case of csAPEX2-GBP bound to Mito-GFP (Fig. 20 A). In the case of csAPEX2-GBP bound to EGFP-IRSp53-WT, staining was observed at the tip of filopodia, coinciding with previous observations (Fig. 20 B) [149,168]. In this last condition, a strong APEX signal was also observed in bud-shaped evaginations, indicating an enrichment of IRSp53 in such structures (Fig. 20 C). In contrast, de-stretched controls transfected with mito-GFP and csAPEX2-GBP did not show any staining at PM evaginations (Fig. 20 D), but the electrodense product was always present in mitochondria.

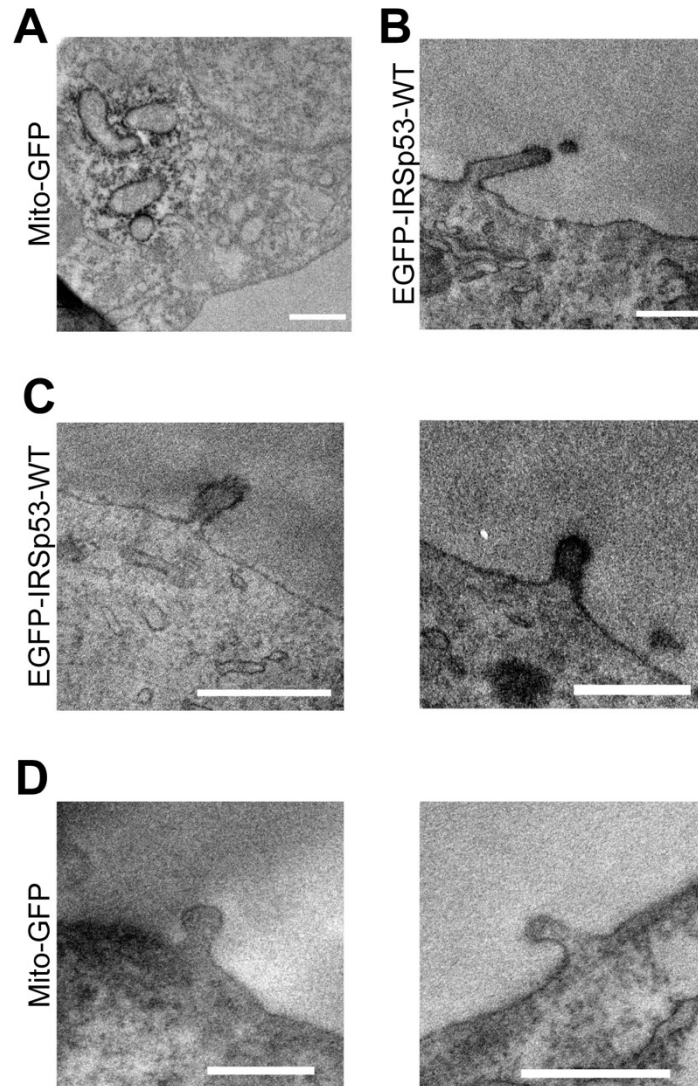


Figure 20: IRSp53 is enriched at stretch-release generated evaginations. (A-B) TEM images of non-stretched IRSp53^{-/-} cells co-transfected with csAPEX2-GBP together with (A, D) mito-GFP or (B, C) EGFP-IRSp53-WT. APEX staining can be observed around mitochondria (A), in the tips of filopodia and up to some extent in the PM of EGFP-IRSp53-WT transfected cells (B), as expected. (C-D) TEM images of PM evaginations coming from cells co-transfected with either APEX2-GBP and (C) EGFP-IRSp53-WT or (D) control condition mito-GFP. APEX staining can be observed at the PM evaginations of EGFP-IRSp53-WT transfected cells marking IRSp53 position. Scale bars are 500 nm.

Knowing that IRSp53 directly recognises evaginations shape, then it seems plausible to hypothesise that different mutants may recognize the structure differently. To examine this possibility the fluorescence dynamics of the different IRSp53 mutants was analysed (Fig. 21 A-F). Those mutants that had little effect on PM evaginations resorption followed a similar decay as the WT form (Fig. 21 A-C). However, the mutants slowing down the resorption followed different dynamics, with an initial recruitment phase before a decay in fluorescence (Fig. 21 D-F). This is illustrated in its most prominent example by the Δ IBAR mutant

(Fig. 21 F). These results probably indicate a delay in the recruitment of IRSp53-WT to the curved PM upon stretch. Indeed, due to the experimental time required to refocus samples and start imaging after compression (around 5-10 s), the acquired time lapses most probably fail to capture the process of PM evagination formation and the recruitment of IRSp53-WT. However, when the process is impaired due to IRSp53 mutations, dynamics are slowed down and recruitment phase can be captured.

This led to the hypothesis that, although presence at the PM is a feature that does not depend on a single domain, recruitment at the curved evaginations could define the efficiency of homeostasis recovery after stretch. To quantify this, the lag time between the timepoints of maximum intensity of the fluorescence signals of the PM and of the different IRSp53 mutant proteins was measured (Fig. 21 G). Confirming the previous assumption, plotting the lag time against fluorescence intensity of the PM marker after 180 s (used as previously as a marker for the efficiency of resorption of the evaginations) led to a strong positive correlation (Fig. 21 H): the more delayed IRSp53 recruitment was with respect to the PM marker, the less efficient the resorption was. Removal of the I-BAR domain displayed the longest lags and the least efficient resorption, supporting the idea that curvature sensing through this domain is needed to couple the mechanical stress to active PM remodelling. If the domain is absent, IRSp53 cannot perform a quick binding to the evagination and start the mechanochemical loop. SH3 domain mutations I403P and W413G also led to long lags and inefficient resorption. Although in this case the I-BAR domain is not impaired, lack of interaction of IRSp53 with NPFs, which could be already bound to the PM and target IRSp53 there [84,181], can delay PM enrichment too. In addition, this impaired interaction most probably affects actin polymerization and, therefore, the subsequent resorption process. Similarly, the I268N-CRIB mutant is probably delayed due to the lack of interaction with active Cdc42 already bound to the PM. Nevertheless, this delay is short and does not impair evagination resorption, also because all the different effectors involved in PM are recruited by IRSp53. In the case of the I-BAR domain alone, which functions is to sense PM curvature and to couple it to active Rac1, the delay in recruitment was similar to SH3 mutants but with a stronger impairment in homeostasis recovery. This suggests that the I-BAR domain alone, which is expected to be already bound to PM to a certain extent before evagination formation[184], keeps on aggregating at the curved structures in accordance with the sensing mechanism proposed for BAR

Chapter 4 – RESULTS

domains[138,171]. However, lack of remaining domains produces a strong effect on evagination flattening.

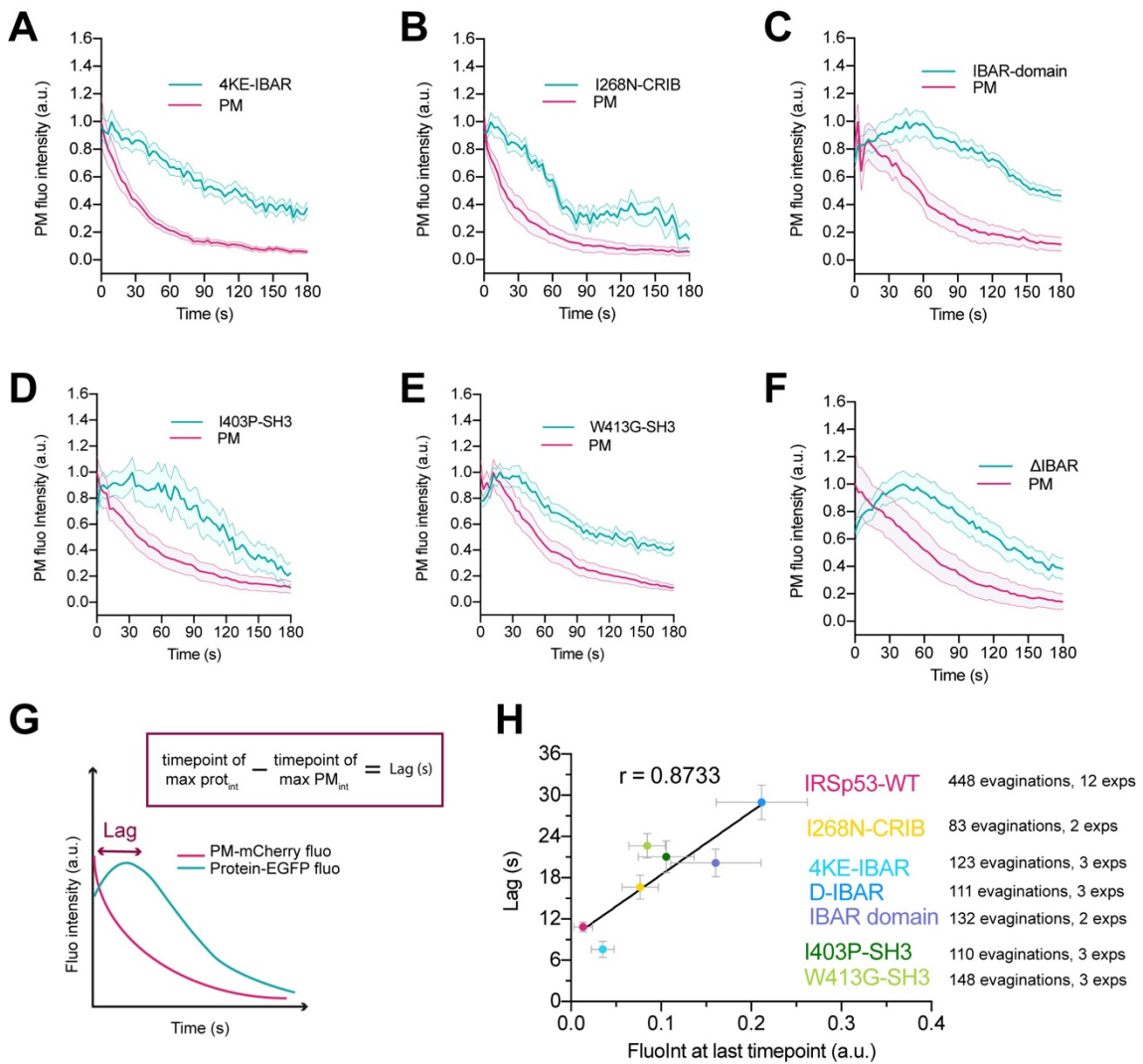


Figure 21: IRSp53 acts as a mechanosensor of PM curvature. (A-F) Corresponding dynamics of PM evaginations upon stretch release quantified through mCh-membrane or GFP coupled to the different IRSp53 mutants. N=15, 13, 14, 9, 12 and 16 cells from 3, 3, 2, 3, 3 and 3 independent experiment. (G) Schematic of how to calculate lag time. Magenta line depicts the behaviour of PM at evaginations upon stretch release quantified through mCh-membrane. Blue line depicts EGFP-IRSp53 or any of its mutants' fluorescence at evaginations upon stretch release. The purple arrow indicates the lag between the PM and IRSp53 signals, i.e., the time difference between the peaks of maximum intensity of both markers. (H) Time lag of WT or mutated IRSp53 plotted against the intensity of fluorescence at the last timepoint of acquisition. R indicates the Pearson correlation coefficient between both variables. Data show mean \pm s.e.m.

Taken together, these data indicate that the recruitment of IRSp53 to the mechanically induced bud-shaped evaginations is necessary for the PM to be successfully remodelled after stretch. The efficiency in the recruitment of this

protein ultimately determines the ability of the cell to set in place the fast mechanism mediating PM flattening in response to the physical perturbation.

4.7. ACTIN POLYMERIZATION IS DRIVEN BY RAC1 AND ARP2/3 ACTIVATION

The results obtained from the mutant's assay suggest that there is an interaction with active Rac1 and further recruitment of NPFs to complete de mechanosensitive loop and successfully perform PM homeostasis recovery after stretch. Previous work on PM ruffling showed that IRSp53 couples Rac1 to the activation of the WRC, and the subsequent nucleation of branched actin filaments mediated by Arp2/3 [72,93,185]. However, activation of Arp2/3 downstream of IRSp53 can also be mediated by Cdc42 and N-WASP [84,163,177] and, additionally, IRSp53 can coordinate the action of formins mDia1 and mDia2, which drive actin polymerization related to filopodia formation [169,186]. Finally, PM reattachment to the actin cortex may also rely on contractile mechanisms mediated by myosin and not only actin polymerization, as in the case of blebs [187]. To discriminate between these mechanisms, IRSp53^{-/-R} cells were treated with different inhibitors and evagination resorption after compression was examined. First, cell treatment with 10 μ M of the specific N-WASP inhibitor Wiskostatin [48] reduced filopodia number as expected [188] (Fig. 22 A and B), but did not modify evagination resorption dynamics (Fig. 22 C-E). Of note, this is consistent with our finding that bud resorption is not impaired in I268N-CRIB mutant condition in which IRSp53 interaction with Cdc42 is impaired.

Chapter 4 – RESULTS

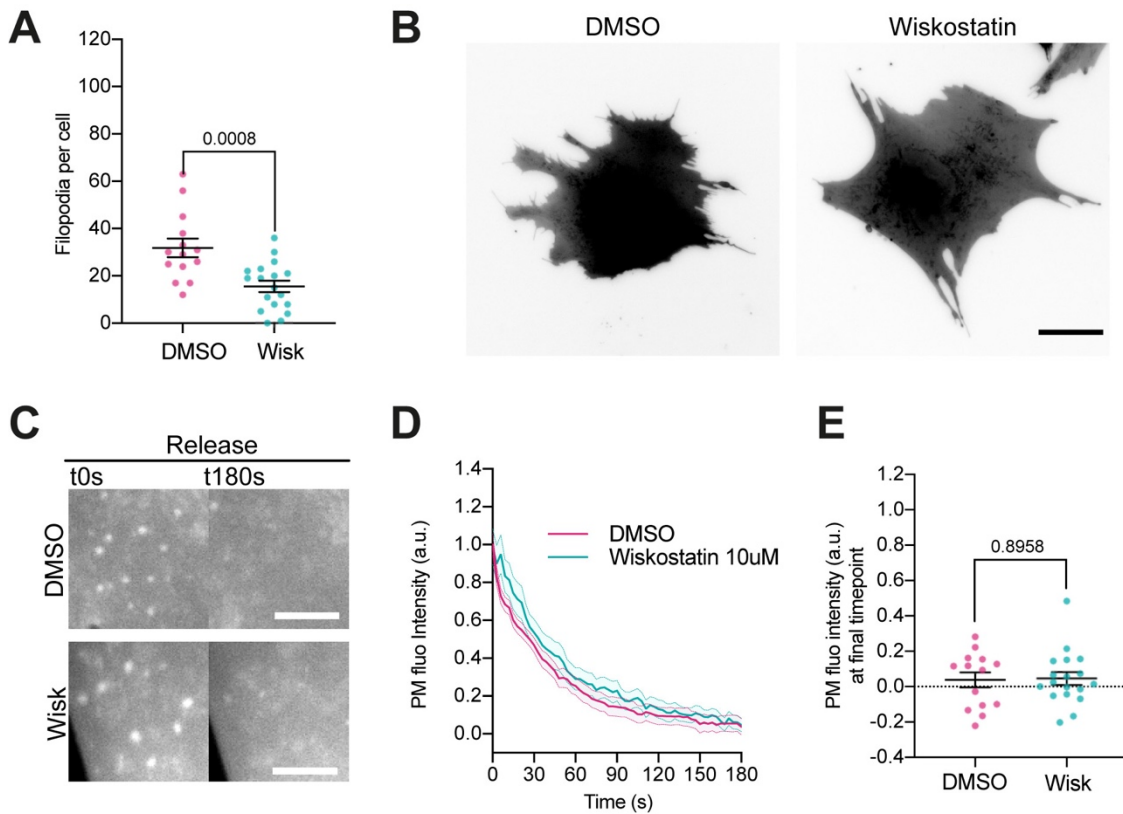


Figure 22: N-WASP plays no role in IRSp53-dependent PM remodeling after stretch. (A) Number of filopodia per cell in 10 μM Wiskostatin or vehicle (DMSO) treated IRSp53^{-/-R} cells. Compound was incubated for 30 min at 37°C before experiments. N= 18 and 14 cells respectively from 3 independent experiments. Statistical significance was assessed through unpaired T-test. (B) Corresponding images of GFP-membrane transfected cells. Scale bar is 20 μm . (C) Images after stretch release of PM evaginations, for IRSp53^{-/-R} cells treated with either vehicle (DMSO) or 10 μM Wiskostatin. Scale bars are 5 μm . PM is marked with EGFP-membrane. (D) Corresponding dynamics of PM evaginations. (E) Differences in PM fluorescence intensity at the final timepoint of acquisition (t180 s after stretch) between DMSO treated control cells and drug treated cells. Statistical significance was assessed through Mann-Whitney test. N= 18 and 14 cells from 3 independent experiments for all cases. Data show mean \pm s.e.m.

Treatment with 15 μM of the formin inhibitor SMIFH2 [189] reduced the number of filopodia as expected [190] (Fig. 23 A and B), but did not affect evagination resorption either (Fig. 23 C-E).

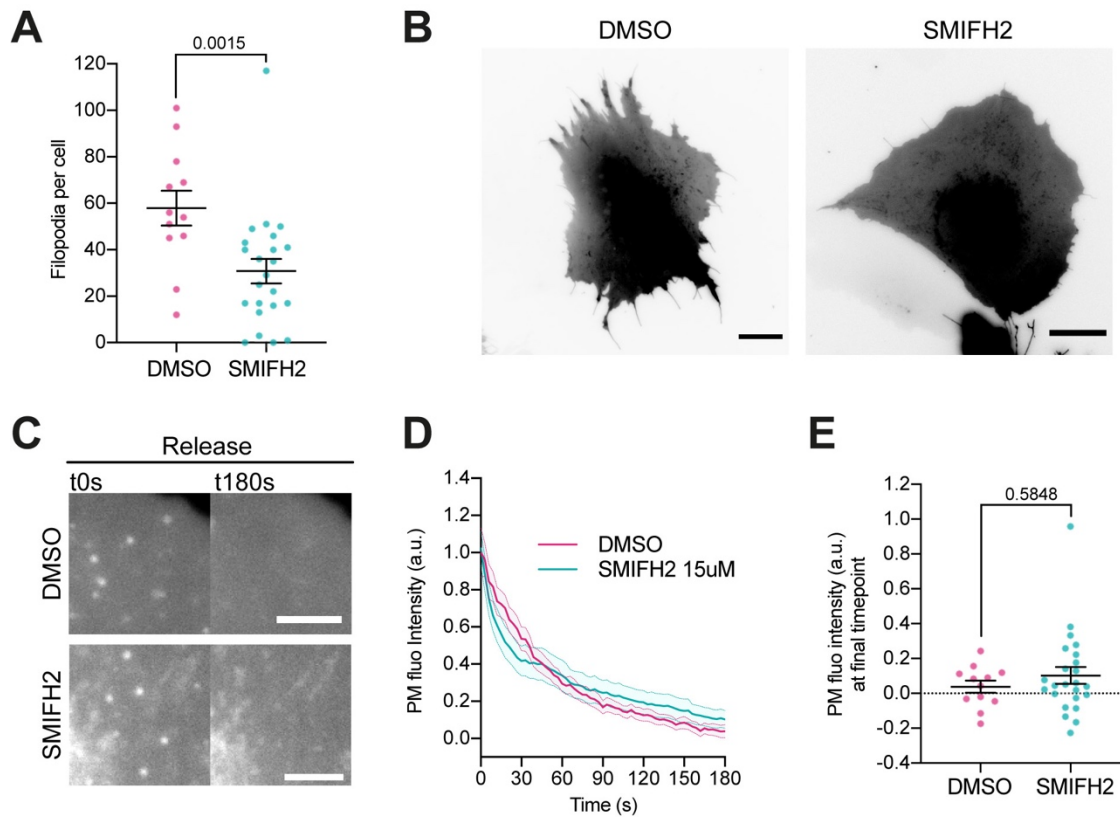


Figure 23: Formins play no role in IRSp53-dependent PM remodeling after stretch. (A) Number of filopodia per cell in 15 μ M SMIFH2 or vehicle (DMSO) treated IRSp53^{-/-R} cells. Compound was incubated for 1 h at 37°C before experiments. N=24 and 13 cells from 4 independent experiments. Statistical significance was assessed through Mann-Whitney test. (B) Corresponding images of GPF-membrane transfected cells. Scale bar is 20 μ m. (C) Images after stretch release of PM evaginations, for IRSp53^{-/-R} cells treated with either vehicle (DMSO) or 15 μ M SMIFH2. Scale bars are 5 μ m. PM is marked with EGFP-membrane. (D) Corresponding dynamics of PM evaginations. (E) Differences in PM fluorescence intensity at the final timepoint of acquisition (t180 s after stretch) between DMSO treated control cells and drug treated cells. Statistical significance was assessed through Mann-Whitney test. N = 24 and 12 cells from 3 independent experiments. Data show mean \pm s.e.m.

Exposing cells to 10 μ M of the myosin II inhibitor Para-nitroblebbistatin (PNB) [191] affected the integrity of stress fibres as expected [192], (Fig. 24 A) but, again, did not impair evagination resorption (Fig. 24 B-D). This result highlights that actin polymerization alone is sufficient to drive PM flattening and no contractility mechanisms are required for the remodelling of stretch-compression resulting topography.

Chapter 4 – RESULTS

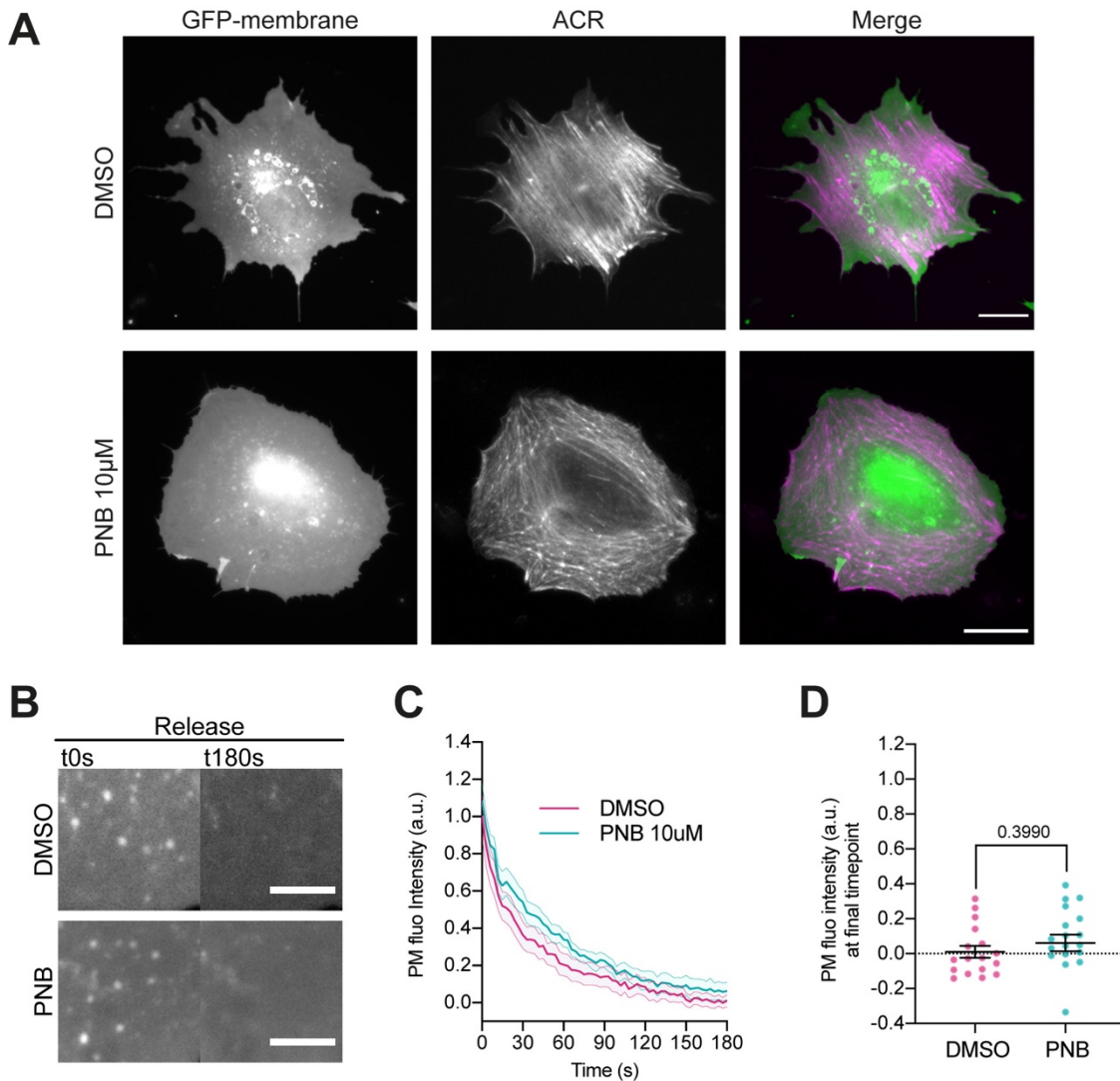


Figure 24: Contractility plays no role in IRSp53-dependent PM remodeling after stretch. (A) IRSp53^{-/-R} MEF after 30 min incubation at 37°C with either 10 µM PNB or vehicle (DMSO). Cells were transfected with GFP-membrane and Actin Chromobody-RFP (ACR) to mark both PM and actin. Scale bar is 20 µm. (B) Images after stretch release of PM evaginations, for IRSp53^{-/-R} cells treated with either vehicle (DMSO) or 10 µM PNB. Scale bars are 5µm. PM is marked with EGFP-membrane. (C) Corresponding dynamics of PM evaginations. (D) Differences in PM fluorescence intensity at the final timepoint of acquisition (t180 s after stretch) between DMSO treated control cells and drug treated cells. Statistical significance was assessed through unpaired T-test. N = 19 and 17 cells from 3 independent experiments. Data show mean ± s.e.m.

Finally and in contrast, treatment with the Arp2/3 inhibitor CK-666 [193] did impair evagination resorption in comparison to DMSO treated controls (Fig. 25). Thus, evagination resorption upon stretch-release involved recruitment of IRSp53, leading to actin polymerization in a myosin-independent and Arp2/3-dependent manner.

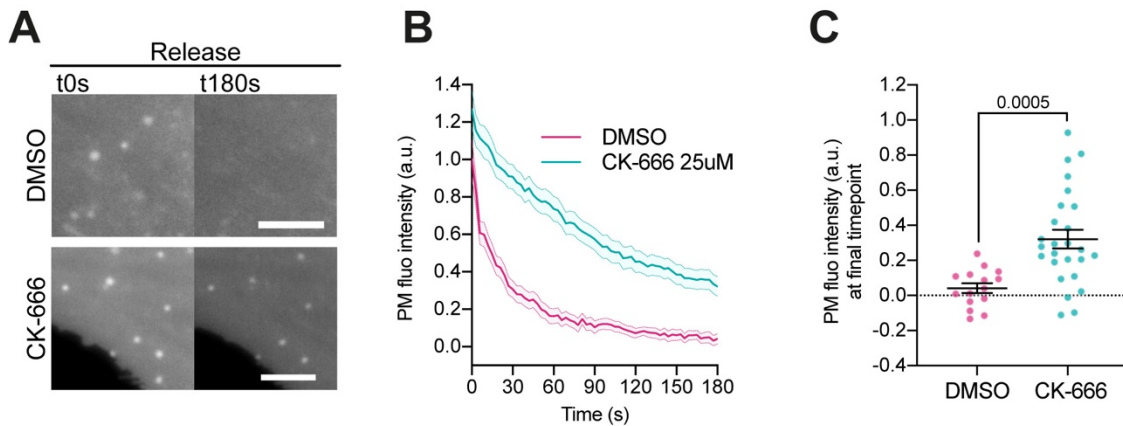


Figure 25: IRSp53 organizes actin polymerization via Arp2/3 activation. (A) Images after stretch release of PM evaginations, for IRSp53^{-/-R} cells treated with either vehicle (DMSO) or 25 μM CK-666. Scale bars are 5 μm. PM is marked with EGFP-membrane. (B) Corresponding dynamics of PM evaginations. (C) Differences in PM fluorescence intensity at the final timepoint of acquisition (t180 s after stretch) between DMSO treated control cells and drug treated cells. Statistical significance was assessed through unpaired T-test. N = 26 and 15 cells from 3 independent experiments. Data show mean ± s.e.m.

As mentioned above, IRSp53 has been described to lead Arp2/3-mediated actin polymerization via the activation of Rac1. Indeed, the role of this small GTPase as a master regulator of actin dynamics and its direct interaction with the I-BAR domain motivated the study of the involvement of Rac1 in our system. The impact of this small GTPase in evagination resorption after stretch was studied by overexpressing constitutively active (G12V) and dominant negative (T17N) forms of Rac1. Confirming its involvement, over-expression of Rac1-G12V speeded up evagination resorption significantly whereas Rac1-T17N slowed it down in NHDF (Fig. 26 A-C). Moreover, overexpression of constitutively active Rac1-G12V accelerated bud resorption even in the background of IRSp53^{-/-} cells (Fig. 26 D-F) further supporting the involvement of this GTPase in the process of evagination resorption but not clarifying how the interaction how the I-BAR protein takes places or if this effect is due to large-scale actin rearrangements induced by the dominant active form of Rac1.

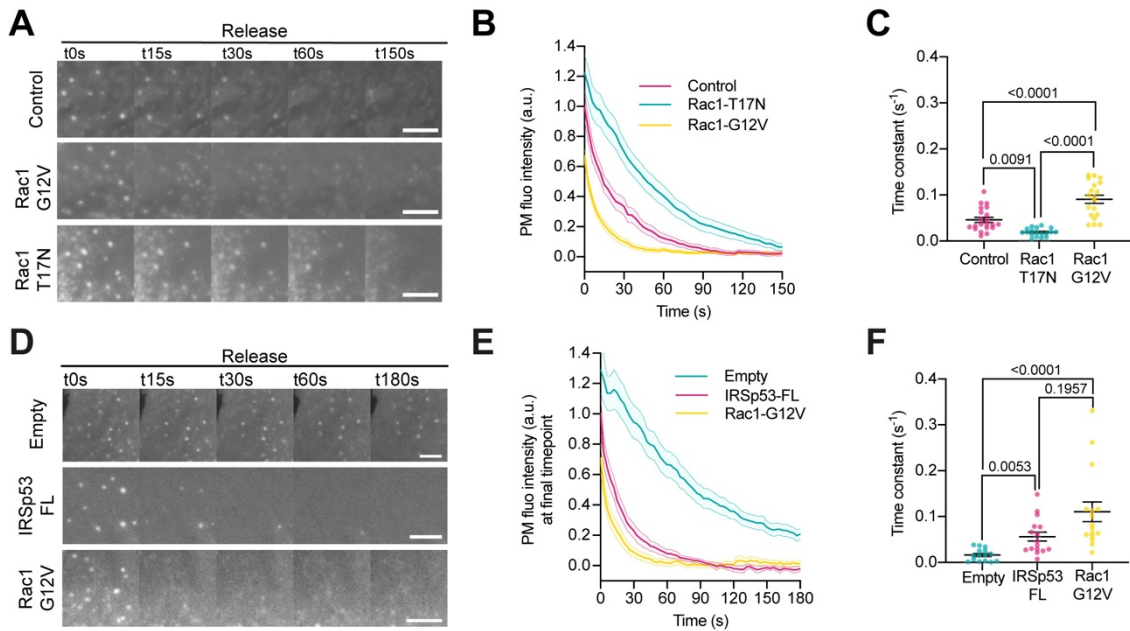


Figure 26: Rac1 is involved in PM remodeling upon stretch. (A) Time course images of PM evaginations after stretch release on NHDF expressing a PM marker alone, or a PM marker plus either a constitutively active (G12V) or a dominant negative (T17N) form of Rac1. PM was tagged with GFP-membrane marker. (B) Corresponding quantification of evagination resorption dynamics after stretch. (C) Time constants resulting from the exponential fitting of the curves in panel (B). Statistical significance was assessed through one-way ANOVA. N=21, 19 and 19 cells from 4 independent experiments. (D) Time course images of PM evaginations after stretch on IRSp53^{-/-} MEF expressing either a constitutively active (G12V) form of Rac1 or EGFP-IRSp53-FL. PM was tagged with either GFP for Rac1-G12V and Empty cells or with mCherry for the EGFP-IRSp53-FL transfected cells. (E) Corresponding quantification of evagination resorption dynamics after stretch. (F) Time constants resulting from the exponential fitting of the curves in panel (E). Statistical significance was assessed through Kruskal-Wallis test. N= at least 19, 16 and 16 cells from 3 independent experiments. For all images scale bars are 5 μ m. Data show mean \pm s.e.m.

4.8.A MECHANICAL MECHANISM FOR ACTIN-MEDIATED EVAGINATION FLATTENING

Previous work on IRSp53-mediated actin polymerization described the formation of out-of-plane protrusions in the form of filopodia or lamellipodia [148,163,169–171,194]. The physical mechanism supporting further protrusion relies on the natural notion that polymerization induces out-of-plane forces on the PM [195], which in the case of polymerization by Arp2/3 should push outwards. At larger scales, polymerization of an actin cortex retracts and flattens cellular blebs, but this mechanism depends on myosin contractility [187], and hence is not applicable here. In contrast, the results recapitulated on this thesis show a novel flattening rather than protruding response. To propose a plausible mechanism, a theoretical model coupling the PM and the actin cortex was

developed (see methods). It was hypothesised that, rather than out-of-plane forces, flattening may be the result of in-plane actin flows around evaginations. Thus, the actin cortex was approximated as a flat 2D active gel. In this model, the PM is adhered to the underlying cortex from which it can delaminate, and experiences frictional in-plane forces proportional to relative slippage [32]. This is coupled to a previous model in the field describing interactions between the PM and curved proteins [154]. Coarse-grained simulations were done reproducing the signalling pathway triggered by IRSp53 localization and leading to actin polymerisation. The polymerisation event is driven by a regulator species with normalized areal density ψ , produced beyond a threshold in IRSp53 enrichment, degraded, and transported by diffusion. ψ dynamics present time-scales comparable to those of actin dynamics. The effect of this regulator is to locally favour actin polymerization by the Arp2/3 complex, and hence bias the competition between a formin-polymerized contractile network component and a branched extensile component [73,155]. Based on these parameters, the mechanical effect of local polymerization by locally reducing contractility was simulated.

This model predicted that curvature-sensitive IRSp53 molecules became enriched in the evagination within a second after its formation. This led to recruitment of the regulator species ψ , resulting in a tension gradient in the vicinity of the evagination. In turn, this induced a centrifugal cortical flow, which frictionally dragged the membrane outwards until flattening. In the absence of curvature, the IRSp53-enriched domain dissolved, the regulator species recovered its uniform baseline, and the cortex recovered its quiescent steady-state (Fig. 27).

Whereas predicted actin flows occur at a scale well below the diffraction limit and can therefore not be observed experimentally, the predicted relative trends of PM and regulator densities qualitatively match our experimental observations when comparing PM and actin (Fig. 13 B) or ezrin (Fig. 13 E).

It has to be noted that in the real system, the proposed mechanism based on in-plane actin flows and cortex-PM friction should compete with the classical mechanism based on out-of-plane forces. This may explain why resorption dynamics in experiments (Fig. 11 C) are significantly longer and less abrupt than those predicted by the model (Fig. 27 B). Predictions are also consistent with the previous observation that evagination resorption is impaired when inhibiting Arp2/3 (Fig. 25) but not myosin or formin activity (Figs. 23 and 24). Indeed, the proposed mechanism in this model is based on a local gradient in extensile versus

Chapter 4 – RESULTS

contractile behaviour around the evagination. This gradient should depend on Arp2/3 (which acts locally at the evagination) and not on formin or myosin, which would regulate overall contractility levels. Thus, the model here described suggests a chemo-mechanical signalling system that autonomously restores homeostasis of PM shape.

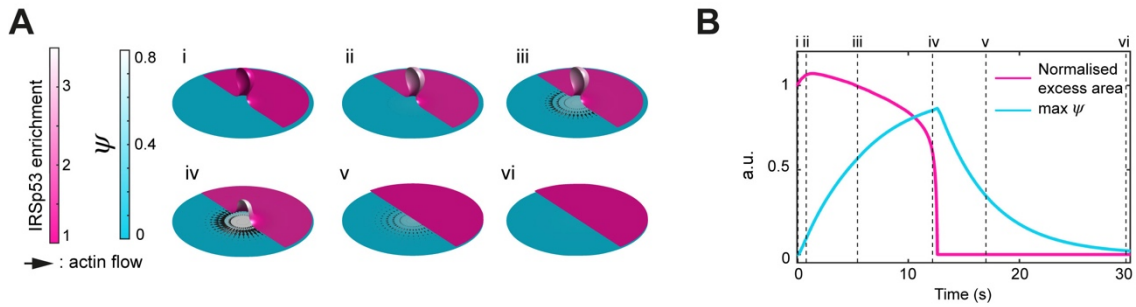


Figure 27: Dynamics of the model of chemo-mechanical signalling. (A) After the formation of the evagination (i), IRSp53 becomes enriched within 1 second (ii), which triggers the local increase in the concentration of actin regulator ψ over about 10 seconds (iii), thus creating a tension gradient and subsequent centrifugal cortex flow dragging and flattening the membrane (iv, v). Once planarity is restored, the IRSp53 domain rapidly disassembles, the actin regulator recovers its steady- state, and the flow ceases (v, vi). Right side magenta bar shows local IRSp53 enrichment from a baseline value of 1. Cyan bar right next to it shows the concentration of an actin regulator ψ . The radius of the membrane patch is 150 nm. **(B)** Corresponding quantifications of PM excess area contained in the evagination and actin regulator concentration ψ . For PM area, 0 corresponds to a flat membrane patch. Timepoints corresponding to configurations shown in (B) are indicated in roman numerals. Both quantifications are normalized to a maximum of 1.

Chaper 5 - DISCUSSION

Cells constantly exchange information with their surroundings, and external inputs are first received by their outermost layer, the PM. This interface, far from being an inert wall, integrates and transmits incoming stimuli, ultimately impacting cell behaviour. In this context, the traditional view of such stimuli as biochemical messengers has now changed to include the concept that physical perturbations are also of major importance [1,58,196]. By sensing and responding to physical and biochemical stimuli, one of the main functions of the PM is to adapt to the changes in shape that cells experience as they migrate or are mechanically deformed in a variety of physiological conditions [63,103,122,197–199]. To date, research in this area has largely focused on the regulation of PM area and tension at the level of the whole cell [53,57,118]. For instance, cell stretch or decrease in medium osmolarity have been commonly used to raise PM tension, unfolding membrane reserves (ruffles, caveolae), inhibiting endocytosis and promoting exocytosis [55,61,121,200,201]. Conversely, cell exposure to a hypertonic solution or cell compression have been employed to decrease PM tension, leading to an increase on the activity of different endocytic pathways [52,59,143,202]. These works have shown that PM tension homeostasis is maintained by regulating PM area through such mechanisms. However, changes in PM area upon mechanical perturbations are necessarily accompanied by changes in topography at the local scale. This is clearly exemplified by caveolae flattening upon cell stretch [62] or creation of PM folds at the sub- μm scale upon cell compression [52]. Curvature also arise when membranes are exposed to either external topographical cues [115,142] or internal pulling by actin filaments [203–205]. Hence, to maintain PM homeostasis, cells should be able not only to

Chapter 5 – DISCUSSION

respond to overall changes in PM tension or area, but also to local changes in PM topography.

To address this problem, this work has used the controlled compression of fibroblasts through the application and release of stretch. The results in this thesis show that stretch-compression cycles generate evaginations on the apical PM of the cells with a size on the 100 nm scale, compatible with the sensing range of I-BAR proteins [168,171]. Due to limitations in TEM sample preparation, which involved peeling off the PDMS membrane in which cells are seeded, it was impossible to check the type of PM folds that may get formed at the basal side. Although in the SEM and fluorescence correlation images there is only a small fraction of bright spots which do not have an apical evagination associated, confocal images of previous work done in the lab have revealed the presence of stretch generated invaginations. These results suggest that this small population of PM folds with no topography correspondence on the SEM image, would likely comprise invaginations formed at the basal side. Due to the different topography of those structures, they would probably follow different mechanisms to be resorbed by the cell than the one proposed in this work. Further evidence of the generation of membrane invaginations generated by stretch-release is discussed in Appendix C.

Also, this thesis has demonstrated the specific role of IRSp53 in recognising stretch-release generated PM evaginations. This mechanism is not due to general cell-scale effects, such as lamellipodial extension [165,176] or endocytosis. Indeed, cell spreading after the stretch-compression cycle was not affected by IRSp53 (Fig. 17 D-G), showing that the flattening happens locally and supporting the hypothesis of evaginations mechanosensing. Nevertheless, it is well known that both endocytosis and exocytosis respond to changes in PM tension [118,201,206]. In concrete, in mammalian cells PM regulatory processes such as clathrin mediated endocytosis (CME) [207,208], micropinocytosis [209], caveolae [61–63,135,143] or the CLIC-GEEC pathway [59,149] are responsive to those changes. Therefore, we expect that such mechanisms play a role too in removing extra membrane when tension drops due to the stretch-compression cycle. Those processes would certainly contribute to the speed of PM flattening after stretch. However, it has to be highlighted that the aforementioned pathways are not specific and do not associate with a determinate topography generated as a result of mechanical stimulation. Instead, the IRSp53 mechanosensing mechanism presented in this work responds to these features. Further, the I268N-CRIB and 4KE-IBAR IRSp53 mutants used in this study strongly impaired CLIC-GEEC

endocytosis [149], but fully rescued evagination resorption (Fig. 18 D and F), showing that IRSp53 affects both phenomena through different mechanisms. The generation of low curvature structures as VLDs through osmotic-shock, a process that was shown to activate the CLIC-GEEC pathway, resulted to be non-affected by the lack of IRSp53, supporting again the specificity of the mechanosensing mechanism proposed in this thesis. Altogether, the finding that IRSp53 is able to couple the mechanically generated PM topography with a biochemical loop mediating flattening and tension restoration at the local scale represents a discovery that adds to the previous knowledge in the field, illustrating a fast and local way for cells to adapt to mechanical perturbations.

Also, the fact that cells have to respond to changes in both PM tension and topography is a requirement that becomes even clearer if one considers recent findings showing that tension does not propagate extensively throughout the whole ensemble of the PM, but dissipates in small areas of less than 5 μm [32].

Therefore, and although no tension measurement has been performed during this study, it would be interesting to use new tools in the field [124] to measure local changes in tension upon stretch-release cycle.

Interestingly, the fission of the evaginations as exosomes was not observed. This would have involved an abrupt change in fluorescence intensity due to the detachment of the structure from the PM and the release of fluorescently labelled vesicles, which are both features that were never recorded under the experimental conditions used here. The slow decrease in fluorescence observed during the recovery phase after stretch correlates with the flattening mechanism proposed in which the evaginations would be decreasing in size and therefore in amount of membrane with time.

Regarding IRSp53 mechanosensing, *in vitro* studies have related the duality between scaffolding and sensing existing around BAR domain containing proteins [210,211] to concentration of the protein in the bulk [140]. Provided that when working at very low expression levels of IRSp53, similar to the endogenous ones, the signal to noise ratio was so small that no quantifications could be done, this study had to be done under over-expression conditions. However, no proof of stabilisation and therefore scaffolding of the evaginations was found during the analysis of dynamics after stretch. This provides support for the hypothesis of evagination sensing and subsequent mechanotransduction event. Also, work done by Prévost and colleagues has shown IRSp53 phase separates in pulled tubes at low tension [171]. This idea could be extrapolated to the system

Chapter 5 – DISCUSSION

presented in this work, reinforcing IRSp53 clustering at the non-tensed evaginations.

To study enrichment with time, quantification trials on this parameter were tried. Unfortunately, they did not yield any significant result due to the low signal to noise ratio achieved during IRSp53 WT or mutated over-expression. These noisy quantifications lead to a magnification of the error that resulted in a bad readout of such dynamics. The low endogenous levels of BAR proteins and the lack of resolution on the Z plane of optical microscopes have made dynamic enrichment quantifications in cell context an issue for the whole field of study. Therefore, the use of APEX staining was the selected technique to counterpart this outcome. Although these experiments were also done under over-expression conditions, ultrathin sectioning of the sample eliminated the background generated by the cytoplasm and TEM imaging allowed to have enough resolution to accurately distinguish the enrichment of the protein. This result, together with the functional assay performed with the mutants, provides a strong support for the mechanosensing mechanism proposed in this thesis.

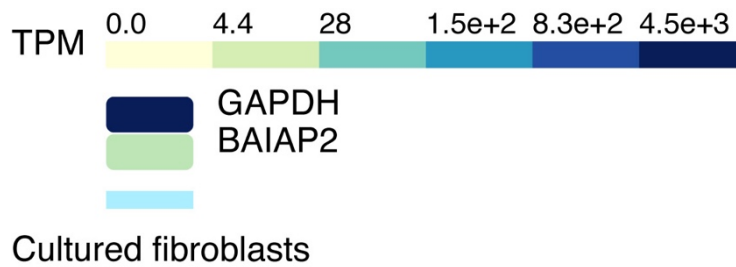


Figure 28: BAIAP2 (gene name of the protein IRSp53) expression levels in cultured fibroblasts compared to GAPDH. Expression levels are shown in transcripts per million reads (TPM²). Data extracted from the GTEx project [212]

The IRSp53-Rac1-WAVE2-Arp2/3 cascade, described here to be involved in evaginations flattening, was earlier associated to membrane ruffling [165,185]. In that sense, it is interesting to observe how this pathway can be readapted to flatten a structure rather than generating a new one (pulling opposite to pushing

² Expression levels on the GTEx Portal are shown in Transcripts Per Million (TPM). This unit is calculated as follows:

$$\text{TPM} = \frac{n_t}{\tilde{l}_t} \left(\sum_{k \in T} \frac{n_k}{\tilde{l}_k} \right)^{-1} \times 10^6$$

where n_t is the number of reads for transcript/gene t , \tilde{l}_t is the normalized transcript/gene length, and T is the set of all transcripts or genes [212].

PM). Understanding how the same cascade can lead to opposite actin dynamics would require further investigation, but the model developed in this work represents a first approach in depicting counterintuitive actin dynamics.

In this regard, it has to be noted that in the proposed molecular loop myosin contractility plays no role. Instead, forces generated by actin polymerization alone and the reattachment of the newly formed network of filaments to the PM seems to be sufficient to pull on the evagination and flatten the structure.

With respect to the role of Rac1 in this system, the order of interaction between this molecule and IRSp53 is a question difficult to address. Other works have already pointed at the dual behaviour of IRSp53 as an upstream and downstream interactor of Rac1 [213]. Indeed, the mechanism proposed in this thesis involving I-BAR mechanosensing and scaffolding of the rest of the partners, represents a compatible hypothesis with those previous findings. Since both active Rac1 and WAVE2 are already present at the PM, it would make sense to think that the sensing of the evaginated structure by IRSp53 and subsequent clustering, would gather them together to start the machinery needed for actin polymerisation. This hypothesis is consistent with the results observed during mutant dynamics, where even when the I-BAR domain is removed, IRSp53 still aggregates at the PM due to the presence of its binding partners that target it there.

Additionally to the mechanosensing mechanism proposed in this work, the explanation for spatial segregation of molecules performing the signalling loop can be related to lipid sorting [214]. This feature has been related to Rac1 spatial compartmentalisation [26] and it is also known that WAVE2 binds preferentially to PIPs [84,93]. Moreover, *in vitro* studies using BAR proteins in general, and IRSp53 in concrete, have extensively demonstrated the preference of these proteins for PIPs binding [93]. Since BAR domain interactions with the PM involve electrostatics [210], it is to be expected that negatively charged lipids would be of preference for these proteins. Having this into account, it is possible to hypothesise that curvature generation might influence the sorting of conical lipids, favouring the sensing of IRSp53 and fostering the presence of Rac1 and WAVE2 to evaginations. This spatial compartmentalisation would direct the interaction between the three of them and therefore, point actin polymerisation to that specific topography.

Another important aspect related to Rac1 role in this system is the involvement of this small GTPase as a master regulator of actin dynamics, directly leading the processes of lamellipodial extension. Therefore, and although there is an effect in evaginations resorption speed when DN Rac1 is expressed, it cannot be ensured

Chapter 5 – DISCUSSION

that this is a direct consequence of the modification on actin dynamics locally at the level of compression-generated evaginations. The possibility that this effect is due to the involvement of Rac1 in lamellipodial extension and actin dynamics at the level of the whole cell has, as well, to be considered.

Finally, while most of the studies have traditionally focused on stretch separately from the subsequent compression provoked by its release [101,102,215], here it is the coupling between both what is studied. This provides a more physiologically relevant view to address cell behaviour, since in our body cells and tissues are often submitted to cyclic stretches rather than the isolated stimulus. Such coupling takes place for instance in heart beating, the musculoskeletal system, or in many developmental scenarios. Thus, and although this remains to be explored, our mechanism could be relevant in events such as the fast compressions of cells embedded in connective tissues [216], the cyclical extensions and contractions undergone by endothelial cells in blood vessels [63], or apical expansion and contractions of amnioserosa cells during dorsal closure in *Drosophila* embryos [217], among many others.

Although the topography adopted by cyclically stretched and compressed cells has not been well characterised *in vivo* due to the high complexity of the required set up, one possible simpler experiment to address this question would involve the use of cell monolayers laying on a substrate emulating a basement membrane and in which the apical side is exposed to a lumen. Such system could be easily coupled to our stretch system and PM topographical rearrangements at the multicellular level after mechanical stimulation could be studied and related to the model proposed in this work. Hopefully, more *in vitro* systems allowing the fine study of biochemical changes triggered by mechanical stimulation, such as the ones exposed in the following works [215,218], would be developed in the next years allowing to bridge the gap between single cell and tissue and organ level.

In conclusion, the findings exposed in this thesis reveal a new mechanosensing mechanism explaining how cells are able to detect physical stimuli at a local, sub- μm scale through their PM, and how this topography modification becomes coupled to a molecular cascade which involves the action of actin polymerising molecules. Altogether, this mechanism offers a quick response for whole cell adaptation to a changing environment.

Chaper 6 - CONCLUSIONS

The aim of this thesis was to unveil the molecular mechanisms by which cells detect and respond to mechanically induced changes in their PM and tension upon the application of stretch-release stimulus. Here, I list the conclusions obtained from this study answering the original question:

1. Mechanical perturbation of cells through physiological stretch-release stimulation results in the formation of bud-shaped evaginations around 115 nm average width in the head and 83 nm average width in the neck that protruded from the apical membrane.
2. The curvature of this evaginations, being 0.03 nm^{-1} for the head and 0.02 nm^{-1} for the neck lays within the range of sensing of I-BAR proteins.
3. Actin is recruited to bud-shaped evaginations within the frame of $\sim 15 \text{ s}$ after their formation.
4. Ezrin is recruited to bud-shaped evaginations within the frame of $\sim 24 \text{ s}$ after their formation, indicating the sealing of the PM and the cortex.
5. IRSp53 mechanosenses the stretch-release generated evaginations and recruits NPFs to mediate a node of actin polymerization that flattens the structure.
6. When IRSp53 is removed, either partially or totally, the flattening of the evaginations and thus, the recovery of PM homeostasis, is impaired.
7. The effect of IRSp53 on actin remodelling is local and does not have any impact on other actin-related processes such as lamellipodia extension after stretch, or in other PM topography remodelling mechanisms, as osmotically induced VLDs.
8. IRSp53 needs both its I-BAR and SH3 domain to be able to couple PM topography to NPFs that will further direct actin polymerisation at the

Chapter 6 – CONCLUSIONS

evaginations. Mutations in these domains substantially delay PM homeostasis recovery after stretch, suggesting that, the longest IRSp53 or the recruited NPFs take to arrive to the evagination, the slower the process is.

9. IRSp53 is enriched at stretch-release generated evaginations, as shown by APEX staining in TEM images.
10. Arp2/3 is the actin polymerising complex mediating flattening of evaginations in this mechanosensitive cascade.
11. Contractility is not involved in PM homeostasis recovery after cell stretch.
12. Rac1 activity influences the polymerisation node either by speeding up or delaying the recovery process after stretch.
13. Theoretical modelling of the mechanosensitive cascade predicts a centripetal flow of actin due to a local decrease in tension that would explain why Arp2/3 branched polymerisation can flatten, instead of pushing, the stretch-release generated evagination.

APPENDIX A – IMMUNOSTAINING PROTOCOL FOR PM BOUND PROTEINS

At the beginning of this thesis, the data gathered by the laboratory in previous work [52] pointed at the formation of invaginations due to stretch-release stimulation of cells. However, the first experiments performed with SEM demonstrated that at the apical side, the PM was protruding due to compression. This suggest that the direction of the PM folds happens in a way to minimise friction with the surrounding media. This behaviour prompted the hypothesis that, if folds were formed at the basal side, then they should bend inwards as the cytosol and the cortex offer less resistance that the PDMS substrate.

Based on this, we decided to perform and immunocolocalisation assay of endogenous N-, F- and I-BARs under the premise that the stretch-release generated structures could act as templates for a mechanosensation event that would lead to PM shape recovery.

To that end immunostainings of several BAR proteins were performed. However, doing this technique involves disruption of PM to allow the entrance of antibodies, which has an impact on the PM itself and in the position of the proteins bound to it. To solve this issue, strong efforts were done in order to improve the immunostaining protocol to preserve the structure of the PM as much as possible.

However, not much literature revising specific immunostaining protocols is available. Therefore, this appendix was included as an attempt to print some findings regarding the improvement of such protocol.

APPENDIX A

The first step for immunostaining is fixation, which involves the preservation of the structure of the sample for further manipulation. There are two types of fixatives, crosslinkers and organic solvents. PFA and Glutaraldehyde lay within the first group. Those two fix proteins by linking their amino groups. On the contrary, organic solvents like methanol and acetone, dehydrogenate proteins and make them precipitate. Crosslinkers are good at preserving cell structure and also are less harmful for fluorescently transfected proteins, however, they are still harsh to phospholipids in the PM, removing a part of them [219]. On their side, organic solvents are quicker in fixation and preserve very well nucleic acid components. Their principal drawback is that they completely destroy the PM leading to cytoplasm leaking and loss of cell content. On the other hand, the crosslinking effects of the first group provoke that some epitopes become masked, thus making antibodies incapable to recognise them [220]. To prevent epitope masking, denaturising protocols involving urea or heat treatment of the sample can be performed in order to expose the hidden epitope [221]. Last, crosslinkers can give high auto-fluorescence (as it is the case for glutaraldehyde), so it is common practice to use a quenching step to eliminate the autofluorescence and to crosslink the possible free amino groups remaining on the sample which contribute to undesired background. Chemicals such as ammonium chloride or sodium borohydride can be used to this end [222–224], but also small amounts of glycine can be added to the blocking buffer in order to prevent this [225].

Another important thing to consider when fixing a sample is the temperature of the fixative. Organic solvents are used at -20°C , while crosslinkers can be used cold (4°C), at RT or even warm (37°C). While increasing the temperature helps in increasing the speed at which the fixative penetrates the tissue, higher temperatures induce cells blebbing while they die, introducing artefacts in the sample [226,227]. Glutaraldehyde fixes faster, but penetrates slower in the tissues, while for PFA is the opposite. This implies that usually a mixture between both would be the most suitable in the majority of the cases.

The next step in fixation involves permeabilising the sample. As mentioned before, organic solvents already remove large amounts of PM phospholipids, making this step unnecessary and shortening the total time of the protocol. However, samples fixed with crosslinkers require further permeabilisation to allow for antibody entrance. Permeabilising agents are detergents which remove phospholipids from the membrane and create holes on it, this is why, when attempting to stain PM bound proteins, this step has to be done with extreme care. The most widely used detergents are Triton-X100 and Tween-20, which

unselectively remove phospholipids from the PM. Both of them are used at concentrations ranging from 0.1 to 0.5% in v/v during 5-10 min. On the milder side of permeabilising agents we have saponins and digitonin, which selectively remove cholesterol and are more suitable for the purpose of BAR protein staining. Those can be used in concentrations similar to Triton and Tween, but Abcam advises concentrations of 100 μ M for digitonin [225]. Nevertheless, it is important to note that the effect of these two can be removed with washings, so it is important to keep them at 0.1% v/v in the washing buffer. Indeed, saponins do not permeabilise nuclear membranes, hence they are not suitable for nuclear proteins.

It is also important to consider election of the buffer for the washings. PBS is often the choice, but variations of this last, such as PBS⁺⁺ supplemented with 1 mM of CaCl₂ and 1 mM of MgCl₂, which stabilise PM and prevent cell detachment, are also interesting options.

Finally, the blocking can also be done in different ways. The object of this step is to prevent undesired binding of the antibody to other substrates that are not the epitope to what it has been raised. The most common blocking solutions include serum, gelatine or milk in concentrations variable from 1 to 5% v/v diluted in the washing buffer of our choice [220,225]. Incubations can span from 30 to 60 min at RT, but on my experience, the longer within that range of times, the better. As mentioned before, a small amount of glycine (Abcam advises 0.3 M) can be added to the blocking solution to crosslink free aldehyde groups which produce high background.

The standard immunostaining procedure in our laboratory included a short fixation step with 4% PFA during 15 min at RT, permeabilization with 0.1% Triton-X100 for 4 min and blocking during 1 h with 2% fish gelatine. While very effective for cytoskeletal proteins, PM was observed to be harmed by using this procedure and the appearance of blebs was observed too. This is why an assay testing different types of fixatives and permeabilising agents was developed.

The efficiency of the standard protocol of the lab to keep the live location of ectopically expressed BAR proteins was also analysed. Controls performed by monitoring the same cell previously transfected with the marked protein plus a membrane marker before and after the addition of 4% PFA showed a partial wash-out of the protein after this step.

After this outcome, different fixatives and permeabilising agents were tested in order to minimize the damaging effects on both PM and its associated proteins. Regarding the fixatives, different PFA concentrations ranging from 2 to 4% in

APPENDIX A

combination with 0.2 to 2% Glutaraldehyde at RT and at 37°C were tested. Fixation with osmotic support, consisting in fixing the samples with 4% PFA plus 0.4% Glutaraldehyde in the presence of 0.8 M Sorbitol to avoid cell permeabilization was also tested. This protocol yielded nice results, however, samples resulted difficult to permeabilise and high concentrations of Triton-X100 had to be used, impairing the proper conservation of PM. Finally, a recent article using a new crosslinker fixative called Glyoxal described better retrieval of antigen targets in the PM as well as in other cell structures when this aldehyde was used [228]. Hence, trials with Glyoxal were also performed.

Regarding permeabilising agents, we tested Triton-X100 in concentrations ranging from 0.1 to 0.5% for 4 min, Tween-20 from 0.1-0.4% for 20 min and saponins from 0.1-1%. But, apart from Triton-X100, none of the other permeabilising agents seemed to alter visually the PM.

After visual analysis of the samples, it was concluded that combination of Glyoxal fixation with the use of saponins gave the best results. Nevertheless, the lack of monoclonal antibodies and the low resolution in the Z plane obtained with optical microscopes prompted the search for alternative staining techniques, such as the APEX2 tag used in the main body of the results of this thesis.

From the screening of BAR proteins performed, very few results could be extracted. As mentioned before, the lack of existence of monoclonal antibodies suitable for immunofluorescence together with the inherent disruption of the PM carried by fixation yielded an inconclusive outcome. However, it was interesting the fact that in the staining against the F-BAR protein FCHO1 some aggregates of the protein were found in close proximity of the areas where stretch-release folds were formed (Fig. 29).

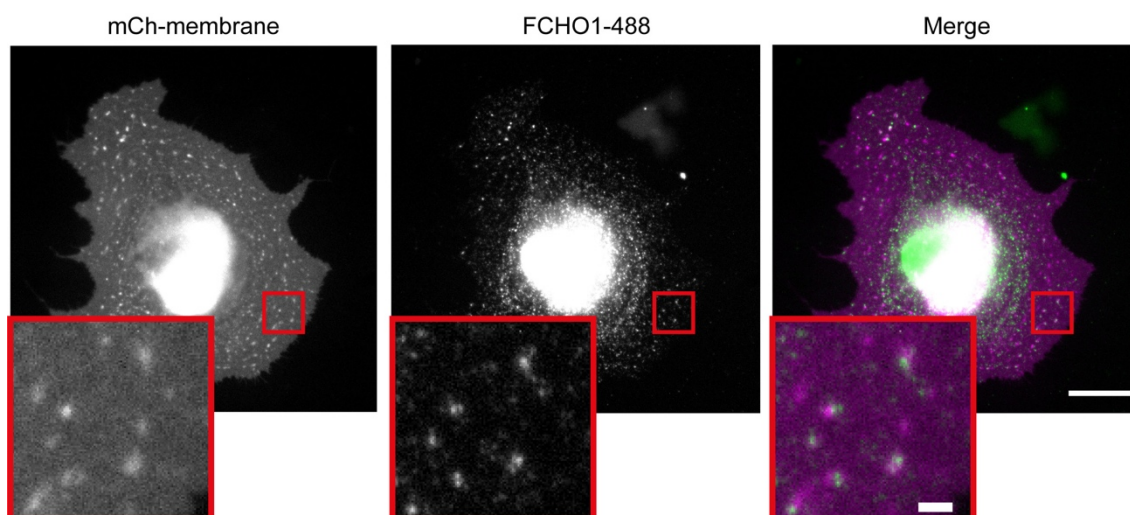


Figure 29: FCHO1 staining in NHDF. After stretch, NHDF cells were fixed in cold glyoxal as explained in the protocol and stained against FCHO1 (HPA041653 Sigma) using a concentration of 1:50 overnight at 4°C. Secondary antibody Alexa-488 (A-21206 ThermoFisher) 1:500 for 90 min at RT. Aggregates can be observed nearby the stretch-release generated PM topography.

Protocol: IF for PM Associated Proteins

Estimated time: 2 days

List of materials

Sample mounting

Compounds	Amount for 1 sample
Prolong™ (ThermoFisher)	30μL
Coverslips of the desired size	1

Fixative solution

Compounds	Amount to prepare 4mL
Distilled H ₂ O	2.835mL
100% ethanol	789μL
Glyoxal	313μL
Acetic acid	30μL

Vortex and bring the pH to 4 or 5 by adding some drops of NaOH 1M. Keep the solution at 4°C. It can be used within the next few days, but ideally prepare it fresh.

APPENDIX A

1X PBS supplemented with NaN_3

Compounds	Amount to prepare 1L
NaN_3	0.2g
PBS 10X	100mL
MQ H_2O	900mL

**You can also use CaCl_2 and MgCl_2 supplemented PBS. The presence of the cations helps on stabilising PM components.*

Saponins Stock solution

Compounds	Amount to prepare 2mL	Final Concentration
Saponins	200 μg	10%
1X PBS	2mL	-

**It must be freshly prepared, as saponins get quickly degraded. Once prepared, the solution can be stored at 4°C for 24h.*

Blocking and Permeabilising (blockperm) Buffer

Compounds	Amount to prepare 40mL	Final Concentration
Fish Gelatine	800 μL	2%
Saponins 10%	400 μL	0.1%
1X PBS	38.8mL	-

Steps

1. Prepare the Fixative solution and cool it down to 4°C by placing it on ice.
2. Prepare a box with some ice and place your samples on it.
3. Quickly remove the media from your samples and add some cold fixative on top.
4. Incubate on ice for 30min + 30min at RT. There is no need to change the fixative.
5. After this time, remove and properly discard fixative and wash your samples 3x10min in PBS.
6. Block and permeabilise your samples with the blockperm buffer 6x10min washings.

7. Meanwhile, prepare your primary antibodies by diluting them at the desired concentration in the blockperm buffer. Place them always on ice.
8. Incubate overnight at 4°C. A good trick is to use 75-80µL of antibody-containing solution and to cover your sample with a 22mm coverslip to prevent from drying. Otherwise you can prepare a humidified chamber (see <https://www.youtube.com/watch?v=GjeLnKbVlrU>)
9. On the next morning remove and discard the coverslips by using tweezers and wash your sample 3x10min with your blockperm buffer. You can increase the washings if at the end of your staining you have a lot of background.
10. Meanwhile, prepare your secondary antibodies by diluting them at the desired concentration in the blockperm buffer. Use an Eppendorf tube wrapped in aluminium foil to protect from light. Keep them always on ice.
11. Use 75-80µL of antibody dilution to cover your sample and incubate for 2h at RT protected from light.
12. Wash 3 quick times with your blockperm buffer to remove the excess of secondary antibody plus 3x10min to completely remove all the unbound antibody.
13. Image your samples or, alternatively mount them using 30µL of Prolong and a coverslip. After mounting leave your sample at least for 24h at RT until prolong gets dried. If your sample is on top of PDMS wait at least 72h before imaging your sample.

**Notes*

- *As PBS is supplemented with NaN₃, samples can be stored post-fixation at 4°C up to 1 week.*
- *You can change glyoxal for other types of fixatives, like PFA or glutaraldehyde or a mixture of these two. Just keep in mind that when using glutaraldehyde for immunostaining you will get a high autofluorescence in green, so make sure you do appropriate controls.*

APPENDIX B – BAR PROTEINS KNOCK-DOWN GENERATION

Together with immunostaining, we approached the question of understanding if compression-generated folds could be recognised by BAR proteins running a silencing assay against different N-, F- and I-BAR candidates. It has to be noted that both immunostaining screening and KD assay were done at the same time as EM experiments, therefore, we were still starting to understand the sign of the curvature of stretch-release generated folds. Indeed, this was a small screening to start with the project and other candidates were planned to be added in case of negative results. Most of the candidates were F-BAR proteins due to their ability to bind shallower curved structures (matching the previous described size for the compression generated folds of ~500nm) and because of their multiple domains to interact with actin.

To this end, stable NHDF lines silencing the N-BAR proteins Amphiphysin and GRAF-1, the F-BAR proteins FCHO1, FBP17 and TOCA1 and the I-BAR protein IRSp53 were generated. Additionally, another cell line expressing a non-targeting shRNA was created as a control.

The results of the silencing assay resulted positive for IRSp53 KD (Fig. 14 A-C). However, other interesting data was obtained for the other BAR proteins and lack of time and the need to focus on one single research line made us abandon the study of the other phenomena.

For Amphiphysin, GRAF-1, FBP17 and TOCA1, no phenotype was observed when knocked-down in NHDF (Fig. 30 A-D). However, it has to be noted that these experiments were only performed once (or twice in the case of GRAF-1) and no statistical analysis could be run on the data due to the low N. Also, no

validation of the KD levels was performed, making impossible to depict any hypothesis from the results obtained.

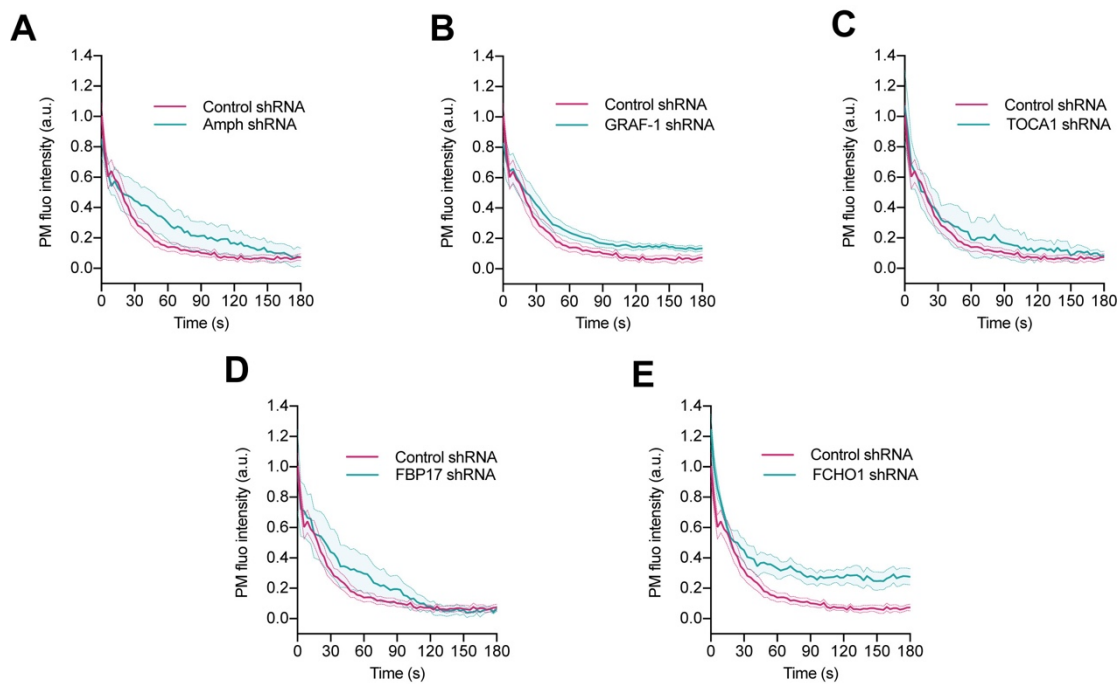


Figure 30: BAR proteins knock-down in NHDF. Time-course dynamics of compression generated PM evaginations in (A) Amphiphysin, (B) GRAF-1, (C) TOCA-1, (D) FBP17 and (E) FCHO1 silencing. Cells were transfected with EGFP-membrane. N = 17, 4, 11, 4, 4 and 5 cells from 4, 1, 2, 1, 1 and 2 independent experiments. Data show mean \pm s.e.m.

Interestingly, and coinciding with what was observed when immunostaining was performed, FCHO1 knock-down produced a milder effect on PM homeostasis recovery after stretch (Fig. 30 E). In this case, the curve describes a first phase following an exponential decay that matches the one of the controls. Nevertheless, after timepoint 45s both curves diverge and while controls complete recovery, FCHO1 KD cells retain some membrane structures. We hypothesized that FCHO1, being one of the first proteins participating in CME [229,230], could have an impact on the endocytic rates of the cell after stretch and, ultimately, this would have an impact in the PM turnover dynamics. Another exciting possibility is that the bright fluorescent spots that we observe through fluorescence imaging that do not have correlation with the 3D SEM imaging could be invaginations being flattened trough FCHO1. This would also explain why there is an exponential decay on one part of the resorption curve, most likely related to the flattening of evaginations through the local IRSp53 mechanism described here, followed by the plateau-like part which could represent not resorbed invaginations in the basal part of the PM. However, understanding if

APPENDIX B

FCHO1 plays an important role in topography remodelling after stretch and weather these two mechanisms conform the two sides of a bigger process involving whole cell homeostasis recovery after stretch would require further investigation.

APPENDIX C – MECHANICAL EFFECTS ON AMPHIPHYSIN TUBULATION IN CELLS

As part of the work by Le Roux et al. [2] in which the remodelling of mechanically generated PM templates by BAR proteins was studied, a series of experiments, comprised on this appendix, were performed.

In their study, Le Roux observed how synthetic lipid bilayers (SLB) stretched and release by the same protocol followed in this thesis, formed tubes and buds upon compression. When the N-BAR protein Amphiphysin was added to the buffer, concentration-dependent remodelling of such membrane structures happened. On the contrary, non-mechanically stimulated SLBs did not display any topographical change mediated by Amphiphysin.

To study if mechanical stimulation through stretch could also trigger Amphiphysin-mediated reshaping in cells, this protein was over-expressed in NHDF. Amphiphysin tubes formed before, during and after stretch (Fig. 31 A), but their number was significantly lowered during the stretch phase (Fig. 31 C), probably due to PM tension increase. Interestingly, when stretch was release, a significant increase in the number of tubes was observed (Fig. 31 C). The tubes formed in localisations near to compression-generated folds, suggesting that maybe the topography formed at the basal PM of the cell can give rise to evaginations which act as a template for Amphiphysin remodelling (Fig. 31 B). Although over-expression of this protein will for sure give levels above physiological conditions, these experiments evoke the fact that mechanical stimulation can act as a trigger for BAR proteins tubulation.

APPENDIX C

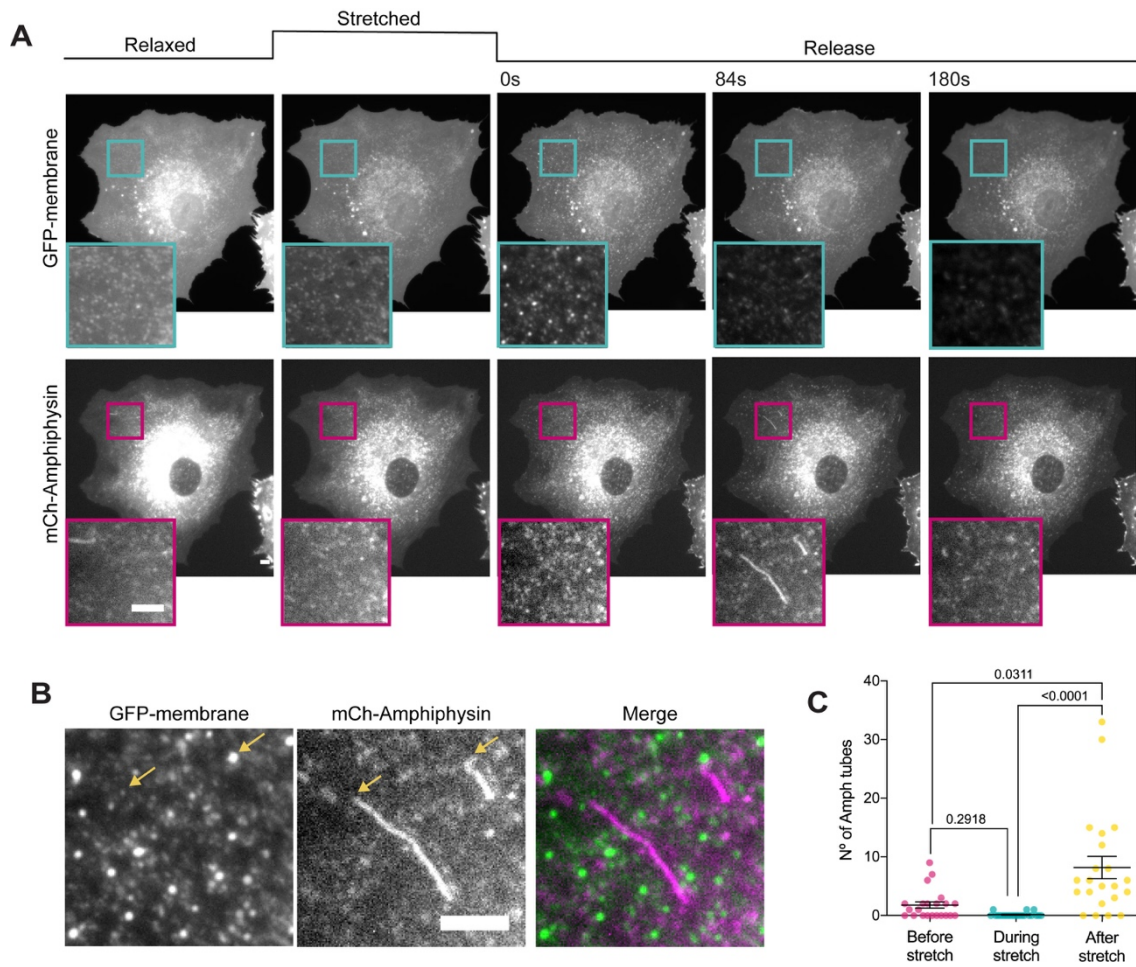


Figure 31: Mechanical stretch triggers Amphiphysin-mediated tubulation in cells. (A) Representative images GFP-membrane and mCh-Amphiphysin transfected cells before, during and after stretch release. **(B)** Detail of membrane and Amphiphysin channels during stretch-induced tubulation. **(C)** Quantification of the number of Amphiphysin tubes at rest, during stretch and once stretch is released (N=22 cells from 3 independent experiments). Scale bars, 5 μ m. Data show mean \pm s.e.m.

APPENDIX D – SEM IMAGES OF COMPRESSION-GENERATED EVAGINATIONS IN IRSp53^{-/-} and IRSp53^{-/-R} MEF

In an attempt to understand if there were morphological discrepancies between the size and shape of compression generated evaginations under the lack of IRSp53, SEM image acquisition of IRSp53^{-/-} and IRSp53^{-/-R} MEF was performed. No differences were observed during those experiments, however, some examples of the images acquired are compiled in this appendix with the purpose of showing the homogeneity of this mechanically generated evaginations and to show some beautiful zooms that perfectly reveal their bud-shaped nature.

APPENDIX D

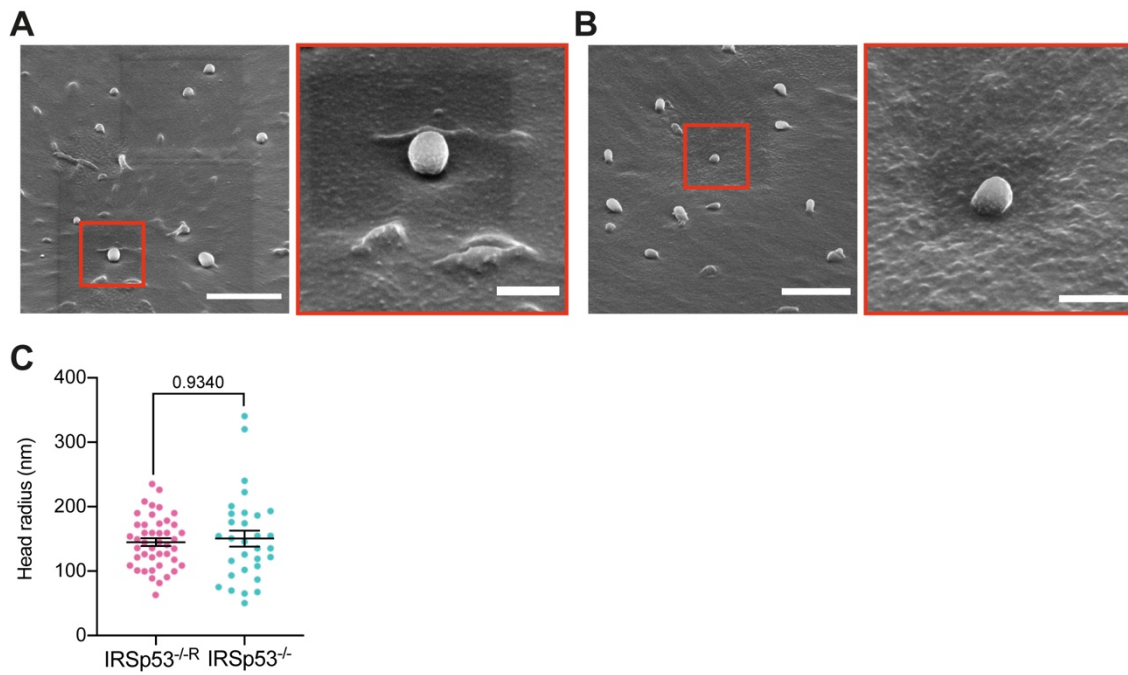


Figure 32: Evaginations ultrastructure in IRSp53^{-R} and IRSp53^{-/-} MEF. (A) PM evaginations generated by stretch-release in the apical side of IRSp53^{-R} MEF. (B) PM evaginations generated by stretch-release in the apical side of IRSp53^{-/-} MEF. Scale bars are 2 μ m for the big images and 500 nm for the insets. (C) Head radius estimation for IRSp53^{-R} and IRSp53^{-/-} cells. Note that here radii are slightly bigger than the ones taken with TEM due to the lack of accuracy in the measurements and the lower resolution of the technique. N = 44 and 31 evaginations from 3 and 3 cells from 1 experiment. Differences were tested through Mann-Whitney test. Data show mean \pm s.e.m.

APPENDIX E – IRSp53 PLASMIDS SEQUENCING

Colour key for sequencing:

Domain	Colour
I-BAR domain	purple
CRIB domain	cyan
SH3 domain	green
Mutations	red

pC1-EGFP-mouse-IRSp53-WT (isoform 4, also known as BAIAP-alpha):

MSLSRSEEMHRLTENVYKTIMEQFNPSLRNFIAMGKNYEKALAGVTFAAKGYFDALVKM
 GELASESQGSKELGDVLFQMAEVHRQIQNQLLEETLKSFHNELLTQLEQKVELDSRYLSA
 ALKKYQTEQRSKGDALDKCQAE LKKLRKKSQGSKNPQKYS DKELQYIDAISNKQGELEN
 YVSDGYKTALTEERRRFCFLVEKQCAVAKNSAAYHSGKELLAQKLPLWQQACADPNKI
 PDRAVQLMQQMANSNGSILPSALSASKSNL **VISDPIPGAKPLVPPELAP**FVGRMSAQE
 NVPVMNGVAGPDS EDYNPWADRKAAQPKSLSP PQSQSKLSDSYSNTLPVRKSVTPKNSY
 ATTENKTLPRSSSMAAG **LERNGRMRVKAI**FSHAAGDNSTLLSFKEGDLITLLVPEARDG
 WHYGESEKTKMRGWFPFSYTRVLDS DGSDRLHMSLQQGKSSSTGNLLDKDDLALPPPDY
 GTSSRAFPTQTAGTFKQRPYSVAVPAFSQGLDDYGARSVSSGSGTLVSTV

pC1-EGFP-mouse-4KE-IRSp53:

MSLRSEEMHRLTENVYKTIMEQFNPSLRNFIAMGKNYEKALAGVTFAAKGYFDALVKMG
 ELASESQGSKELGDVLFQMAEVHRQIQNQLLEETLKSFHNELLTQLEQKVELDSRYLSAA
 LKKYQTEQRSKGDALDKCQAE **EE**LR**EE**SQGSKNPQKYS DKELQYIDAISNKQGELENY
 VSDGYKTALTEERRRFCFLVEKQCAVAKNSAAYHSGKELLAQKLPLWQQACADPNKI P
 DRAVQLMQQMANSNGSILPSALSASKSNL **VISDPIPGAKPLVPPELAP**FVGRMSAQEN
 VPVMNGVAGPDS EDYNPWADRKAAQPKSLSP PQSQSKLSDSYSNTLPVRKSVTPKNSYA
 TTENKTLPRSSSMAAG **LERNGRMRVKAI**FSHAAGDNSTLLSFKEGDLITLLVPEARDGW

APPENDIX E

HYGESEKTKMRGWFPFSYTRVLDS DGSDRLHMSLQQGKSSSTGNLLDKDDLALPPPDYGTSSRAFPQTAGTFKQRPYSVAVPAFSQGLDDYGARSVSSGSGTLVSTG

pC1-EGFP-mouse-I268N-IRSp53:

MSLSRSEEMHRLTENVYKTIMEQFNPSLRNFIAMGKNYEKALAGVTFAAKGYFDALVKMGELASESQGSKELGDVLFQMAEVHRQIQNQLLEETLKSFHNELLTQLEQKVELDSRYLSAALKKYQTEQRSKGDALDKCQAE LKKLRKKSQGSKNPQKYS DKELQYIDAISNKQGELENYVSDGYKTALTEERRRFCFLVEKQCAVAKNSAAYHSGKGKELLAQKLPLWQQACADPNKIPDRAVQLMQQMANSNGSILPSALSASKSNLVNSDPIPGAKPLVPPELAPFVGRMSAQENVPVMNGVAGPDSE DYNPWADRKAAQPKSLSP PQSQSKLSDSYSNTLPVRKSVTPKNSYATTENKTLPRSSSMAAGLERNGRMRVKAI FSHAAGDNSTLLSFKEGDLITLLVPEARDGWHYGESEKTKMRGWFPFSYTRVLDS DGSDRLHMSLQQGKSSSTGNLLDKDDLALPPPDYGTSSRAFPQTAGTFKQRPYSVAVPAFSQGLDDYGARSVSSGSGTLVSTG

pC1-EGFP-mouse-I403P-IRSp53:

MSLSRSEEMHRLTENVYKTIMEQFNPSLRNFIAMGKNYEKALAGVTFAAKGYFDALVKMGELASESQGSKELGDVLFQMAEVHRQIQNQLLEETLKSFHNELLTQLEQKVELDSRYLSAALKKYQTEQRSKGDALDKCQAE LKKLRKKSQGSKNPQKYS DKELQYIDAISNKQGELENYVSDGYKTALTEERRRFCFLVEKQCAVAKNSAAYHSGKGKELLAQKLPLWQQACADPNKIPDRAVQLMQQMANSNGSILPSALSASKSNLVISDPIPGAKPLVPPELAPFVGRMSAQENVPVMNGVAGPDSE DYNPWADRKAAQPKSLSP PQSQSKLSDSYSNTLPVRKSVTPKNSYATTENKTLPRSSSMAAGLERNGRMRVKAI FSHAAGDNSTLLSFKEGDLPTLLVPEARDGWHYGESEKTKMRGWFPFSYTRVLDS DGSDRLHMSLQQGKSSSTGNLLDKDDLALPPPDYGTSSRAFPQTAGTFKQRPYSVAVPAFSQGLDDYGARSVSSGSGTLVSTG

pC1-EGFP-human-IRSp53-WT

MSLSRSEEMHRLTENVYKTIMEQFNPSLRNFIAMGKNYEKALAGVTYAAKGYFDALVKMGELASESQGSKELGDVLFQMAEVHRQIQNQLLEMLKSFHNELLTQLEQKVELDSRYLSAALKKYQTEQRSKGDALDKCQAE LKKLRKKSQGSKNPQKYS DKELQYIDAISNKQGELENYVSDGYKTALTEERRRFCFLVEKQCAVAKNSAAYHSGKGKELLAQKLPLWQQACADPSKIPERAVQLMQQVASNGATLPSALSASKSNLVISDPIPGAKPLVPPELAPFVGRMSAQES TPIMNGVTGPDGEDYSPWADRKAAQPKSLSP PQSQSKLSDSYSNTLPVRKSVTPKNSYATTENKTLPRSSSMAAGLERNGRMRVKAI FSHAAGDNSTLLSFKEGDLITLLVPEARDGWHYGESEKTKMRGWFPFSYTRVLDS DGSDRLHMSLQQGKSSSTGNLLDKDDLAI PPDYGAASRAFPQATASGFKQRPYSVAVPAFSQGLDDYGARSMSSGSGTLVSTV

pC1-EGFP-IBAR-domain

MSLSRSEEMHRLTENVYKTIMEQFNPSLRNFIAMGKNYEKALAGVTYAAKGYFDALVKMGELASESQGSKELGDVLFQMAEVHRQIQNQLLEMLKSFHNELLTQLEQKVELDSRYLSAALKKYQTEQRSKGDALDKCQAE LKKLRKKSQGSKNPQKYS DKELQYIDAISNKQGELENYVSDGYKTALTEERRRFCFLVEKQCAVAKNSAAYHSGKGKELLAQKLPLWQQACADPSKIPERAVQLMQQVASN

pC1-EGFP-ΔIBAR

SGLRSGATLPSALSASKSNLVISDPIPGAKPLVPPELAPFVGRMSAQESTPIMNGVTGPDGEDYSPWADRKAAQPKSLSP PQSQSKLSDSYSNTLPVRKSVTPKNSYATTENKTLPRSSSMAAGLERNGRMRVKAI FSHAAGDNSTLLSFKEGDLITLLVPEARDGWHYGESEKTKMRGWFPFSYTRVLDS DGSDRLHMSLQQGKSSSTGNLLDKDDLAI PPDYGAASRAFPQATASGFKQRPYSVAVPAFSQGLDDYGARSMSSGSGTLVSTV

pC1-EGFP-ΔW413G-IRSP53

MSLSRSEEMHRLTENYKTIMEQFNPSLRNFIAMGKNYEKALAGVTYAAKGYFDALVKM
GELASESQGSKELGDVLFQMAEVHRQIQNQLLEMLKSFHNELLTQLEQKVELDSRYLSA
ALKKYQTEQRSKGDALDKCQAEKLRKKSQGSKNPQKYSKELQYIDAI SNKQGELEN
YVSDGYKTALTEERRRFCFLVEKQCAVAKNSAAYHSGKELLAQKLPLWQQACADPSKI
PERAVQLMQQVASNGATLPSALSASKSNLVISDPIPGAKPLVVPPELAPFVGRMSAQES
TPIMNGVTGPDGEDYSPWADRKAAQPKSLSPQSQSKLSDSYSNTLPVRKSVTPKNSYA
TTENKTLPRSSSMAAGLERNGRMRVKAI FSHAAGDNSTLLSFKEGDLITLLVPEARDG**G**
HYGESEKTKMRGWFPFSYTRVLDS DGSDRLHMSLQQGKSSSTGNLLDKDDLAI PPPDYG
AASRAFPAQ TASGFKQRPYSVAVPAFSQGLDDYGARSMSSGSGTLVS

APPENDIX F – ANALYSIS CODE FOR MEMBRANE EVAGINATIONS DYNAMICS

```

%for 10 reservoirs and 1 cell, with a txt file called PI
%load matrices
clear all
prompt = 'number of cells';
N = input(prompt);
Size = N*10;

%Initialize final matrices
ResMatrixm = zeros(61,Size);
ResMatrixi = zeros(61,Size);
rm = zeros(61,Size);
fm = zeros(61,Size);
om = zeros(61,Size);
ri = zeros(61,Size);
fi = zeros(61,Size);
oi = zeros(61,Size);

%Analyze each individual file, calculate the reservoir final integrate
%density (bilayer subtraction and cell intensity normalization) and
place
%it in the complete matrix

for i=0:N-1;

    [file,path1] = uigetfile('*.txt','Select all Files of the membrane
channel');
    cd(path1);
    C = readmatrix(file);

    %Prepare full matrix
    Time = C(1:61);
    Res = C(end-60:end,2:41);
    Cell = C(end-60:end,42:45);

```

```

%separate areas and MeanI
resA = Res(:,1:2:end);
resI = Res(:,2:2:end);

%separate reservoir mean I from flat bilayer mean I
resIr = resI(:,1:2:end);
resIf = resI(:,2:2:end);

%separate reservoir area from flat bilayer area
resAr = resA(:,1:2:end);
%resAf = resA(:,2:2:end);

%calculate Int Density of reservoirs and bilayer
resIntDr = resAr.*resIr;
resIntDf = resAr.*resIf;

%subtract reservoir from background
IntDsub = resIntDr-resIntDf;

%mean intensity and area matrices of cell and outside
CellI = Cell(:,2);
CellA = Cell(:,1);
OutsideI = Cell(:,4);
%OutsideA = Cell(:,3);

%Calculate cell Int Density and subtract background
CellIntD = CellI.*CellA;
OutsideIntD = OutsideI.*CellA;
CellIntDsub = CellIntD-OutsideIntD;

%final normalised reservoir intensity and their mean
ResNorm = IntDsub./CellIntDsub;
MeanResNorm = mean(ResNorm,2);

%fill matrix of all reservoirs for all cells and for the mean
ResMatrixm(:,1+10*i:10+10*i)=ResNorm*10000
MeanResMatrixm(:,i+1)=MeanResNorm*10000;

%matrix of outside Integrated densities
IntDo = OutsideI.*resAr

%fill matrix for enrichment
rm(:,1+10*i:10+10*i)=resIntDr;
fm(:,1+10*i:10+10*i)=resIntDf;
om(:,1+10*i:10+10*i)=IntDo;
end;

for i=0:N-1;

file = uigetfile('*..*','Select all Files of the protein channel');
C = readmatrix(file);

%Prepare full matrix
Time = C(1:61);
Res = C(end-60:end,2:41);
Cell = C(end-60:end,42:45);

%separate areas and MeanI
resA = Res(:, 1:2:end);

```

APPENDIX F

```
resI = Res(:,2:2:end);

%separate reservoir mean I from flat bilayer mean I
resIr = resI(:,1:2:end);
resIf = resI(:,2:2:end);

%separate reservoir area from flat bilayer area
resAr = resA(:,1:2:end);
%resAf = resA(:,2:2:end);

%calculate Int Density of reservoirs and bilayer
resIntDr = resAr.*resIr;
resIntDf = resAr.*resIf;

%subtract reservoir from background
IntDsub = resIntDr-resIntDf;

%mean intensity and area matrices of cell and outside
CellI = Cell(:,2);
CellA = Cell(:,1);
OutsideI = Cell(:,4);
%OutsideA = Cell(:,3);

%Calculate cell Int Density and subtract background
CellIntD = CellI.*CellA;
OutsideIntD = OutsideI.*CellA;
CellIntDsub = CellIntD-OutsideIntD;

%final normalised reservoir intensity and their mean
ResNorm = IntDsub./CellIntDsub;
MeanResNorm = mean(ResNorm,2);

%fill matrix of all reservoirs for all cells and their mean
ResMatrixi(:,1+10*i:10+10*i)=ResNorm*10000;
MeanResMatrixi(:,i+1)=MeanResNorm*10000;

%matrix of outside Integrated densities
IntDo = OutsideI.*resAr

%fill matrix for enrichment
ri(:,1+10*i:10+10*i)=resIntDr;
fi(:,1+10*i:10+10*i)=resIntDf;
oi(:,1+10*i:10+10*i)=IntDo;
end;

%Export the matrix of all reservoirs intensity (subtracted and
corrected)

%prompt = 'Time of destretch';
%T = input(prompt);
%ResMatrixDestr = ResMatrix(T:end,:);
%writematrix(ResMatrixDestr, 'ResMatrixDestr.xlsx');
path = uigetdir
cd (path);

%Enrichment calculations from PRC routine xarxa_data_analysis_v2

minsig = 0.05; %Minimum membrane signal allowed
```

```

fi2 = fi; % Flat area, irsp53.
fm2 = fm; % Flat area, membrane.
oi2 = oi; % Outside cell, irsp53.
om2 = om; % Outside cell, membrane.
ri2 = ri; % Reservoir, irsp53.
rm2 = rm; % Reservoir, membrane.

% Signal to noise ratios

nfi = (fi2-oi2)./oi2;
nfm = (fm2-om2)./om2;
nri = (ri2-fi2)./fi2;
nrm = (rm2-fm2)./fm2;

ratiot = [];
indit = [];
indmt = [];
badt = [];
endintensity = [];
for i=1:size(fi,2);
    bad = min(find(movmean(nrm(:,i),3) < minsig));
    if isempty(bad) == 1;
        bad = size(fi,1)+1;
    end;
    if bad > 1;
        [trash,indi] = max(nri(1:bad-1,i));
        [trash,indm] = max(nrm(1:bad-1,i));

        ratioflat = (fi2(indi,i)-oi2(indi,i))./(fm2(indi,i)-
om2(indi,i)); %Ratio in flat region
        ratiosres = (ri2(indi,i)-fi2(indi,i))./(rm2(indi,i)-
fm2(indi,i)); % Ratio in reservoir
        ratiot(end+1) = ratiosres./ratioflat; % Ratio of ratios
        indit(end+1) = indi;
        indmt(end+1) = indm;
        endintensity(end+1) = ResMatrixm(end,i);
        badt(end+1) = bad;
    end;

end;

indit = 3*indit;
indmt = 3*indmt;
lag = indit -indmt;

results = [ratiot' indit' indmt' lag' endintensity'];
results(end+1,:) = NaN;

writematrix(results,'tempres.xlsx');
% figure, plot(mean(nrm,2))
% title('Signal to noise ratio, membrane');
% figure, plot(mean(nri,2))
% title('Signal to noise ratio, irsp53');

```

APPENDIX G – PUBLICATIONS AND CONFERENCES

CONFERENCES

- 2021 Life at the Periphery: Mechanobiology of the Cell Surface - EMBO | EMBL Symposium
Poster Presentation: A local mechanosensing mechanism mediated by IRSp53 controls membrane shape homeostasis in response to cell stretch.
- 2019 Actin-based mechanosensation and force generation in health and disease - Universidad Internacional de Andalucía
Poster presentation: Curvature-Sensing Proteins in Stretch-associated Membrane Remodelling.
- 2019 Cell polarity and membrane dynamics - EMBO Workshop
Poster presentation: Curvature-Sensing Proteins in Stretch-associated Membrane Remodelling.
- 2018 Biomedicine PhD day – Universitat de Barcelona
Best poster award: Curvature-Sensing Proteins in Stretch-associated Membrane Remodelling.

PUBLICATIONS

1. **X. Quiroga**, N. Walani, A. Chavero, A. Mittens, A. Disanza, F. Tebar, X. Trepal, R. G. Parton, G. Scita, M. I. Geli, M. Arroyo, A. L. Le Roux, P. Roca-Cusachs. A local mechanosensing mechanism mediated by IRSp53 controls membrane shape homeostasis in response to cell stretch. (submitted)

2. L. Le Roux, C. Tozzi, N. Walani, **X. Quiroga**, D. Zalvidea, X. Trepas, M. Staykova, M. Arroyo, P. Roca-Cusachs. Dynamic mechanochemical feedback between curved membranes and BAR protein self-organization. Nat. Comm. (under review). Impact factor: 12.121 (6/71 Multidisciplinary Sciences)
3. I. Andreu, B. Falcones, S. Hurst, N. Chahare, **X. Quiroga**, A. L. Le Roux, Z. Kechagia, A. E. M. Beedle, A. Elósegui-Artola, X. Trepas, R. Farré, T. Betz, I. Almendros, P. Roca-Cusachs. The force loading rate drives cell mechanosensing through both reinforcement and fluidization. Nat. Comm. (accepted). Impact factor: 12.121 (6/71 Multidisciplinary Sciences)
4. A. L. Le Roux, **X. Quiroga**, N. Walani, M. Arroyo, P. Roca-Cusachs. The plasma membrane as a mechanochemical transducer. Philos. Trans. R. Soc. B Biol. Sci. 374 (2019). Impact factor: 5.680 (15/442 Biology and Biochemistry)

LIST OF ABBREVIATIONS

ACG	Actin chromobody green
ACR	Actin chromobody red
ADP	Adenosine diphosphate
AFM	Atomic force microscopy
ALPS	Amphipathic lipid-packing sensor motif
ANOVA	Analysis of variance
APEX	Ascorbate peroxidase
Arp2/3	Actin-related protein-2/3
ATP	Adenosine triphosphate
BAR	Bin-Amphiphysin-Rvs
BAIAP2	Brain-specific angiogenesis inhibitor 1-associated protein 2
CCTα	Choline-phosphate cytidyltransferase A
Cdc42	Cell division control protein 42 homolog
CLIC-GEEC	Clathrin-independent carriers and GPI-anchored proteins enriched early endosomal compartments
CME	Clathrin-mediated endocytosis
CMV	Cytomegalovirus
CRIB	Cdc42/Rac interactive binding motif
ECM	Extracellular matrix
EGF	Epidermal growth factor
EGFP	Enhanced green fluorescent protein
EHD2	EH domain-containing protein 2
EM	Electron microscopy
Eps8	Epidermal growth factor receptor kinase substrate 8

ERM	Ezrin, Radixin and Moesin
EYFP	Enhanced yellow fluorescent protein
DAB	Diaminobenzidine
DAG	Diacylglycerol
DIAPH1	Diaphanous homolog protein 1
DMEM	Dulbecco's modified Eagle's medium
DMSO	Dimethyl sulfoxide
DNA	Deoxyribonucleic acid
F-actin	Filamentous actin
F-BAR	FER/CIP homology BAR domain
FBP17	Formin-binding protein 1
FBS	Foetal bovine serum
FERM	Four-point-one ERM domain
FH	Formin homology
FYVE	Fab1p, YOTB, Vac1p and EEA1 domain
G-actin	Globular actin
GAP	GTPase-activating protein
GEF	Guanine exchange factor
GDP	Guanidine diphosphate
GFP	Green fluorescent protein
GPCR	G protein coupled receptor
GTP	Guanidine triphosphate
GUV	Giant unilamellar vesicle
HEK	Human embryonic kidney
I-BAR	Inverse BAR domain
IRSp53	Insulin receptor substrate p53, although the recommended name is BAIAP2
JMY	Junction-mediated regulatory protein
KD	Knock-down
KO	Knock-out
L_d	Liquid disordered
L_o	Liquid ordered
mCherry	Monomeric cherry
MEF	Mouse embryonic fibroblasts
MGC	Mechanically gated channel
mTORC2	Mammalian target of rapamycin complex 2
N-BAR	Normal BAR domain

LIST OF ABBREVIATIONS

NHDF	Normal human dermal fibroblasts
NPF	Nucleation promoting factor
NT	Non-targeting
N-WASP	Neural Wiskott-Aldrich syndrome protein
PA	Phosphatidic acid
PB	Phosphate buffer
PBS	Phosphate buffer saline
PC	Phosphatidyl choline
PDMS	Polydimethyl siloxane
PE	Phosphatidyl ethanolamine
PFA	Paraformaldehyde
PH	Pleckstrin homology domain
PI	Phosphatidyl inositol
PIPs	Phosphoinositides
PIP2	Phosphatidyl inositol 4,5 biphosphate
PIP3	Phosphatidyl inositol 3,4,5 biphosphate
PIP5K	Phosphatidyl inositol phosphate 5 kinase
PLC	Phospholipase C
PLD2	Phospholipase D 2
PM	Plasma membrane
PMMA	Polymetacrylate
PNB	Para-nitroblebbistatin
PS	Phosphatidyl serine
PX	Phox homology domain
Rac1	Ras-related C3 botulinum toxin substrate 1
RCB	Rac binding domain
RFP	Red fluorescent protein
RhoA	Transforming protein RhoA (from Ras homolog family member A)
RNA	Ribonucleic acid
RT	Room temperature
SEM	Scanning electron microscopy
SH3	Src homology 3 domain
shRNA	Short hairpin RNA
SLB	Synthetic lipid bilayer
S₀	Solid-like
TEM	Transmission electron microscopy

LIST OF ABBREVIATIONS

TMB	Tandem-monomer-binding
TORC2	Target of rapamycin complex 2
TPM	Transcripts per million
TRP	Transient receptor potential
VLDs	Vacuole-like dilations
WASP	Wiskott-Aldrich syndrome protein
WAVE	Wiskott-Aldrich syndrome protein family member 2
WH2	Wasp homology 2 domain
WRC	WAVE regulatory complex
WT	Wild type

REFERENCES

- 1 Le Roux, A.L. *et al.* The plasma membrane as a mechanochemical transducer. , *Philosophical Transactions of the Royal Society B: Biological Sciences*, 374. (2019)
- 2 Le Roux, A.-L. *et al.* (2020) Dynamic Mechanochemical feedback between curved membranes and BAR protein self-organization. *bioRxiv* DOI: 10.1101/2020.09.23.310169
- 3 Cooper, G. (2000) *The Cell: A Molecular Approach*, (2nd edn) Sinauer Associates.
- 4 Alberts B, Johnson A, Lewis J, *et al.* (2002) *Molecular Biology of the Cell*, (4th edn) Garland Science.
- 5 City, N.Y. *et al.* (2003) Membrane lipids: where they are and how they behave. 299, 1006–1007
- 6 Harayama, T. and Riezman, H. (2018) Understanding the diversity of membrane lipid composition. *Nat. Rev. Mol. Cell Biol.* 19, 281–296
- 7 Suetsugu, S. *et al.* (2014) Phospholipids and Membrane-Deforming Proteins. *Physiol Rev* 94, 1219–1248
- 8 Slotte, J.P. Biological functions of sphingomyelins. , *Progress in Lipid Research*, 52. (2013) , 424–437
- 9 Shurer, C.R. *et al.* (2019) Physical Principles of Membrane Shape Regulation by the Glycocalyx. *Cell* 177, 1757-1770.e21
- 10 Lorent, J.H. *et al.* (2020) Plasma membranes are asymmetric in lipid unsaturation, packing and protein shape. *Nat. Chem. Biol.* DOI: 10.1038/s41589-020-0529-6
- 11 Devaux, P.F. and Morris, R. Transmembrane asymmetry and lateral domains in biological membranes. , *Traffic*, 5. 01-Apr-(2004) , John Wiley & Sons, Ltd, 241–246
- 12 Harvey Lodish, Arnold Berk, S Lawrence Zipursky, Paul Matsudaira, David Baltimore, and J.D. (2000) *Molecular Cell Biology*, (4th edn)

- 13 Singer, S.J. and Nicolson, G.L. (1971) The structure and chemistry of mammalian cell membranes. *Am. J. Pathol.* 65, 427–437
- 14 Ritchie, K. *et al.* The fence and picket structure of the plasma membrane of live cells as revealed by single molecule techniques (Review). , *Molecular Membrane Biology*, 20. (2003) , 13–18
- 15 Kusumi, A. *et al.* Paradigm shift of the plasma membrane concept from the two-dimensional continuum fluid to the partitioned fluid: High-speed single-molecule tracking of membrane molecules. , *Annual Review of Biophysics and Biomolecular Structure*, 34. (2005) , 351–378
- 16 de la Serna, J.B. *et al.* There is no simple model of the plasma membrane organization. , *Frontiers in Cell and Developmental Biology*, 4. 29-Sep-(2016) , Frontiers Media S.A.
- 17 Sadegh, S. *et al.* (2017) Plasma membrane is compartmentalized by a self-similar cortical actin meshwork. *Phys. Rev. X* 7,
- 18 Huang, J. and Feigenson, G.W. (1999) A microscopic interaction model of maximum solubility of cholesterol in lipid bilayers. *Biophys. J.* 76, 2142–2157
- 19 Sengupta, P. *et al.* Lipid rafts, fluid/fluid phase separation, and their relevance to plasma membrane structure and function. , *Seminars in Cell and Developmental Biology*, 18. (2007) , 583–590
- 20 Sevcsik, E. and Schütz, G.J. (2016) With or without rafts? Alternative views on cell membranes. *BioEssays* 38, 129–139
- 21 Sezgin, E. *et al.* The mystery of membrane organization: Composition, regulation and roles of lipid rafts. , *Nature Reviews Molecular Cell Biology*, 18. (2017) , Nature Publishing Group, 361–374
- 22 Bigay, J. and Antonny, B. Curvature, Lipid Packing, and Electrostatics of Membrane Organelles: Defining Cellular Territories in Determining Specificity. , *Developmental Cell*, 23. 13-Nov-(2012) , 886–895
- 23 Diz-Muñoz, A. *et al.* In pursuit of the mechanics that shape cell surfaces. , *Nature Physics*, 14. (2018) , 648–652
- 24 Kapus, A. and Janmey, P. (2013) Plasma membrane-cortical cytoskeleton interactions: A cell biology approach with biophysical considerations. *Compr. Physiol.* 3, 1231–1281
- 25 De Craene, J.O. *et al.* Phosphoinositides, major actors in membrane trafficking and lipid signaling pathways. , *International Journal of Molecular Sciences*, 18. 15-Mar-(2017) , MDPI AG, 634
- 26 Maxwell, K.N. *et al.* Clustering of Rac1: Selective Lipid Sorting Drives Signaling. , *Trends in Biochemical Sciences*, 43. (2018) , 75–77
- 27 Riggi, M. *et al.* (2018) Decrease in plasma membrane tension triggers PtdIns(4,5)P₂ phase separation to inactivate TORC2. *Nat. Cell Biol.* 20, 1043–1051
- 28 Moeendarbary, E. and Harris, A.R. (2014) Cell mechanics: Principles, practices, and prospects. *Wiley Interdiscip. Rev. Syst. Biol. Med.* 6, 371–388

REFERENCES

- 29 Sens, P. and Plastino, J. Membrane tension and cytoskeleton organization in cell motility. , *Journal of Physics Condensed Matter*, 27. (2015) , 273103
- 30 Sitarska, E. and Diz-muñoz, A. (2020) Pay attention to membrane tension : mechanobiology of the cell surface. *Curr. Opin. Cell Biol.* 66, 1–12
- 31 Diz-Muñoz, A. *et al.* (2013) Use the force: membrane tension as anorganizer of cell shape and motility. *Trends Cell Biol.* 23, 47–53
- 32 Shi, Z. *et al.* (2018) Cell Membranes Resist Flow. *Cell* 175, 1769-1779.e13
- 33 Suetsugu, S. *et al.* (2014) Dynamic shaping of cellular membranes by phospholipids and membrane-deforming proteins. *Physiol. Rev.* 94, 1219–1248
- 34 Parmryd, I. and Önfelt, B. Consequences of membrane topography. , *FEBS Journal*, 280. Jun-(2013) , 2775–2784
- 35 Antony, B. (2011) Mechanisms of Membrane Curvature Sensing. *Annu. Rev. Biochem.* 80, 101–123
- 36 Cornell, R.B. and Northwood, I.C. Regulation of CTP:phosphocholine cytidyltransferase by amphitropism and relocalization. , *Trends in Biochemical Sciences*, 25. 01-Sep-(2000) , Elsevier, 441–447
- 37 McMahan, H.T. and Boucrot, E. (2015) Membrane curvature at a glance. *J. Cell Sci.* 128, 1065–1070
- 38 Bassereau, P. *et al.* (2018) The 2018 biomembrane curvature and remodeling roadmap. *J. Phys. D. Appl. Phys.* 51, 343001
- 39 Gallop, H.T.M.& J.L. (2005) Membrane curvature and mechanisms of dynamic cell membrane remodelling. *Nature* 438, 590–596
- 40 Lecuit, T. and Lenne, P.F. Cell surface mechanics and the control of cell shape, tissue patterns and morphogenesis. , *Nature Reviews Molecular Cell Biology*, 8. (2007) , 633–644
- 41 Doherty, G.J. and McMahan, H.T. (2008) Mediation, Modulation, and Consequences of Membrane-Cytoskeleton Interactions. *Annu. Rev. Biophys.* 37, 65–95
- 42 Mattila, P.K. and Lappalainen, P. Filopodia: Molecular architecture and cellular functions. , *Nature Reviews Molecular Cell Biology*, 9. (2008) , 446–454
- 43 Faix, J. and Rottner, K. The making of filopodia. , *Current Opinion in Cell Biology*, 18. (2006) , 18–25
- 44 Small, J.V. *et al.* (2002) The lamellipodium: where motility begins. *Trends Cell Biol.* 12, 8–11
- 45 Raucher, D. and Sheetz, M.P. (1999) *Characteristics of a Membrane Reservoir Buffering Membrane Tension*, 77
- 46 Charras, G.T. (2008) A short history of blebbing. *J. Microsc.* 231, 466–478
- 47 Lim, F.Y. *et al.* (2012) The size, shape, and dynamics of cellular blebs. *EPL* 100, 28004
- 48 Tsujita, K. *et al.* (2015) Feedback regulation between plasma membrane tension and membrane-bending proteins organizes cell polarity during

- leading edge formation. *Nat. Cell Biol.* 17, 749–758
- 49 Goudarzi, M. *et al.* (2017) Bleb Expansion in Migrating Cells Depends on Supply of Membrane from Cell Surface Invaginations. *Dev. Cell* 43, 577–587.e5
- 50 Diz-Muñoz, A. *et al.* (2016) Steering cell migration by alternating blebs and actin-rich protrusions. DOI: 10.1186/s12915-016-0294-x
- 51 Reichman-Fried, M. and Raz, E. (2016) Blood, blebs and lumen expansion. *Nat. Cell Biol.* 18, 366–367
- 52 Kosmalska, A.J. *et al.* (2015) Physical principles of membrane remodelling during cell mechanoadaptation. *Nat. Commun.* 6, 7292
- 53 Gauthier, N.C. *et al.* (2012) Mechanical feedback between membrane tension and dynamics. *Trends Cell Biol.* 22, 527–535
- 54 Kumari, S. *et al.* (2010) Endocytosis unplugged: multiple ways to enter the cell. *Cell Res.* 20, 256–275
- 55 Wang, G. and Galli, T. (2018) Reciprocal link between cell biomechanics and exocytosis. *Traffic* DOI: 10.1111/tra.12584
- 56 Hamill, O.P. and Martinac, B. (2001) Molecular Basis of Mechanotransduction in Living Cells. *Physiol. Rev.* 81 (2), 685–740
- 57 Gauthier, N.C. *et al.* (2011) Temporary increase in plasma membrane tension coordinates the activation of exocytosis and contraction during cell spreading. *Proc. Natl. Acad. Sci. U. S. A.* 108, 14467–72
- 58 Apodaca, G. (2002) Modulation of membrane traffic by mechanical stimuli. *Am. J. Physiol. Renal Physiol.* 282, F179–F190
- 59 Thottacherry, J.J. *et al.* (2018) Mechanochemical feedback control of dynamin independent endocytosis modulates membrane tension in adherent cells. *Nat. Commun.* 9,
- 60 Mayor, S. *et al.* (2014) Clathrin-independent pathways of endocytosis. *Cold Spring Harb. Perspect. Biol.* 6, 1–21
- 61 Gervásio, O.L. *et al.* (2011) Caveolae respond to cell stretch and contribute to stretch-induced signaling. *J. Cell Sci.* 124, 3581–3590
- 62 Sinha, B. *et al.* (2011) Cells respond to mechanical stress by rapid disassembly of caveolae. *Cell* 144, 402–413
- 63 Cheng, J.P.X. *et al.* (2015) Caveolae protect endothelial cells from membrane rupture during increased cardiac output. *J. Cell Biol.* 211, 53–61
- 64 Ingber, D.E. (2006) Cellular mechanotransduction: putting all the pieces together again. *FASEB J.* 20, 811–827
- 65 Köster, D. V. and Mayor, S. Cortical actin and the plasma membrane: Inextricably intertwined. , *Current Opinion in Cell Biology*, 38. (2016) , 81–89
- 66 Dominguez, R. and Holmes, K.C. (2011) Actin Structure and Function. *Annu. Rev. Biophys.* 40, 169–186
- 67 Svitkina, T. (2018) The actin cytoskeleton and actin-based motility. *Cold Spring Harb. Perspect. Biol.* 10,

REFERENCES

- 68 Siton-Mendelson, O. and Bernheim-Groswasser, A. Functional Actin Networks under Construction: The Cooperative Action of Actin Nucleation and Elongation Factors. , *Trends in Biochemical Sciences*, 42. (2017) , 414–430
- 69 Pollard, T.D. Regulation of actin filament assembly by Arp2/3 complex and formins. , *Annual Review of Biophysics and Biomolecular Structure*, 36. (2007) , 451–477
- 70 Breitsprecher, D. and Goode, B.L. (2013) Formins at a glance. *J. Cell Sci.* 126, 1–7
- 71 Svitkina, T.M. Actin Cell Cortex: Structure and Molecular Organization. , *Trends in Cell Biology*. (2020)
- 72 Goley, E.D. and Welch, M.D. The ARP2/3 complex: An actin nucleator comes of age. , *Nature Reviews Molecular Cell Biology*, 7. (2006) , 713–726
- 73 Chugh, P. and Paluch, E.K. (2018) The actin cortex at a glance. *J. Cell Sci.* 131,
- 74 Cartagena-Rivera, A.X. *et al.* (2016) Actomyosin Cortical Mechanical Properties in Nonadherent Cells Determined by Atomic Force Microscopy. *Biophys. J.* 110, 2528–2539
- 75 Chikina, A.S. *et al.* (2019) Time-resolved ultrastructure of the cortical actin cytoskeleton in dynamic membrane blebs. *J. Cell Biol.* 218, 445–454
- 76 Chugh, P. *et al.* (2017) Actin cortex architecture regulates cell surface tension. *Nat. Cell Biol.* 19, 689–697
- 77 Fritzsche, M. *et al.* (2016) Actin kinetics shapes cortical network structure and mechanics. *Sci. Adv.* 2,
- 78 McClatchey, A.I. (2014) ERM proteins at a glance. *J. Cell Sci.* 127, 3199–3204
- 79 Ponuwei, G.A. (2016) A glimpse of the ERM proteins. *J. Biomed. Sci.* 23,
- 80 Kunda, P. *et al.* (2008) Moesin Controls Cortical Rigidity, Cell Rounding, and Spindle Morphogenesis during Mitosis. *Curr. Biol.* 18, 91–101
- 81 Salbreux, G. *et al.* Actin cortex mechanics and cellular morphogenesis. , *Trends in Cell Biology*, 22. (2012) , 536–545
- 82 Schink, K.O. *et al.* (2016) Phosphoinositides in Control of Membrane Dynamics. *Annu. Rev. Cell Dev. Biol.* 32, 143–171
- 83 Yin, H.L. and Janmey, P.A. (2003) Phosphoinositide Regulation of the Actin Cytoskeleton. *Annu. Rev. Physiol.* 65, 761–789
- 84 Kurisu, S. and Takenawa, T. The WASP and WAVE family proteins. , *Genome biology*, 10. (2009) , 226
- 85 Tadaomi Takenawa and Miki, and H. WASP and WAVE family proteins: key molecules for rapid rearrangement of cortical actin filaments and cell movement. *J. Cell Sci.* 114, 1801–1809
- 86 Ramalingam, N. *et al.* (2010) Phospholipids regulate localization and activity of mDia1 formin. *Eur. J. Cell Biol.* 89, 723–732
- 87 Gorelik, R. *et al.* (2011) Mechanisms of plasma membrane targeting of

- formin mDia2 through its amino terminal domains. *Mol. Biol. Cell* 22, 189–201
- 88 Senju, Y. and Lappalainen, P. (2019) Regulation of actin dynamics by PI(4,5)P2 in cell migration and endocytosis. *Curr. Opin. Cell Biol.* 56, 7–13
- 89 Breitbart, H. and Finkelstein, M. (2015) , Regulation of Sperm Capacitation and the Acrosome Reaction by PIP2 and Actin Modulation. , in *Asian Journal of Andrology*, 17, pp. 597–600
- 90 Chou, J. *et al.* (2002) *Distribution of gelsolin and phosphoinositol 4,5-bisphosphate in lamellipodia during EGF-induced motility*, 34
- 91 Raucher, D. *et al.* (2000) Phosphatidylinositol 4,5-bisphosphate functions as a second messenger that regulates cytoskeleton-plasma membrane adhesion. *Cell* 100, 221–228
- 92 Maxwell, K.N. *et al.* (2018) Rac1 Nanoscale Organization on the Plasma Membrane Is Driven by Lipid Binding Specificity Encoded in the Membrane Anchor. *Mol. Cell. Biol.* 38,
- 93 Suetsugu, S. *et al.* (2006) Optimization of WAVE2 complex-induced actin polymerization by membrane-bound IRSp53, PIP3, and Rac. *J. Cell Biol.* 173, 571–585
- 94 Lundmark, R. *et al.* (2008) The GTPase-Activating Protein GRAF1 Regulates the CLIC/GEEC Endocytic Pathway. *Curr. Biol.* 18, 1802–1808
- 95 Ligeti, E. and Settleman, J. Regulation of RhoGAP specificity by phospholipids and prenylation. , *Methods in Enzymology*, 406. (2006) , 104–117
- 96 Halstead, J.R. *et al.* (2010) Rac controls PIP5K localisation and PtdIns(4,5)P2 synthesis, which modulates vinculin localisation and neurite dynamics. *J. Cell Sci.* 123, 3535–3546
- 97 Pleines, I. *et al.* (2009) Rac1 is essential for phospholipase C- γ 2 activation in platelets. *Pflugers Arch. Eur. J. Physiol.* 457, 1173–1185
- 98 Eyckmans, J. *et al.* A Hitchhiker’s Guide to Mechanobiology. , *Developmental Cell*, 21. 19-Jul-(2011) , Cell Press, 35–47
- 99 Elosegui-Artola, A. *et al.* (2016) Mechanical regulation of a molecular clutch defines force transmission and transduction in response to matrix rigidity. *Nat. Cell Biol.* 18, 540–548
- 100 Kechagia, J.Z. *et al.* Integrins as biomechanical sensors of the microenvironment. , *Nature Reviews Molecular Cell Biology*, 20. (2019) , 457–473
- 101 Gudipaty, S.A. *et al.* (2017) Mechanical stretch triggers rapid epithelial cell division through Piezo1. *Nature* 543, 118–121
- 102 Chen, Y. *et al.* Tensile and compressive force regulation on cell mechanosensing. , *Biophysical Reviews*, 11. (2019) , 311–318
- 103 Maksym, G.N. (2010) Mechanics of Airway Smooth Muscle Cells and the Response to Stretch. In *Stud Mechanobiol Tissue Eng Biomater* pp. 201–245, Springer-Verlag Berlin Heidelberg

REFERENCES

- 104 Birukova, A.A. *et al.* (2006) Differential regulation of pulmonary endothelial monolayer integrity by varying degrees of cyclic stretch. *Am. J. Pathol.* 168, 1749–1761
- 105 Skutek, M. *et al.* (2001) Cyclic mechanical stretching enhances secretion of Interleukin 6 in human tendon fibroblasts. *Knee Surgery, Sport. Traumatol. Arthrosc.* 9, 322–326
- 106 Kültz, D. Cellular osmoregulation: Beyond ion transport and cell volume. *Zoology*, 104. (2001) , 198–208
- 107 Rossy, J. *et al.* Role of mechanotransduction and tension in t cell function. *Frontiers in Immunology*, 9. (2018) , 1–11
- 108 Cheng, G. *et al.* (2009) Micro-environmental mechanical stress controls tumor spheroid size and morphology by suppressing proliferation and inducing apoptosis in cancer cells. *PLoS One* 4,
- 109 Lang, F. (2007) Mechanisms and Significance of Cell Volume Regulation. *J. Am. Coll. Nutr.* 26, 613S-623S
- 110 Shi, Z.D. and Tarbell, J.M. (2011) Fluid flow mechanotransduction in vascular smooth muscle cells and fibroblasts. *Ann. Biomed. Eng.* 39, 1608–1619
- 111 Janmey, P.A. and McCulloch, C.A. (2007) Cell Mechanics: Integrating Cell Responses to Mechanical Stimuli. *Annu. Rev. Biomed. Eng.* 9, 1–34
- 112 Goetz, J.G. *et al.* (2014) Endothelial cilia mediate low flow sensing during zebrafish vascular development. *Cell Rep.* 6, 799–808
- 113 le Noble, F. *et al.* (2004) Flow regulates arterial-venous differentiation in the chick embryo yolk sac. *Development* 131, 361–375
- 114 Oria, R. *et al.* (2017) Force loading explains spatial sensing of ligands by cells. *Nature* 552, 219–224
- 115 Lou, H.Y. *et al.* (2019) Membrane curvature underlies actin reorganization in response to nanoscale surface topography. *Proc. Natl. Acad. Sci. U. S. A.* 116, 23143–23151
- 116 Shoham, N. *et al.* (2012) Static mechanical stretching accelerates lipid production in 3T3-L1 adipocytes by activating the MEK signaling pathway. *Am. J. Physiol. - Cell Physiol.* 302, 429–441
- 117 Pinot, M. *et al.* (2018) Feedback between membrane tension, lipid shape and curvature in the formation of packing defects. *bioRxiv* DOI: 10.1101/389627
- 118 Pontes, B. *et al.* Membrane tension: A challenging but universal physical parameter in cell biology. *Seminars in Cell and Developmental Biology*, 71. (2017) , 30–41
- 119 Andreu, I. *et al.* The force loading rate drives cell mechanosensing through both reinforcement and fluidization. DOI: 10.1101/2021.03.08.434428
- 120 Staykova, M. *et al.* (2013) Confined bilayers passively regulate shape and stress. *Phys. Rev. Lett.* 110, 1–5

- 121 Riggi, M. *et al.* (2019) TORC2 controls endocytosis through plasma membrane tension. *J. Cell Biol.* 218, 2265–2276
- 122 Diz-Muñoz, A. *et al.* (2016) Membrane Tension Acts Through PLD2 and mTORC2 to Limit Actin Network Assembly During Neutrophil Migration. *PLoS Biol.* 14, 1–30
- 123 Hatzakis, N.S. *et al.* (2009) How curved membranes recruit amphipathic helices and protein anchoring motifs. *Nat. Chem. Biol.* 5, 835–841
- 124 Colom, A. *et al.* A fluorescent membrane tension probe. DOI: 10.1038/s41557-018-0127-3
- 125 Steward, R.L. *et al.* (2011) Mechanical stretch and shear flow induced reorganization and recruitment of fibronectin in fibroblasts. *Sci. Rep.* 1,
- 126 Trieu, D. *et al.* (2014) A microfluidic device to apply shear stresses to polarizing ciliated airway epithelium using air flow. *Biomicrofluidics* 8, 064104
- 127 Jones, T. *et al.* (2020) Light-Inducible Generation of Membrane Curvature in Live Cells with Engineered BAR Domain Proteins. *ACS Synth. Biol.* 9, 893–901
- 128 Fernandez, A. *et al.* (2017) Cell-Shaping Micropatterns for Quantitative Super-Resolution Microscopy Imaging of Membrane Mechanosensing Proteins. *ACS Appl. Mater. Interfaces* 9, 27575–27586
- 129 Von Erlach, T.C. *et al.* (2018) Cell-geometry-dependent changes in plasma membrane order direct stem cell signalling and fate. *Nat. Mater.* 17, 237–242
- 130 Ranade, S.S. *et al.* Mechanically Activated Ion Channels. , *Neuron*, 87. 23-Sep-(2015) , Cell Press, 1162–1179
- 131 Woo, S.H. *et al.* (2014) Piezo2 is required for Merkel-cell mechanotransduction. *Nature* 509, 622–626
- 132 Xu, J. *et al.* (2018) GPR68 Senses Flow and Is Essential for Vascular Physiology Article GPR68 Senses Flow and Is Essential for Vascular Physiology. *Cell* 173, 762–775
- 133 Kozera, L. *et al.* (2009) Caveolae act as membrane reserves which limit mechanosensitive ICl,swell channel activation during swelling in the rat ventricular myocyte. *PLoS One* 4,
- 134 Singh, V. and Lamaze, C. Membrane tension buffering by caveolae: a role in cancer? , *Cancer and Metastasis Reviews*, 39. (2020) , 505–517
- 135 Torrino, S. *et al.* (2018) EHD2 is a mechanotransducer connecting caveolae dynamics with gene transcription. *J. Cell Biol.* 217, 4092–4105
- 136 Berchtold, D. *et al.* (2012) Plasma membrane stress induces relocalization of Slm proteins and activation of TORC2 to promote sphingolipid synthesis. *Nat. Cell Biol.* 14, 542–547
- 137 Simunovic, M. and Voth, G.A. (2015) Membrane tension controls the assembly of curvature-generating proteins. *Nat. Commun.* 6,
- 138 Simunovic, M. *et al.* (2015) When Physics Takes Over: BAR Proteins and

REFERENCES

- Membrane Curvature. *Trends Cell Biol.* 25, 780–792
- 139 Sorre, B. *et al.* (2009) Curvature-driven lipid sorting needs proximity to a demixing point and is aided by proteins. *Proc. Natl. Acad. Sci. U. S. A.* 106, 5622–5626
- 140 Sorre, B. *et al.* (2012) Nature of curvature coupling of amphiphysin with membranes depends on its bound density. *Proc. Natl. Acad. Sci. U. S. A.* 109, 173–8
- 141 Peter, B.J. *et al.* (2004) BAR Domains as Sensors of Membrane Curvature : The Amphiphysin BAR Structure. *Science (80-.)*. 303, 495–499
- 142 Zhao, W. *et al.* (2017) Nanoscale manipulation of membrane curvature for probing endocytosis in live cells. *Nat. Nanotechnol.* 12, 750–756
- 143 Echarri, A. *et al.* (2019) An Abl-FBP17 mechanosensing system couples local plasma membrane curvature and stress fiber remodeling during mechanoadaptation. *Nat. Commun.* 10,
- 144 Disanza, A. *et al.* (2013) CDC42 switches IRSp53 from inhibition of actin growth to elongation by clustering of VASP. *EMBO J.* 32, 2735–2750
- 145 Weiss, S.M. *et al.* (2009) IRSp53 Links the Enterohemorrhagic E. coli Effectors Tir and EspFU for Actin Pedestal Formation. *Cell Host Microbe* 5, 244–258
- 146 Sawallisch, C. *et al.* (2009) The insulin receptor substrate of 53 kDa (IRSp53) limits hippocampal synaptic plasticity. *J. Biol. Chem.* 284, 9225–9236
- 147 Bogdanov, A.M. *et al.* (2012) Anti-Fading Media for Live Cell GFP Imaging. *PLoS One* 7, 53004
- 148 Disanza, A. *et al.* (2006) Regulation of cell shape by Cdc42 is mediated by the synergic actin-bundling activity of the Eps8-IRSp53 complex. *Nat. Cell Biol.* 8, 1337–1347
- 149 Sathe, M. *et al.* (2017) Small GTPases and BAR domain proteins regulate branched actin to make clathrin and dynamin independent endocytic vesicles. DOI: 10.1101/170753
- 150 Soriano-castell, D. *et al.* (2017) ROCK1 is a novel Rac1 effector to regulate tubular endocytic membrane formation during clathrin-independent endocytosis. *Sci. Rep.* DOI: 10.1038/s41598-017-07130-x
- 151 Carpenter, A.E. *et al.* (2006) CellProfiler: Image analysis software for identifying and quantifying cell phenotypes. *Genome Biol.* 7, R100
- 152 Arroyo, M. and Desimone, A. (2009) Relaxation dynamics of fluid membranes. *Phys. Rev. E - Stat. Nonlinear, Soft Matter Phys.* 79,
- 153 Scita, G. *et al.* IRSp53: crossing the road of membrane and actin dynamics in the formation of membrane protrusions. , *Trends in Cell Biology*, 18. (2008) , 52–60
- 154 Tozzi, C. *et al.* (2019) Out-of-equilibrium mechanochemistry and self-organization of fluid membranes interacting with curved proteins. *New J. Phys.* 21,

- 155 Suarez, C. and Kovar, D.R. Internetwork competition for monomers governs actin cytoskeleton organization. , *Nature Reviews Molecular Cell Biology*, 17. (2016) , 799–810
- 156 Maiuri, P. *et al.* (2015) Actin flows mediate a universal coupling between cell speed and cell persistence. *Cell* 161, 374–386
- 157 Casares, L. *et al.* (2015) Hydraulic fracture during epithelial stretching. *Nat. Mater.* 14, 343–351
- 158 Flores, L.R. *et al.* (2019) Lifeact-GFP alters F-actin organization, cellular morphology and biophysical behaviour. *Sci. Rep.* 9, 1–13
- 159 Fritzsche, M. *et al.* (2014) Quantitative analysis of ezrin turnover dynamics in the actin cortex. *Biophys. J.* 106, 343–353
- 160 Ebrahimkuty, M.P. and Galic, M. Receptor-Free Signaling at Curved Cellular Membranes. , *BioEssays*, 41. 04-Oct-(2019) , John Wiley and Sons Inc., 1900068
- 161 Carman, P.J. and Dominguez, R. BAR domain proteins—a linkage between cellular membranes, signaling pathways, and the actin cytoskeleton. , *Biophysical Reviews*, 10. 01-Dec-(2018) , Springer Verlag, 1587–1604
- 162 Henne, W.M. *et al.* (2010) FCHo Proteins Are Nucleators of Clathrin-Mediated Endocytosis. *Science* (80-.). 328, 1281–1284
- 163 Kim, B.L. *et al.* (2008) The Cdc42 effector IRSp53 generates filopodia by coupling membrane protrusion with actin dynamics. *J. Biol. Chem.* 283, 20454–20472
- 164 Tsai, F.C. *et al.* (2018) Ezrin enrichment on curved membranes requires a specific conformation or interaction with a curvature-sensitive partner. *Elife* 7, 1–27
- 165 Miki, H. *et al.* (2000) IRSp53 is an essential intermediate between Rac and WAVE in the regulation of membrane ruffling. *Nature* 408, 732–735
- 166 Miki, H. and Takenawa, T. (2002) WAVE2 serves a functional partner of IRSp53 by regulating its interaction with Rac. *Biochem. Biophys. Res. Commun.* 293, 93–99
- 167 Yamagishi, A. *et al.* (2004) A Novel Actin Bundling/Filopodium-forming Domain Conserved in Insulin Receptor Tyrosine Kinase Substrate p53 and Missing in Metastasis Protein. *J. Biol. Chem.* 279, 14929–14936
- 168 Breuer, A. *et al.* (2019) Quantitative investigation of negative membrane curvature sensing and generation by I-BARs in filopodia of living cells. *Soft Matter* 15, 9829–9839
- 169 Goh, W.I. *et al.* (2012) mDia1 and WAVE2 proteins interact directly with IRSp53 in filopodia and are involved in filopodium formation. *J. Biol. Chem.* 287, 4702–4714
- 170 Kast, D.J. and Dominguez, R. (2019) IRSp53 coordinates AMPK and 14-3-3 signaling to regulate filopodia dynamics and directed cell migration. *Mol. Biol. Cell* 30, 1285–1297

REFERENCES

- 171 Prévost, C. *et al.* (2015) IRSp53 senses negative membrane curvature and phase separates along membrane tubules. *Nat. Commun.* 6,
- 172 Suetsugu, S. *et al.* (2006) The RAC binding domain/IRSp53-MIM homology domain of IRSp53 induces RAC-dependent membrane deformation. *J. Biol. Chem.* 281, 35347–35358
- 173 Millard, T.H. *et al.* (2005) Structural basis of filopodia formation induced by the IRSp53/MIM homology domain of human IRSp53. *EMBO J.* 24, 240–250
- 174 Zampighi, G.A. *et al.* (1995) Discrete and Reversible Vacuole-like Dilations Induced by Osmomechanical Perturbation of Neurons. *J. Membr. Biol.* 145, 33–47
- 175 Morris, C.E. and Homann, U. (2001) Cell surface area regulation and membrane tension. *J. Membr. Biol.* 179, 79–102
- 176 Nakagawa, H. *et al.* IRSp53 is colocalised with WAVE2 at the tips of protruding lamellipodia and filopodia independently of Mena. , *Journal of Cell Science*, 116. (2003) , 2577–2583
- 177 Kast, D.J. *et al.* (2014) Mechanism of IRSp53 inhibition and combinatorial activation by Cdc42 and downstream effectors. *Nat. Struct. Mol. Biol.* 21, 413–422
- 178 Mattila, P.K. *et al.* (2007) Missing-in-metastasis and IRSp53 deform PI(4,5)P2-rich membranes by an inverse BAR domain-like mechanism. *J. Cell Biol.* 176, 953–964
- 179 Choi, J. *et al.* (2005) Regulation of dendritic spine morphogenesis by insulin receptor substrate 53, a downstream effector of Rac1 and Cdc42 small GTPases. *J. Neurosci.* 25, 869–879
- 180 Robens, J.M. *et al.* (2010) Regulation of IRSp53-Dependent Filopodial Dynamics by Antagonism between 14-3-3 Binding and SH3-Mediated Localization. *Mol. Cell. Biol.* 30, 829–844
- 181 Bisi, S. *et al.* (2020) IRSp53 controls plasma membrane shape and polarized transport at the nascent lumen in epithelial tubules. *Nat. Commun.* 11, 1–23
- 182 Martell, J.D. *et al.* (2017) Electron microscopy using the genetically encoded APEX2 tag in cultured mammalian cells. *Nat. Protoc.* 12, 1792–1816
- 183 Ariotti, N. *et al.* (2018) Ultrastructural localisation of protein interactions using conditionally stable nanobodies. *PLoS Biol.* 16, 1–11
- 184 Sudhaharan, T. *et al.* (2019) Superresolution microscopy reveals distinct localisation of full length IRSp53 and its I-BAR domain protein within filopodia. *Sci. Rep.* 9,
- 185 Abou-Kheir, W. *et al.* (2008) Membrane targeting of WAVE2 is not sufficient for WAVE2-dependent actin polymerization: A role for IRSp53 in mediating the interaction between Rac and WAVE2. *J. Cell Sci.* 121, 379–390

- 186 Fujiwara, T. *et al.* (2000) Rho small G-protein-dependent binding of mDia to an Src homology 3 domain-containing IRSp53/BAIAP2. *Biochem. Biophys. Res. Commun.* 271, 626–629
- 187 Charras, G.T. *et al.* (2006) Reassembly of contractile actin cortex in cell blebs. *J. Cell Biol.* 175, 477–490
- 188 Yang, W. *et al.* (2020) TRPV4 activates the Cdc42/N-wasp pathway to promote glioblastoma invasion by altering cellular protrusions. *Sci. Rep.* 10, 14151
- 189 Rizvi, S.A. *et al.* (2009) Identification and Characterization of a Small Molecule Inhibitor of Formin-Mediated Actin Assembly. *Chem. Biol.* 16, 1158–1168
- 190 Wakayama, Y. *et al.* (2015) Cdc42 mediates Bmp - Induced sprouting angiogenesis through Fmnl3-driven assembly of endothelial filopodia in zebrafish. *Dev. Cell* 32, 109–122
- 191 Képiró, M. *et al.* (2014) Para-nitroblebbistatin, the non-cytotoxic and photostable myosin II inhibitor. *Angew. Chemie - Int. Ed.* 53, 8211–8215
- 192 Tojkander, S. *et al.* (2012) Actin stress fibers - Assembly, dynamics and biological roles. *J. Cell Sci.* 125, 1855–1864
- 193 Hetrick, B. *et al.* (2013) Small molecules CK-666 and CK-869 inhibit actin-related protein 2/3 complex by blocking an activating conformational change. *Chem. Biol.* 20, 701–712
- 194 Connolly, B.A. *et al.* (2005) Tiam1-IRSp53 Complex Formation Directs Specificity of Rac-Mediated Actin Cytoskeleton Regulation. *Mol. Cell. Biol.* 25, 4602–4614
- 195 Gov, N.S. Guided by curvature: Shaping cells by coupling curved membrane proteins and cytoskeletal forces. , *Philosophical Transactions of the Royal Society B: Biological Sciences*, 373. 26-May-(2018) , Royal Society Publishing
- 196 Beedle, A.E.M. *et al.* (2015) Mechanobiology-chemical origin of membrane mechanical resistance and force-dependent signaling. *Curr. Opin. Chem. Biol.* 29, 87–93
- 197 Innocenti, M. (2018) New insights into the formation and the function of lamellipodia and ruffles in mesenchymal cell migration. *Cell Adhes. Migr.* 12, 401–416
- 198 Li, X. *et al.* (2021) The effects of cardiac stretch on atrial fibroblasts: Analysis of the evidence and potential role in atrial fibrillation. *Cardiovasc. Res.* 00, 1–21
- 199 Aragona, M. *et al.* (2020) Mechanisms of stretch-mediated skin expansion at single-cell resolution. *Nature* 584, 268–273
- 200 Dai, J. *et al.* (1998) Membrane tension in swelling and shrinking molluscan neurons. *J. Neurosci.* 18, 6681–6692
- 201 Lemièrre, J. *et al.* (2018) Rapid adaptation of endocytosis, exocytosis and eisosomes after an acute increase in membrane tension in yeast cells.

REFERENCES

- bioRxiv* DOI: 10.1101/342030
- 202 Wang, S. *et al.* (2011) Endocytic response of type I alveolar epithelial cells to hypertonic stress. *Am J Physiol Lung Cell Mol Physiol* 55905, 560–568
- 203 Galic, M. *et al.* (2012) External push and internal pull forces recruit curvature-sensing N-BAR domain proteins to the plasma membrane. *Nat. Cell Biol.* 14, 874–881
- 204 Itoh, T. *et al.* (2005) Dynamin and the actin cytoskeleton cooperatively regulate plasma membrane invagination by BAR and F-BAR proteins. *Dev. Cell* 9, 791–804
- 205 Renard, H.-F. *et al.* (2015) Endophilin-A2 functions in membrane scission in clathrin-independent endocytosis. *Nature* 517, 493–6
- 206 Masters, T. a *et al.* (2013) Plasma membrane tension orchestrates membrane trafficking, cytoskeletal remodeling, and biochemical signaling during phagocytosis. *Proc. Natl. Acad. Sci. U. S. A.* 110, 11875–80
- 207 Bucher, D. *et al.* (2018) Clathrin-Adaptor ratio and membrane tension regulate the flat-To-curved transition of the clathrin coat during endocytosis. *Nat. Commun.* 9,
- 208 Boulant, S. *et al.* (2011) Actin dynamics counteract membrane tension during clathrin-mediated endocytosis. *Nat. Cell Biol.* 13, 1124–1132
- 209 Loh, J. *et al.* (2019) An acute decrease in plasma membrane tension induces macropinocytosis via PLD2 activation. *J. Cell Sci.* 132,
- 210 Baumgart, T. *et al.* (2011) Thermodynamics and mechanics of membrane curvature generation and sensing by proteins and lipids. *Annu. Rev. Phys. Chem.* 62, 483–506
- 211 Ren, G. *et al.* (2006) The BAR Domain Proteins : Molding Membranes in Fission , Fusion , and Phagy The BAR Domain Proteins : Molding Membranes in Fission , Fusion , and Phagy. *Microbiol. Mol. Biol. Rev.* 70, 37–120
- 212 The Common Fund of the Office of the Director of the National Institutes of Health, and by NCI, NHGRI, NHLBI, NIDA, NIMH, and N. The Genotype-Tissue Expression (GTEx) Project. , *The data used for the analyses described in this manuscript were obtained from: the GTEx Portal on 05/06/21.*
- 213 Funato, Y. *et al.* (2004) IRSp53/Eps8 complex is important for positive regulation of Rac and cancer cell motility/invasiveness. *Cancer Res.* 64, 5237–5244
- 214 Callan-Jones, A. *et al.* Curvature-driven lipid sorting in biomembranes. , *Cold Spring Harbor Perspectives in Biology*, 3. (2011) , 1–14
- 215 Massou, S. *et al.* (2020) Cell stretching is amplified by active actin remodelling to deform and recruit proteins in mechanosensitive structures. *Nat. Cell Biol.* 22, 1011–1023
- 216 Zhao, Z. *et al.* Mechanotransduction pathways in the regulation of cartilage chondrocyte homeostasis. , *Journal of Cellular and Molecular Medicine*, 24. 01-May-(2020) , Blackwell Publishing Inc., 5408–5419

- 217 Jayasinghe, A.K. *et al.* (2013) Apical oscillations in amnioserosa cells: Basolateral coupling and mechanical autonomy. *Biophys. J.* 105, 255–265
- 218 Latorre, E. *et al.* (2018) Active superelasticity in three-dimensional epithelia of controlled shape. *Nature* 563, 203–208
- 219 Idevall-Hagren, O. and De Camilli, P. (2015) Detection and manipulation of phosphoinositides. *Biochim. Biophys. Acta - Mol. Cell Biol. Lipids* 1851, 736–745
- 220 Hoff, F. (2015) , How to Prepare Your Specimen for Immunofluorescence Microscopy. , *Leica Microsystems*. [Online]. Available: <https://www.leica-microsystems.com/science-lab/how-to-prepare-your-specimen-for-immunofluorescence-microscopy/>
- 221 Hayashi, T. *et al.* Antigen Retrieval to Improve the Immunocytochemistry Detection of Sigma-1 Receptors and ER Chaperones. DOI: 10.1007/s00418-011-0811-5
- 222 Nybo, K. (2012) GFP imaging in fixed cells. *Biotechniques* 52, 359–360
- 223 Tagliaferro, P. *et al.* (1997) Immunofluorescence and glutaraldehyde fixation. A new procedure based on the Schiff-quenching method. *J. Neurosci. Methods* 77, 191–197
- 224 Lee, S. *et al.* (2013) Autofluorescence generation and elimination: A lesson from glutaraldehyde. *Chem. Commun.* 49, 3028–3030
- 225 Abcam Immunocytochemistry and immunofluorescence staining protocol. , *Abcam webinar*.
- 226 Hobro, A.J. and Smith, N.I. (2017) An evaluation of fixation methods: Spatial and compositional cellular changes observed by Raman imaging. *Vib. Spectrosc.* 91, 31–45
- 227 Kopek, B.G. *et al.* (2017) Diverse protocols for correlative super-resolution fluorescence imaging and electron microscopy of chemically fixed samples. *Nat. Protoc.* 12, 916–946
- 228 Richter, K.N. *et al.* (2018) Glyoxal as an alternative fixative to formaldehyde in immunostaining and super-resolution microscopy. *EMBO J.* DOI: 10.15252/embj.201695709
- 229 Taylor, M.J. *et al.* (2011) A high precision survey of the molecular dynamics of mammalian clathrin-mediated endocytosis. *PLoS Biol.* 9,
- 230 Umasankar, P.K. *et al.* (2012) Distinct and separable activities of the endocytic clathrin-coat components Fcho1/2 and AP-2 in developmental patterning. *Nat. Cell Biol.* 14, 488–501

“A vida é a merenda dos campeões”

Ataque Escampe